Spring 1-1-2017

Autoignition Studies of Gasoline Surrogate Fuels in the Advanced Fuel Ignition Delay Analyzer

Drew Morales Cameron
University of Colorado at Boulder, dmcameron08@gmail.com

Autoignition Studies Of Gasoline Surrogate Fuels In The Advanced Fuel Ignition Delay Analyzer

by

Drew Morales Cameron

B.S., Seattle University, 2015

A thesis submitted to the

Faculty of the Graduate School of the

University of Colorado in partial fulfillment

of the requirement for the degree of

Master of Science

Department of Mechanical Engineering

2017

This thesis entitled:
Autoignition Studies Of Gasoline Surrogate Fuels
In The Advanced Fuel Ignition Delay Analyzer
written by Drew Morales Cameron
has been approved for the Department of Mechanical Engineering

Professor John Daily

Professor Peter Hamlington

Professor Nicole Labbe

Date_____

The final copy of this thesis has been examined by the signatories, and we find that both the content and the form meet acceptable presentation standards of scholarly work in the above mentioned discipline.

Abstract

Drew Morales Cameron (M.S., Mechanical Engineering)

Autoignition Studies Of Gasoline Surrogate Fuels In The Advanced Fuel Ignition Delay Analyzer

Thesis directed by Professor John Daily and Dr. Bradley Zigler (NREL)

Improving vehicle efficiency is a substantial way to reduce CO_2 emissions from the transportation sector. The most limiting factor of spark ignition (SI) gasoline engine efficiency is the phenomenon known as knocking. The current methods to characterize fuel knock resistance are with the Research Octane Number (RON) and Motor Octane Number (MON) methods. However, it has been shown that these engine-based test methods do not directly predict knock resistance in modern direct injection (DI) gasoline engines, especially under boosted conditions. Alternative test devices have been used to more directly study ignition kinetics. Constant volume combustion chambers (CVCCs) have been used to obtain valuable autoignition data at a broader ranger of pressure and temperature conditions than the single point engine operating conditions of the RON and MON tests. This study uses a new CVCC to study gasoline range fuels at engine relevant conditions to collect autoignition data on a set of simple gasoline surrogate fuels and correlate these data to the fuel chemistry and properties. A set of nine gasoline surrogates, with and without oxygenates were tested in the Advanced Fuel Ignition Delay Analyzer (AFIDA). The main outputs of this study are 3D surfaces of autoignition (ignition delay time) as a function of pressure and temperature. These data more completely characterize ignition delay at a wide range of engine relevant conditions, providing more insight than the RON and MON tests. Linear regression was performed between the ignition delay time and the fuel composition and properties, however significant correlations were not found. This study paves the way for more

complex, full-boiling range gasoline fuels to be characterized in the AFIDA, fuels which are too complex to model with chemical kinetics.

Dedication

This thesis is dedicated this to my parents Denise Morales and Don Cameron whose love, support, and scientific encouragement helped me accomplish my goals. I also dedicate this thesis in memory of David Helete who made me the scientist I am today. I could not have done this with out any of you.

Acknowledgments

This research was conducted as part of the Co-Optimization of Fuels & Engines (Co-Optima) project sponsored by the U.S. Department of Energy - Office of Energy Efficiency and Renewable Energy, Bioenergy Technologies and Vehicle Technologies Offices. Co-Optima is a collaborative project of several national laboratories initiated to simultaneously accelerate the introduction of affordable, scalable, and sustainable biofuels and high-efficiency, low-emission vehicle engines. Work at the National Renewable Energy Laboratory (NREL) was performed under Contract No. DE347AC36-99GO10337.

I want to thank Bradley Zigler for giving me the opportunities and guidance to succeed since I first joined his research group as a Science Undergraduate Laboratory Intern in 2014 at NREL. I would also like to personally acknowledge the laboratory assistance I received from my colleges Matt Ratcliff, Earl Christensen, Lisa Fouts, Gina Chupka, Riley Abel and especially Jon Luecke without whose knowledge, and support this research would not have been possible. I would like to thank Dr. Daily for advising me and supporting my ambition throughout this project. I would also like to acknowledge Philipp Seidenspinner and ASG Analytik-Service Gesellschaft mbH, Germany for their technical support and collaboration with NREL on the Advanced Fuel Ignition Delay Analyzer.

Contents

Chapter

Tables

Figures

Acronym List

AFIDA: Advanced Fuel Ignition Delay Analyzer

ASTM: American Society for Testing and Materials

AVFL: Advanced/Vehicles/Fuels/Lubricants

BDC: Bottom Dead Center

CN: Cetane Number

CRC: Coordinating Research Council

DCN: Derived Cetane Number

DHA: Detailed Hydrocarbon Analysis

DI: Direct Injection

FACE: Fuels for Advanced Combustion Engines

G-CN: Generic Cetane Number

GHG: Greenhouse Gas

HPLC: High Performance Liquid Chromatography

ID: Ignition Delay

IQT: Ignition Quality Tester

LLNL: Lawrence Livermore National Laboratory

LTHR: Low-Temperature Heat Release

MON: Motor Octane Number

NREL: National Renewable Energy Laboratory

NTC: Negative Temperature Coefficient

ON: Octane Number

PRF: Primary Reference Fuel

RCM: Rapid Compression Machine

RON: Research Octane Number

S: (Octane) Sensitivity

SI: Spark Ignition

TDC: Top Dead Center

TRF: Toluene Reference Fuel

TSF: Toluene Standardization Fuel

CHAPTER 1

Introduction

1.1 Motivation

In the United States, the transportation sector consumes a significant amount of petroleum (see Figure 1 and Figure 2), and is therefore a significant contributor of greenhouse gas (GHG) emissions [1]. Light duty vehicles dominate the transportation sector (see Figure 3), and the majority of those vehicles are powered by spark ignition (SI) internal combustion engines [2,3]. It is crucial to increase efficiency of SI engines to reduce these emissions.

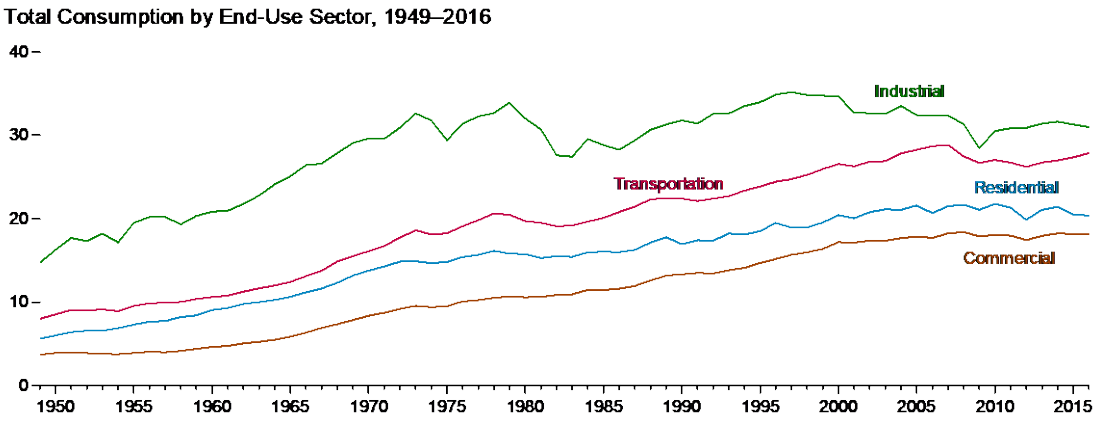

Figure 1: United States total energy consumption by end-use sector, 1949-2016 in Quadrillion (10^{15}) British Thermal Units (BTUs) [1].

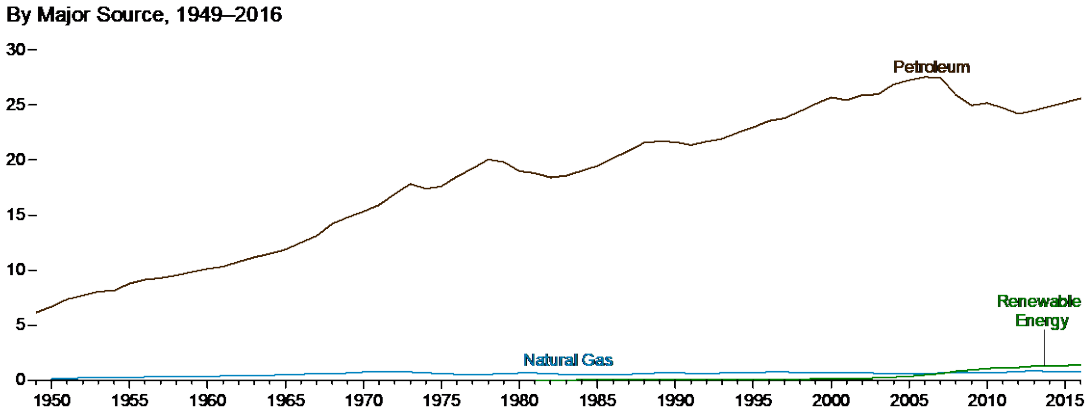

Figure 2: United States total transportation sector energy consumption by major source, 1949-2016 in Quadrillion BTUs [1].

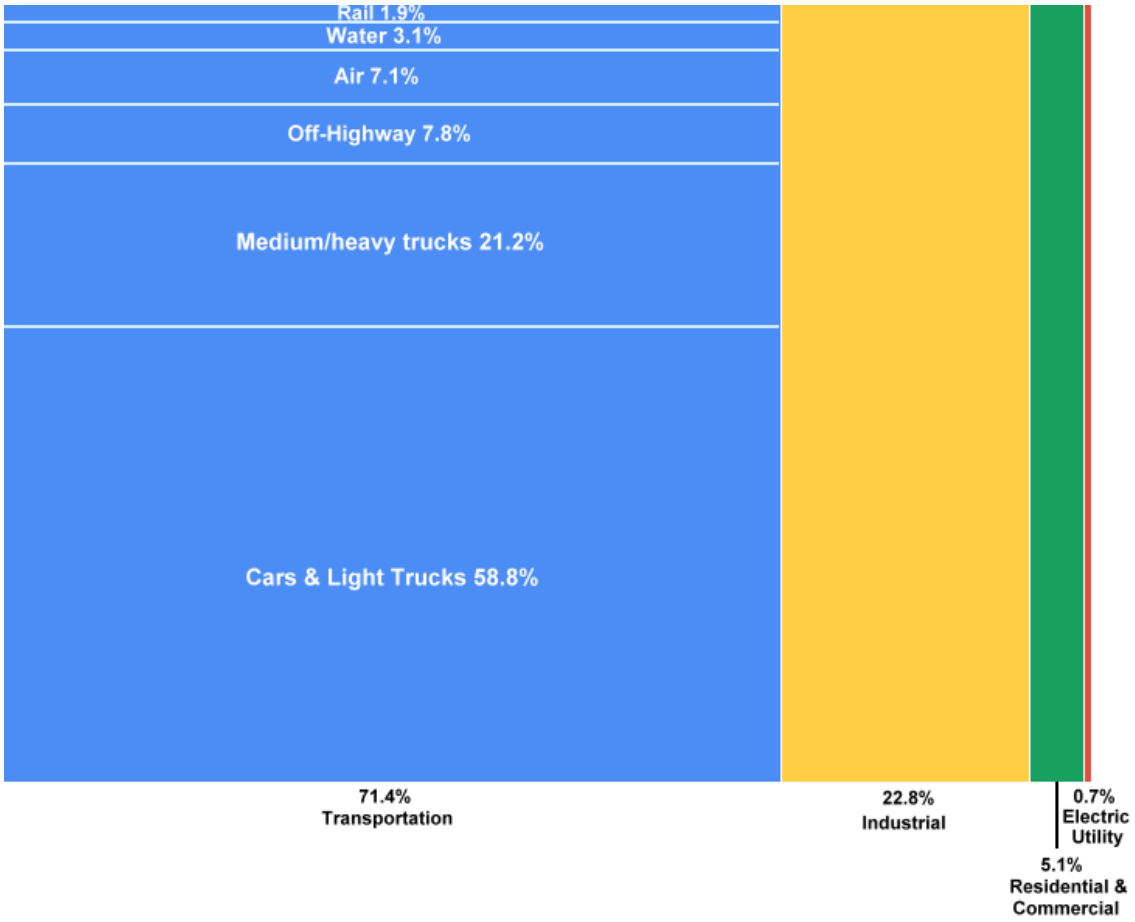

Figure 3: United States total petroleum consumption by sector, 2016 [2].

The phenomena of knock, has long been a limiting factor of SI engine efficiency [4]. Fuel knocking refers to the autoignition of unburned gasoline fuel/air mixture (endgas) as the flame front propagates across the combustion chamber [5]. Figure 4 is a visual representation of a normal combustion event in an SI engine (A) to a knocking event (B). It is named fittingly as extreme knocking is signified by the loud sound of an unintentional combustion event, which can cause extensive engine damage. Smaller knocking events cause a decrease in efficiency and interference with the engine cycles. In SI engines, efficiency is limited by the compression ratio, which is the ratio of the volume of the cylinder when the piston is at bottom dead center (BDC) to the volume of the cylinder when the piston is at top dead center (TDC) [6]. Compression ratio is related to the Carnot cycle efficiency by Equation (1.1), where r is the compression ratio and k

is the specific heat ratio [6]. For the advancement of SI engines the knocking propensity of fuels must be accurately characterized at modern engine relevant conditions.

$$\eta = 1 - \frac{1}{r^{k-1}} \tag{1.1}$$

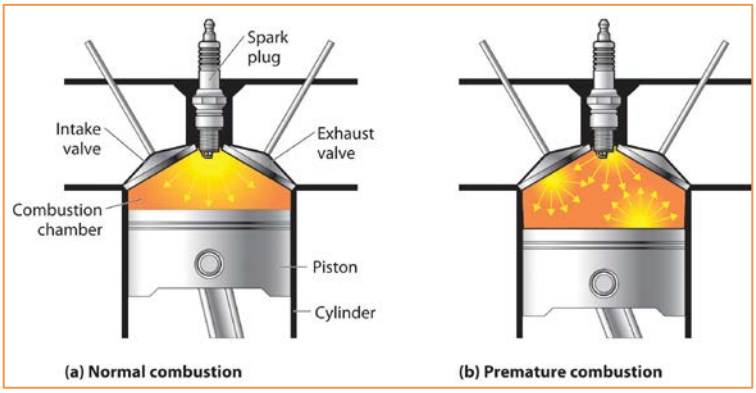

Figure 4: Comparison of a normal combustion event (A), to a knocking, or premature combustion event in (B) in an SI engine [7].

1.2 Background

As automotive companies employ novel technologies such as down-sizing, down-speeding, and turbocharging to increase efficiency, all of which rely on increased combustion temperatures and pressures, it is critical to accurately characterize the knocking potential of fuels [8]. The current method to characterize the knocking potential is known as the octane number (ON), which corresponds to the fuel's resistance to knocking autoignition. The two related methods used for gasoline fuels are, Research Octane Number (RON) and Motor Octane Number (MON) [9,10], the average of which is commonly shown on commercial gasoline fuel pumps. In these tests the fuel's knocking quality is compared to that of Primary Reference Fuels (PRFs), which are volumetric mixtures of iso-octane and n-heptane. The PRFs define the octane rating. Iso-octane is the definition of ON 100 and n-heptane is the definition of ON 0. The RON and MON tests are conducted at specific engine conditions, lower intake temperatures and slower engine speeds, versus higher intake temperatures and faster engine speeds respectively [11]. The

difference between RON and MON is known as the octane sensitivity (S), which indicates the difference in performance at different engine conditions. The RON and MON octane rating methods involve engine testing with technology dating to the 1920s, and have been shown to no longer directly predict knock resistance in modern SI engines, especially those with gasoline direct injection [2,8]. The RON and MON tests also fail to evaluate significant fuel chemistry effects that biofuels have in resisting knock [12,13]. The engine research and development community requires more accurate methods of quantifying a fuel's knock resistance to support advanced SI engine development with simultaneous changes in fuel blend composition.

1.3 Current Work

Significant work has been carried out in shock tubes, rapid compression machines (RCMs), and chemical kinetic simulations to characterize fuels and examine the ignition delay (ID) times in these various set-ups. ID time is the time it takes for a fuel to combust after it has been introduced to the system and is frequently used to measure the ignitability of the fuel. Studies in the Ignition Quality Tester (IQT), a constant volume combustion chamber (CVCC) or similar devices can be used to compliment RCM, and shock tube work. While the capabilities of RCM and shock tube devices are improving they have previously been limited to homogenous mixtures, and high-volatility fuels [14, 15, 16, 17]. Additionally these tests have long set-up/testing times, making it difficult to test large fuel sets efficiently [18]. While these tests are valuable there is a need to characterize high quantities of lower-volatility fuels in CVCCs like the IQT.

Similar kinetics data can be obtained in single-cylinder engines, however these tests are complex and typically less repeatable [18]. Additionally large volumes of fuel are required for these engine tests compared to the hundreds of mL or less, which is required to run extensive

testing in most CVCCs. The small volume of fuel required for CVCCs make them ideal for screening new fuels that are not available in high quantities. While there are many competing methods for characterizing fuels the IQT and similar devices provide important information and can be helpful both in screening new fuels, but also in providing validation of chemical kinetic models for complex fuel mixtures [19]. CVCCs also have the advantage of providing purely quiescent ambient conditions, which are not obtainable in flow devices such as shock tubes, RCM, and engines [20]. The higher ID times in the IQT allows for the mixture to reach a quasi-homogenous state, which allows the fuel chemistry effects on ignition delay to be studied with minimal interference from the fuel spray physics [19].

1.4 Research Plan

The goal of this research is to develop a methodology to evaluate the ignition behavior of gasoline surrogate fuels (both simple and complex) using a research CVCC and subsequently develop correlations between fuel properties, composition, and autoignition characteristics. This research was conducted at the National Renewable Energy Laboratory (NREL) with the use of the IQT and newer CVCC, the Advanced Fuel Ignition Delay Analyzer (AFIDA). The original goal was to study a set of 19 complex surrogate gasoline blends in cooperation with the Coordinating Research Council, who developed the fuels and studied them extensively in both direct injection (DI) and port fuel injection SI engines. The fuels would be analyzed in the IQT and correlations developed with the fuel properties, as well as chemical makeup to follow. However, the course of research was altered and a reduced set of simpler gasoline surrogate fuels was studied in the AFIDA instead.

These parametric ignition delay studies of gasoline surrogates in the AFIDA will help enable a bridge to link differences in fuel chemistry and how those differences impact engine

knock limits and thus, engine efficiency. The current standard for evaluating knocking potential of gasoline, RON and MON no longer describe knock performance in direct terms for modern DISI engines. Octane sensitivity (S), the difference between RON and MON has become more relevant and indicative of knocking potential than RON or MON alone [11]. Higher S, and lower MON actually helps efficiency in boosted DI engines, counter-intuitive to logic that a higher MON and RON rating equates to higher auto ignition, or knock, resistance. This study will more fully describe knock resistance than RON or MON alone, as these tests will be conducted over a broad ranger of parametric space of temperature and pressure compared to the single operating points of RON and MON tests. This study will also pave the way for further autoignition studies of complex gasoline range blends relevant to engine operating conditions, as shock tubes and most RCMs tend to operate at higher temperatures and lower pressures than engines. Although improvements have been made in these more fundamental devices for ignition kinetics measurements, shock tubes and RCMs are still challenging to operate with wide boiling range fuels. This research will also enable the AFIDA to provide support in validating chemical kinetic mechanisms. Currently chemical kinetic mechanisms are available to model simple fuels blends; some of the components this study uses, such as iso-octane, and n-heptane have well-established models. However blending effects (especially with oxygenates) have not been extensively studied under engine-relevant conditions. More importantly, more realistic, complex gasoline surrogates and real, full-boiling range gasolines are not currently modeled with detailed kinetic mechanisms. This study is establishing the groundwork with simple surrogate blends that will enable NREL to transition to full-boiling range gasolines, which are not simple to model, and would need well-controlled, engine-relevant experimental validation which the AFIDA can support.

CHAPTER 2

Experimental

2.1 Fuel Sets

The Coordinating Research Council (CRC) is a non-profit organization that directs studies on the interaction between automotive/other mobility equipment and petroleum products [21]. The Advanced Vehicles/Fuels/Lubricants 20 (AVFL-20) study investigates efficiency advantages for increased octane number fuels that may be available from ethanol or other blend components in modern light-duty vehicles [22]. For this study the CRC developed a fuel matrix to allow exploration of a wide range of ethanol content (10 to 30 vol. %), RON (91 to 102), and sensitivity (S=RON-MON) (6 to 7 and 10 to 12) [22]. Further studies with this AVFL-20 fuel set have been conducted as part of the AVFL-30/31 project. The objective of this project is to evaluate combustion properties of the AVFL-20 test fuel set using a laboratory ignition characterization method to develop correlations between fuel properties, composition, and autoignition characteristics [22]. The CRC shared the fuel set with NREL for this study to be conducted in NREL's research CVCCs.

After initial testing on the AVFL-20 fuel matrix and working through experiments and equipment setbacks, a different set of fuels as seen in Table 1 was eventually chosen for testing and correlation work instead. The new set of fuels is publicly available and does not require CRC panel permission for publication thus expediting the research process. This fuel set had been used in a previous single cylinder research engine study of knock limited engine performance and particulate matter emissions at NREL, and was designed to vary heat of vaporization (HOV) while keeping RON and S close to constant [23]. The fuel set, with the exception of FACE research gasoline B, consists of simple surrogate blends with up to six different components,

toluene, iso-octane, n-heptane, ethanol, anisole, and p-cresol. Toluene, iso-octane, and n-heptane were blended into Primary Reference Fuels (PRF), Toluene Standardization Fuels (TSF), and Toluene Reference Fuel (TRF) with ethanol, anisole, and p-cresol blended by volume percent as noted (i.e. E25=25 vol. % ethanol) [24, 25]. Before either set of fuels was tested in a CVCC initial screening was done with a fuel from CRC AVFL-24. AVFL-24 developed a set of fuels known as the Fuels for Advanced Combustion Engines (FACE) research gasolines [26]. The FACE gasoline matrix is composed of 10 fuels designed around the four properties of aromatic content, RON, S, and normal-paraffin content [26]. These fuels were designed by the CRC FACE working group, produced by Chevron Philips Chemical Company, and made available in research quantities to enable advanced combustion researchers to make comparison of results from different laboratories of the same, well defined fuel set [26]. Due to the large quantity of these fuels, and the similarities in properties (fuel boiling point, RON) to the AVFL-30 fuels, FACE B was selected from the matrix to conduct initial screening with until the test procedure was vetted. While the original AVFL-20 fuel set consists of gasoline range fuels and would be interesting to analyze due to the available detailed hydrocarbon analysis (DHA), span of RON, span of S, and span of ethanol content, the new fuel set in Table 1 is ultimately a better fit for this study, with more tractable data and simple chemical compositions with which to correlate.

Table 1: Properties of fuel set.

Fuel	Density (g/mL)	RON	S	HOV (kj/kg)
PRF 100	0.692	100	0	303
TSF99.8	0.820	99.8	11.1	390
E25 in TRF88	0.754	101.6	10.7	489
E40 in TRF71	0.770	99.2	12.2	595
E20 + 2% p-cresol in TRF88	0.757	101.1	9.4	472
E20 + 6% anisole in TRF88	0.769	99.9	9.6	472
TRF88	0.742	87	5.2	348

E25 in FACE B	0.720	105.6	11.8	485
FACE B	0.697	95.8	3.4	340

2.2 Ignition Quality Tester

2.2.1 Ignition Quality Tester: Design

The Ignition Quality Tester (IQT) is a CVCC with a spray injection system, intended to measure the combustion propensity of diesel fuels [27, 28, 29, 30]. The Derived Cetane Number (DCN) is the metric for rating the propensity of a fuel to ignite, analogous to how the ON rates the anti-knocking propensity of gasoline fuels [31]. The DCN is mathematically derived, by relating a measured ignition delay time to a cetane number measured by ASTM D613 single cylinder engine-based method [32]. The IQT was designed to run samples of diesel fuels to determine the DCN. The IQT is intended to control chamber temperature, chamber pressure, and air-fuel ratio, while the ignition delay time and the DCN are measured. The IQT holds pressure and temperature constant, while the fuel is injected into the chamber. Under these conditions the fuel will autoignite; the time from start of injection to rapid pressure rise, and thus combustion of the fuel is called the ignition delay (ID) time measurement, and is on the order of ones to hundreds of milliseconds.

The IQT consists of a 3 main components, which can be seen in Figure 5: a heated chamber (1), a fuel injection system (2), and computer (3) that runs the software to control the tests and analyze the results. The fuel injection system consists of a pneumatically driven mechanical fuel pump with a single-hole S-type delayed (inward-opening) pintle nozzle [19,33]. The injector nozzle is cooled by a closed loop liquid-to-air cooling system [34]. The fuel line is pressurized to 50 psi during tests, and 2600±50 psi during injections.

Figure 5: Ignition Quality Tester device, with 3 main components. 1: Combustion chamber. 2: Fuel delivery system. 3: Computer/software controls [34].

A cross section of the combustion chamber can be seen in Figure 6. The combustion chamber is electrically heated, and thermally insulated. The front end houses the fuel injector, and thermocouples to monitor the nozzle temperature. The back of the combustion chamber houses a pressure transducer. The pressure transducer measures the pressure in the chamber during the injection and the combustion event, to obtain data for the pressure profile. A thermocouple referred to as ‘air back temperature’ is in close proximity to the pressure transducer to monitor temperature and pressure in the same area of the chamber. Two other thermocouples measure the internal temperature of the chamber, the average of which is reported in the software. Additionally two other thermocouples monitor the outer surface temperature of the combustion chamber.

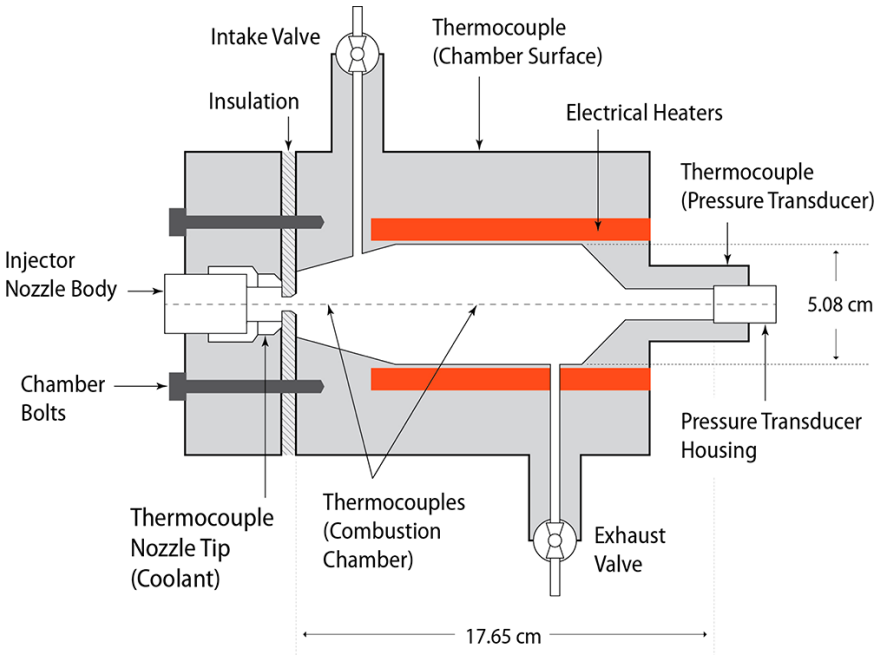

Figure 6: Cross section schematic of the IQT combustion chamber [19].

The software enables the user to control the test, and collects data from the pressure transducer, chamber thermocouples, and needle lift of the injector. While the test is being conducted plots are updated in real time of the needle lift profile and the pressure trace. The needle lift plot essentially shows when and how much fuel is being injected into the chamber. The pressure trace shows the change in chamber pressure over time. The software also processes the data and outputs DCN and ID time measurements. This software defines ID time as the time from the start of injection, to the 'pressure recovery point' (calculates as 138kPa above the initial chamber pressure based on ASTM D6890 conditions) [31, 35]. The software calculates DCN from ID time according to an empirical correlation relating ID time to Cetane Number as measured in the single cylinder cetane rating engine [31, 32].

2.2.2 Ignition Quality Tester: Derived Cetane Number Test

The IQT is designed to run under DCN conditions, using a 20.9% oxygen balance nitrogen diluent at a chamber pressure of 310 psi (~21 bar) [32]. ASTM D6890 requires

verification of IQT calibration each time the instrument is used. The combustion skin temperature is adjusted so that pure n-heptane has a measured ignition delay of 3.78 ± 0.03 milliseconds before DCN measurements begin [32]. The resulting air temperature for DCN conditions is typically around 545°C. Each test consists of 15 pre-injections to stabilize conditions and 32 main (measured) injections. The result is an average ID time that is taken over all 32 main injections. The software calculates DCN from ID according to an empirical correlation relating ID to Cetane Number as measured in the single cylinder cetane rating engine, as show in Figure 7 [31, 32].

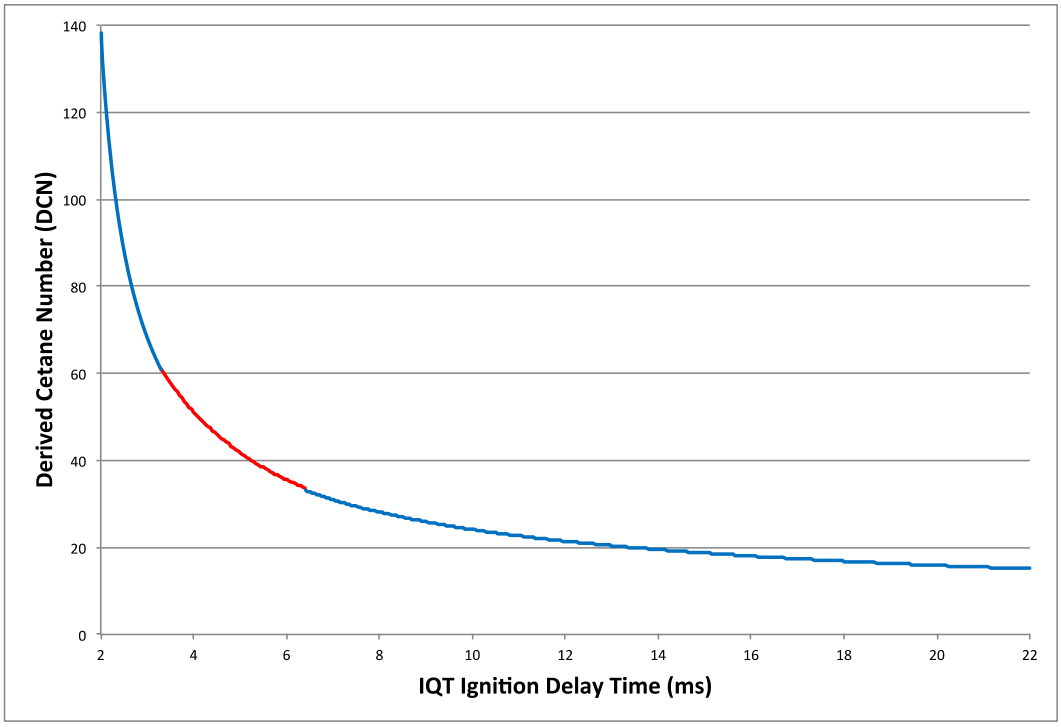

Figure 7: Plot of Derived Cetane Number versus Ignition Delay Time in the IQT. The red portion represents the normal range of DCN values for diesel-like fuels.

2.2.3 Modified Ignition Quality Tester: Temperature Sweep Test

The IQT was originally designed to measure diesel fuels over an ignition delay range from 3.1 ms to 6.5 ms (64 DCN to 33 DCN), and as such the software's definition of ID time, is inaccurate for gasoline range fuels [31]. Many diesel fuels ignite in one stage and have short

ignition delay times, where gasoline fuels can have 2-stage ignition defined by low-temperature heat release (LTHR), and then the main ignition event. NREL developed a LabVIEW-based independent control system to allow for much longer ID measurements and to adjust the definition of start of combustion, for gasoline fuels [32]. With the independently controlled system, ID time is calculated by a user defined fixed pressure point, above the initial chamber pressure, to describe the entire ignition event [32]. Prior research conducted by NREL focused on the ability to produce IQT data suitable for kinetic mechanism development feedback, as the ID time from the IQT inherently includes both physical ID effects (spray breakup and evaporation) as well as chemical kinetic ID effects [32,33].

Another unique capability of the NREL's modified IQT is to test fuels across a temperature range, as opposed to a single temperature condition in the DCN tests [32, 35]. For this test the IQT chamber is pressurized to a user specified pressure, typically 10, 20, or 30 bar using 20.9% oxygen in nitrogen balance and heated to approximately 730 °C, as measured by the air back thermocouple in the IQT. The amount of fuel injected is adjusted for each fuel to maintain a fuel-air equivalence ratio (ϕ) of 1 at an air back temperature of 700 °C, charged to 145 psi. Once the test is started, the heaters are turned off to let the temperature drop gradually throughout the test. This test allows for the collection of chemical kinetic combustion data over a wide range of temperatures. Five pre-injections are done at the beginning of the test. The main injections are allowed to continue until the ignition delay becomes >400 ms or the air back thermocouple temperature reaches approximately 375 °C. The temperature drop from ~700 °C to ~ 375 °C takes around two hours. Main injections are performed about every 30 seconds. The mass of fuel injected is kept constant through this test, however the number of moles in the chamber is increasing as the temperature drops by the ideal gas law as pressure and volume

remain constant, thus creating leaner conditions as the test progresses to low temperatures. The mass of fuel injected is adjusted mechanically by inserting varying thickness of shims that effectively changes the pneumatic pressure intensifier stroke. The process of changing shim is extensive and requires the user to take apart the fuel reservoir while testing is stopped. Thus it is not possible to adjust the mass of fuel injected during the test.

2.2.4 Ignition Quality Tester: FACE B Trials

The IQT has been used to conduct temperature sweep tests in previous studies on gasoline range fuels. However, most studies have been centered on PRFs or surrogate gasoline blends, consisting of a few components. The lower boiling point of gasoline blends compared to PRFs and diesel fuels poses a challenge to conducting tests in the IQT. Since fuel in the IQT reservoir, transfer lines, and injector nozzle is pressurize at 50 psi before the pressure is ramped up to ~2600 psi for an injection event, lower boiling point fuel fractions can begin to boil within the IQT fuel system at high chamber temperatures (and pressures) that increase the heat transfer to the injector tip. Previously gasoline surrogate blends that encounter boiling issues have been run in the IQT at NREL. To remedy this issue in the past, the bleed off valve (A) as seen in Figure 8, which is located near the injector nozzle was opened and closed right before the injection. This expelled the vaporized fuel from the line, and replenished it with un-boiled fuel. For previous gasoline surrogate blends this was successful in maintaining the fuel-air equivalence ratio throughout the test for the surrogate blends, which can be confirmed by the needle lift profile. The area under the needle lift profile represents the mass of fuel injected, thus when significant changes occur in the profile it is clear the global air fuel ratio is changing.

The AVFL-20 gasoline blends, as well as FACE B, have low initial boiling points, thus fuel boiling was expected during these tests in the IQT. The boiling would negatively affect the

amount of fuel injected during the temperature sweep test, and result in an inconsistent fuel-air ratio. To accommodate the high quantity of AVFL-20 samples (19 different fuel blends) to be tested in the IQT (57 different tests at 2 hours each) a few options were explored to modify the IQT and automate a solution to prevent fuel boiling. The first option is to chill the sample and the second is to automate the opening and closing of the bleed off valve. Unfortunately the fuel cannot be chilled in the nozzle where the boiling is occuring. The nozzle is in close proximity to the combustion chamber and to sufficiently cool the fuel, would compromise the constant chamber temperature requirement. Thus to accommodate the high quantity of gasoline range AVFL-20 fuels it was decided to design and install an automated bleed off valve.

Figure 8: Image of the IQT device. Of importance is the circled bleed off valve [34].

The ASCO EF8262H006V solenoid valve was chosen for this application. It is rated for use with fuel and oil, and can withstand pressures of 120 psi. The valve would be situated in line with the original system, and replace the original bleed off valve. This set up can be seen in Figure 9. After procuring the parts, installing the system, and coding the controls, by NREL colleagues Jon Luecke, Riley Abel, and Jon Burton. Tests with FACE B were attempted. This test revealed that the new automated system did not work. In fact the automated system was not

injecting any fuel into the chamber. A few hypotheses were formulated to explain the lack of injection. One hypothesis is that the seal of the solenoid valve is leaking during the injection event. The pressure in the fuel line increases sharply ~2600 psi when the fuel is injected, this surpasses the 120 psi the valve is rated for, thus causing fuel to bypass the valve and preventing the pressure in the line from reaching the value needed for injection. The other hypothesis is that the volume added to the fuel line with the solenoid valve configuration, could be too large, thus preventing the pressure from being reached and the injection from occurring. Unfortunately it would take time and resources to attempt to fix the solenoid valve system, thus moving forward the tests were conducted while manually purging the bleed off valve.

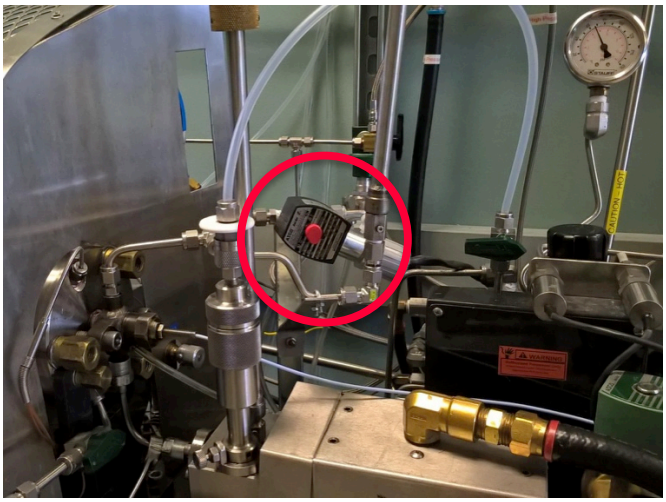

Figure 9: Image of the IQT with the automated solenoid valve replacing the typical manual bleed off valve.

After some initial testing with FACE B in the IQT, which has a similar boiling point to the AVFL-20 samples, it was discovered that the sample was still boiling regardless of the fuel bleed off. As the test continued the needle lift profile of the injected fuel was consistently decreasing. Additionally the fuel reservoir needed to be refueled partway during the tests, as well as opened and evacuated at the end of the test. Each time the fuel reservoir was opened fuel boiling was visibly observable. This study was continued and temperature sweeps were

conducted at 5, 10 and 15 bar, changing the fuel reservoir often and bleeding the fuel off after each injection to try to mitigate the boiling issues. Figure 10 shows the temperature sweep data for FACE B at 15 bar, it is clear the ID time is very inconsistent due to fuel boiling, especially at lower temperatures. The test starts at 725 °C and drops steadily throughout the test until around 400 °C. At the lower temperatures the fuel has been heated in the reservoir for the duration of the high temperature tests and thus sees more extreme vaporization affecting the fuel-air ratio. It is clear from this data that the AVFL-20 fuel set cannot be consistently run in the IQT per the original plan.

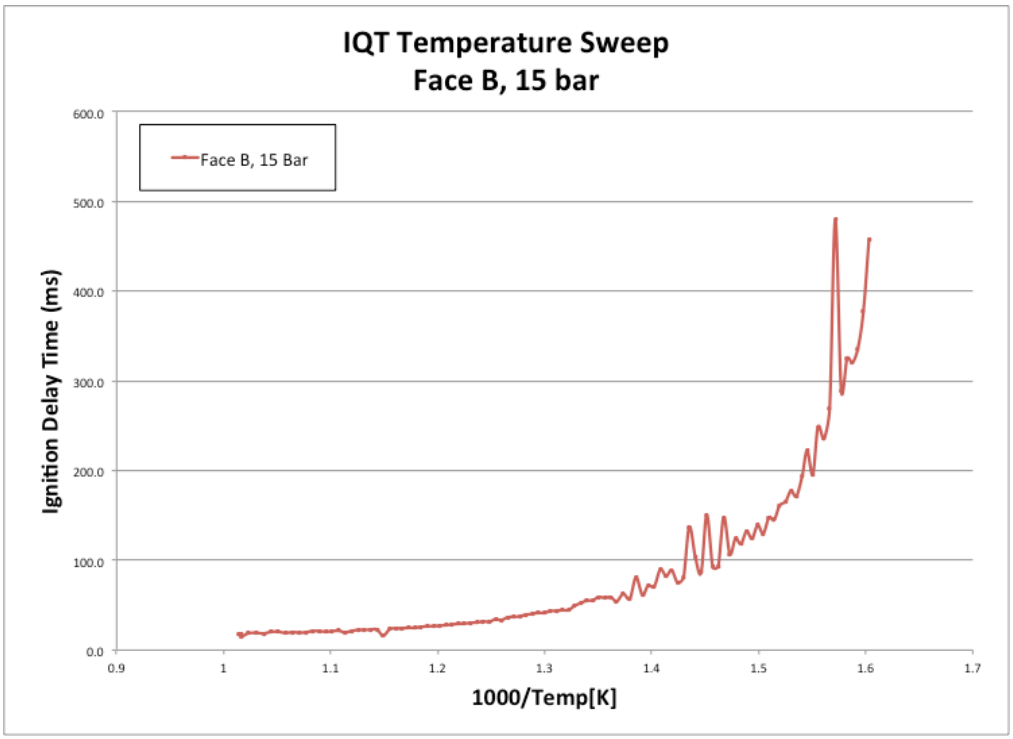

Figure 10: Inverse temperature versus ID time for FACE B conducted at 15 bar in the IQT.

2.3 Advanced Fuel Ignition Delay Analyzer

2.3.1 Advanced Fuel Ignition Delay Analyzer: Introduction

Upon completion of the FACE B trials in the IQT, the possibility of running the tests in NREL's new research CVCC the Advanced Fuel Ignition Delay Analyzer (AFIDA) was

explored [36]. In June 2016, NREL acquired the AFIDA 2805, a constant volume research combustion chamber indented to measure Generic Cetane Number (G-CN, similar to DCN) of diesel fuels, in addition to custom parametric studies of ignition delay. This was around the time the FACE B trial experiments were being conducted in the IQT. The AFIDA is ideal for this study since the fuel line is highly pressurized to support a common-rail type piezoelectric fuel injector, which also avoids fuel boiling. The AFIDA was designed for the fully automated determination of the ignition behavior, G-CN and analysis of exhaust gases of diesel fuels [37]. The advantages of testing in the AFIDA include: automated design with a 16-place autosampling carousel, high user control of test parameters, no temperature tuning required for standardized cetane number tests (unlike other constant volume devices), high repeatability, high fuel line pressure using a high-performance liquid chromatography (HPLC) pump, and use of a common rail type piezoelectric fuel injector. The use of the common rail type piezoelectric fuel injector significantly reduces the spray physics dominated portion of overall ID time, allowing greater focus on the chemical kinetics dominated portion of ID. The experiments were not originally planned in the AFIDA, since the device is new both on the market and to NREL, making extensive fuel mapping and device characterization necessary before experiments could be conducted. Still, the AFIDA is ideal for this study since the fuel line can be highly pressurized, up to 2100 bar to avoid fuel boiling. For this reason as well as more precise temperature control, the AFIDA, was chosen to complete the study. NREL's AFIDA is one of four units custom built for non-standard (G-CN), flexible operation, and is currently the only such AFIDA located outside of Europe.

2.3.2 Advanced Fuel Ignition Delay Analyzer: Design

The AFIDA is a fully automated ignition delay analyzer. The device consists of the combustion chamber, fuel delivery system, and computer software that controls the device. The device set up can be seen in Figure 11. Figure 12 shows a schematic of the main components in the AFIDA. The AFIDA has a maximum chamber temperature of 1000 K, a maximum initial charge pressure of 50 bar, and a maximum line pressure of 1200 bar. The fuel delivery system consists of a fully automated sample selection carousel, with a 16 sample capacity at 40 mL per sample. The fuel carousel is capable of heating the fuels, enabling testing of fuels that are solid at room temperature. A high-pressure pump draws the fuel out of the vial and pressurizes it into the curing tube. [37] A Bosch piezoelectric diesel injector injects a precisely defined amount of fuel into the electrically heated and pressurized combustion chamber. Under these conditions the fuel will autoignite, causing a pressure rise in the chamber. A dynamic pressure transducer and multiple thermocouples closely monitor the combustion chamber, the orientation of which can be seen in Figure 12. The AFIDA has very accurate temperature control, and high repeatability compared to the IQT. To achieve temperature conditions in the IQT the temperature dithers around the set point; the heaters are constantly cycling off and on causing the temperature to bouncing above and below the set point. This method is not ideal; as ID time is highly temperature dependent. In contrast the AFIDA has very precise temperature control. The AFIDA ramps the temperature slightly above the set point and then runs the test when the temperature decreases to the set point. The fuel does not inject until the temperature condition is met, even if that means repeating this process. Additionally the AFIDA performs 12 injection cycles at each test condition, with pressure traces evaluated for repeatability.

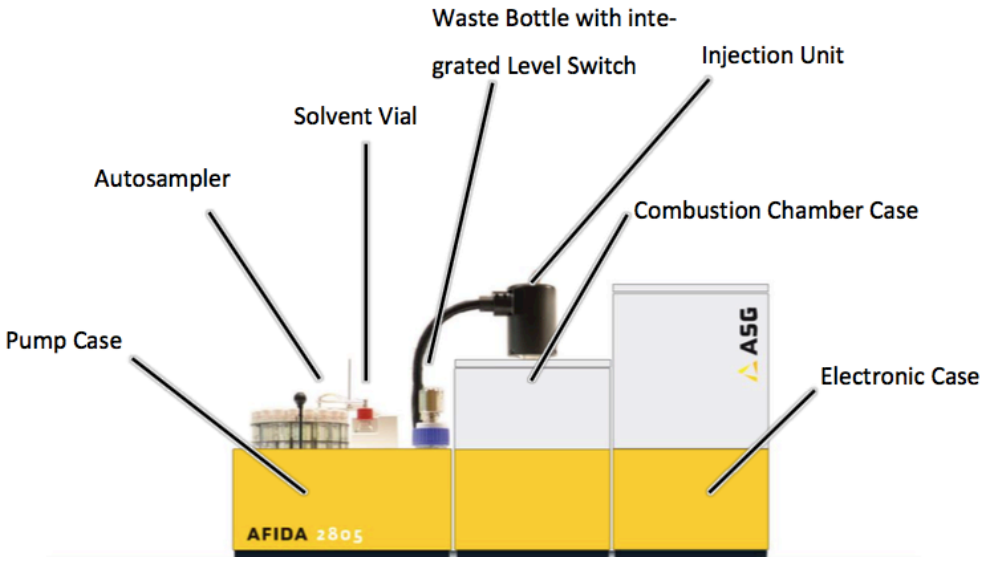

Figure 11: Image of the AFIDA 2805, with the main components identified [37].

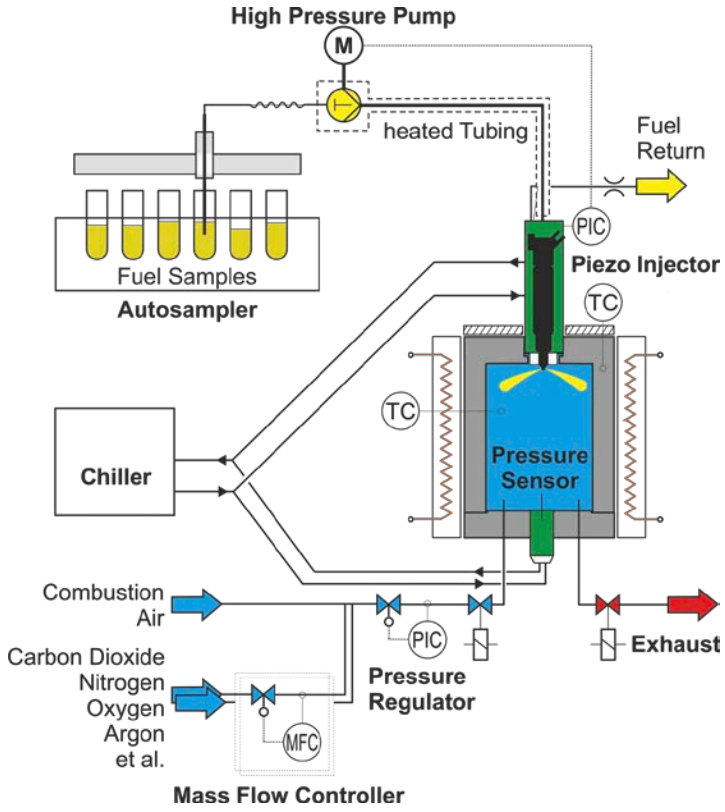

Figure 12: Schematic of the AFIDA, highlighting inputs for the test process with combustion air and fuel input noted, along with the exhaust from the chamber after the test had concluded [37].

2.3.3 Advanced Fuel Ignition Delay Analyzer: Sample Data

The AFIDA performs 12 injections at each temperature and pressure condition, Figure 13 shows the pressure trace for each injection as well as the average for FACE B at 16 bar and 450°C. These data illustrate the repeatability of experiments in the AFIDA. Figure 14 shows what the average pressure trace data at each temperature condition looks like across the entire temperature sweep. LTHR can be seen from 525 °C to 400 °C.

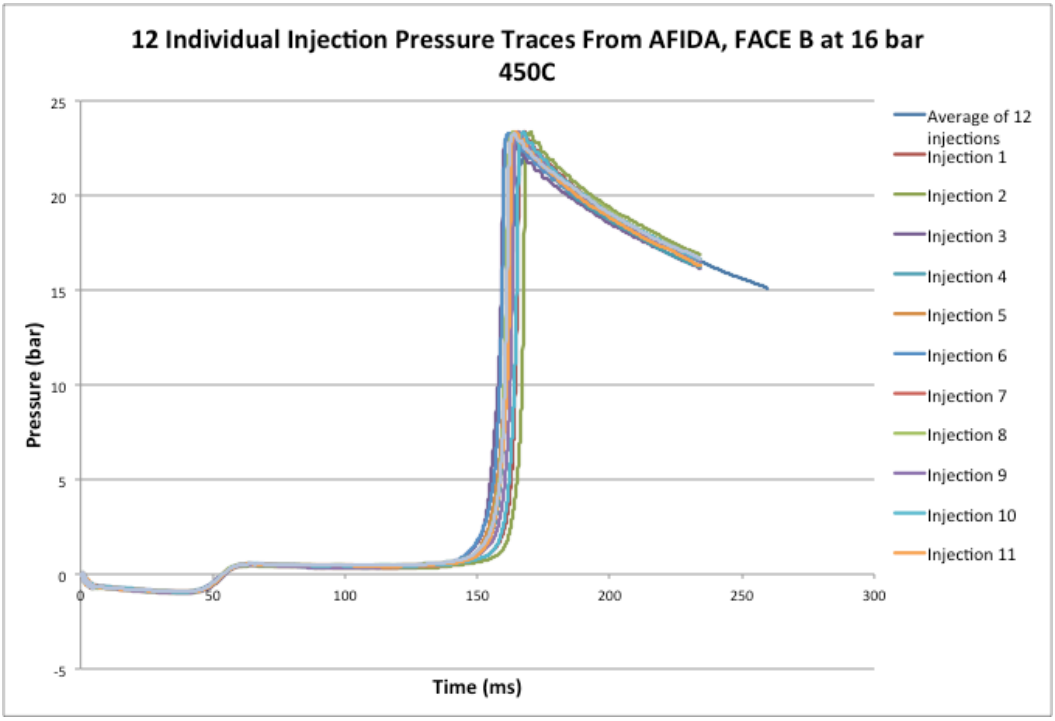

Figure 13: 12 individual pressure traces as well as the average from the AFIDA of FACE B at 16 bar and 450°C.

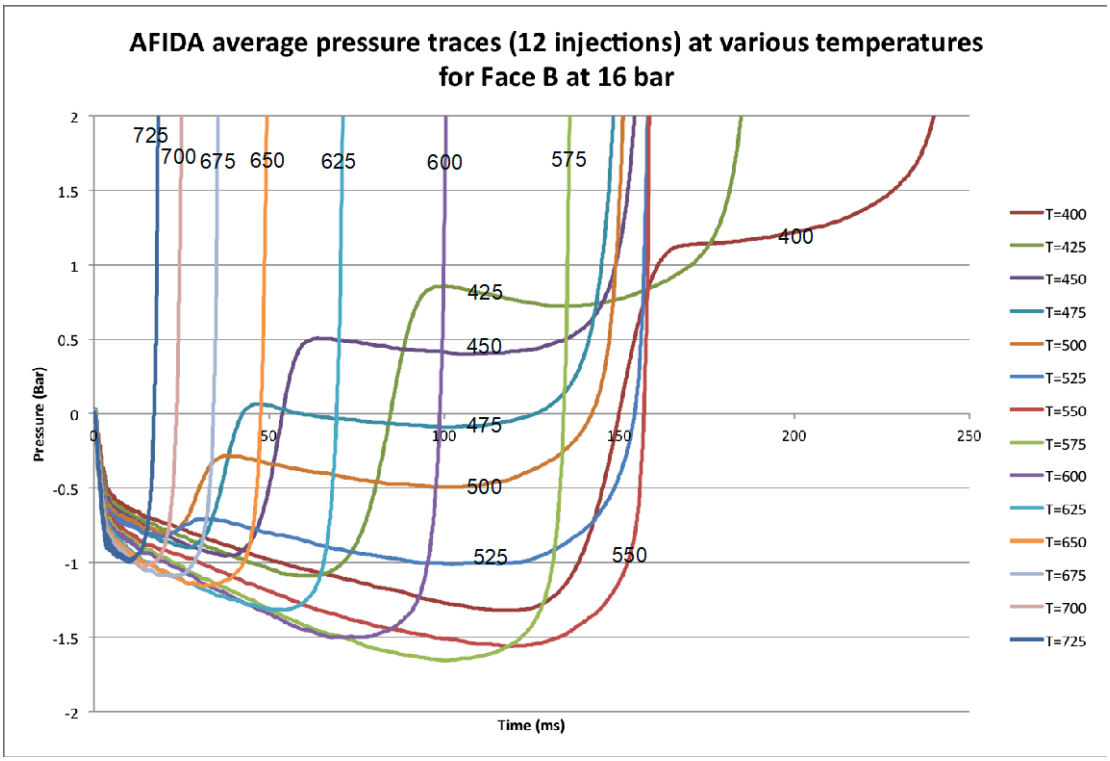

Figure 14: Average pressure trace for each temperature is plotted for FACE B at 16 bar.

2.3.4 Advanced Fuel Ignition Delay Analyzer: ϕ Calculations

In order to run temperature sweeps in the AFIDA, as opposed to the G-CN tests that it is designed to run, extensive characterization was required. Jon Luecke at NREL ran experiments to determine the moles of fuel injected as the injection duration changed, as well as moles of air filling the chamber at different temperature and pressure conditions. These experiments were necessary to determine the fuel-air equivalence ratio of the experiments to be conducted in the AFIDA. The moles of air in the chamber cannot be calculated since the temperature in the chamber is unknown. While thermocouples monitor the chamber temperature, it is only the temperature at one point and does not account for the temperature gradients from the wall to the center of the chamber. The average temperature of the chamber is unknown, thus to determine the moles of air in the chamber experimentally the chamber was filled at 5, 10, and 20 bar pressure conditions at 25 °C, and 400-700 °C in 100 °C increments. Once the chamber stabilized

it was exhausted in an evacuated sampling canister. The canister volume is known, and the pressure was read with a high accuracy pressure gauge. The volume of the canister (about 95% of total volume) was added to the 5% that was left in the chamber (less accurate). The moles of air are calculated with the ideal gas law at room temperature for the canister and at chamber temperature for the 5% remaining volume. While using the temperature of the chamber causes errors, the canister method is highly accurate and accounts for 95% of the total measurement. To determine O_2 in the chamber at various pressures, the ideal gas law was used to determine the theoretical moles of air in the chamber. The average theoretical temperature for the experimental number of moles of air in the chamber is taken over the range of pressures 6-26 bar at 5 bar increments. This average theoretical temperature is then linearly correlated to the actual chamber temperature. The linear fit is then used to determine the fuel-air equivalence ratio of a given fuel at a specific temperature pressure condition. The number of moles of O_2 is then calculated using the ideal gas law, but instead of chamber temperature, the linear fit equation is used. To calculate the moles of fuel injected, experiments were conducted at different injection durations, and the mass of 60 injections of certification diesel fuel were measured experimentally with 1600 bar fuel pressure at 0-4000 μs in 500 μs increments. The fuel was injected into a tube that was then removed from the injector and weighed. There are some errors associated with this method as fuels have different properties that effect the injection, however testing with a more volatile fuel would result in errors due to fuel evaporation and loss of mass in transferring the tube from the nozzle to the scale. This test was conducted 3 different times at each injection duration condition. The density of the fuel is used to determine the volume of fuel injected. The results were plotted and a correlation was established between the injection duration and the volume of fuel injected. One of the significant challenges of using the AFIDA is attempting to inject stoichiometric

mixtures. The AFIDA was primarily designed for G-CN measurements, and intended for diesel range fuels where the global equivalence ratio would be lean. To study gasoline range fuels, where stoichiometric or slightly lean conditions are of interest, the fuel injector piezo crystal must be energized for long periods of time to inject more fuel. However, fuel pressure drops during injection, as the fuel line volume is small and the HPLC fuel pump cannot quickly ramp up pressure during an injection event to maintain pressure. NREL is working on modifying the AFIDA fuel system for these types of studies, but the work is still early stage. When using an optional fuel line with higher internal volume (to maintain a higher pressurized reservoir to reduce pressure drop during injection) instead of the standard fuel line, the maximum injection duration achievable is 2500 μs, after that the percent error between the measured volume of fuel injected and the curved fit used to predict the volume of fuel injected becomes too high. Between 2500 μs and 3000 μs, the error jumps from -0.15% to -5.23%. With these experiential results the fuel-air equivalence ratio can be determined at each temperature and pressure condition given the fuel injection duration. The fuel-air equivalence ratio is calculated per Equation 2.1, as the ratio of moles of fuel to moles of oxidizer actual, to moles of fuel to moles of oxidizer at stoichiometric conditions.

$$\boldsymbol{\phi} = \frac{\left(\mathbf{n_{fuel}}/\mathbf{n_{ox}}\right)_{\mathbf{actual}}}{\left(\mathbf{n_{fuel}}/\mathbf{n_{ox}}\right)_{\mathbf{stoich}}} \tag{2.1}$$

A ϕ of 1 indicates that there is the exact amount of oxygen needed to react with the fuel, greater than 1 indicates there is excess fuel after the reaction and is referred to as rich, less than 1 indicates there is excess air after the reaction and is referred to as lean.

2.3.5 Advanced Fuel Ignition Delay Analyzer: Iso-octane And N-heptane Mapping

Iso-octane (RON 100) and n-heptane (RON 0) were mapped in the AFIDA by Jon Luecke to examine the differences in ID time as percent oxygen balance in nitrogen diluent, and

pressure varied. The AFIDA chamber volume, 0.4 L, is greater than the 0.2 L volume of the IQT, thus a lower oxygen concentration in nitrogen balance was required to obtain ϕ of 1 (calculated per the method in Section 2.2.4), since the AFIDA is fuel limited to maintain stoichiometry. Tests were conducted at with 21%, 10%, and 3% O_2. Figure 15 shows a comparison of iso-octane ran at 3% O_2, and 10% O_2, at 11 bar and ϕ of 1. Data were collected from 725 °C - 475 °C. Some data are missing due to insufficient data collection, or exceedingly high ID times. From these data it is clear that the ignition delay times are too long and not relevant to typical engine operating space. Moreover the ID time is in the thousands of ms at a temperature of 475 °C, as further temperature sweeps will test down to 425 °C this will only exacerbate the issue. For this reason, further tests will use 21% O_2 and lower ϕ values, to obtain quicker and more relevant ID times. Additionally it was discovered that the AFIDA test sequence software cycles the chiller off around 650 ms after the fuel has been injected. This causes a rise in the pressure trace, and then a drop when the chiller comes back on ~100ms later. This interference with the data can be seen in Figure 16. As a result any ignition delay time after 650 ms is not accurate. While ID times past 650 ms are not engine-relevant, this physical issue places an upper limit on the ID time data.

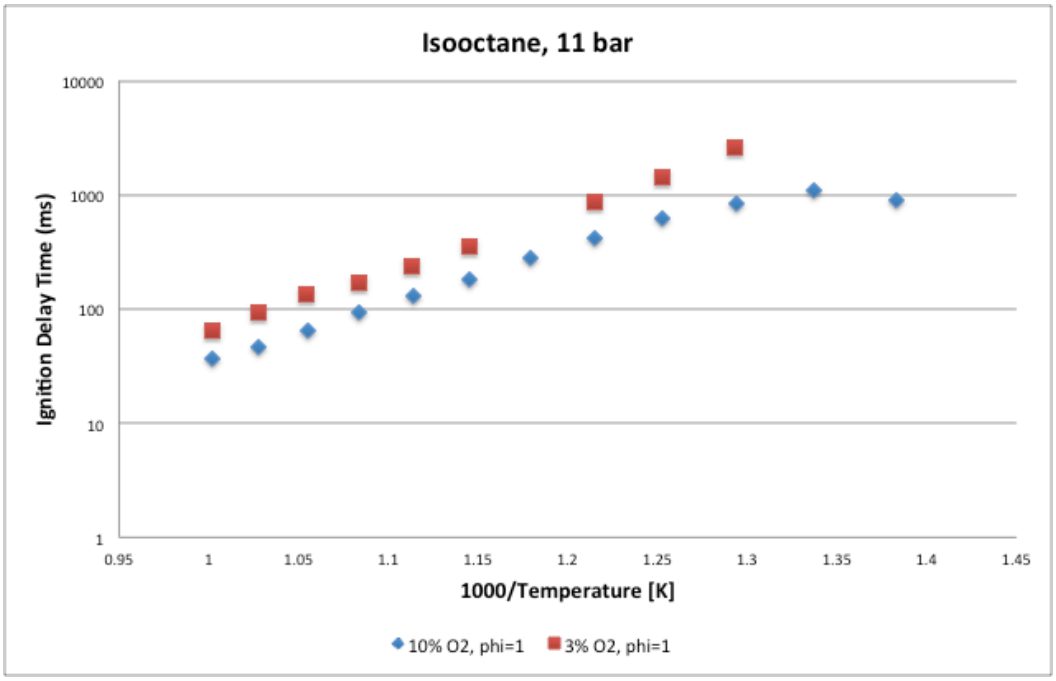

Figure 15: Temperature versus ID time for iso-octane, at 11 bar and a $\phi = 1$, for 3% and 10% O_2.

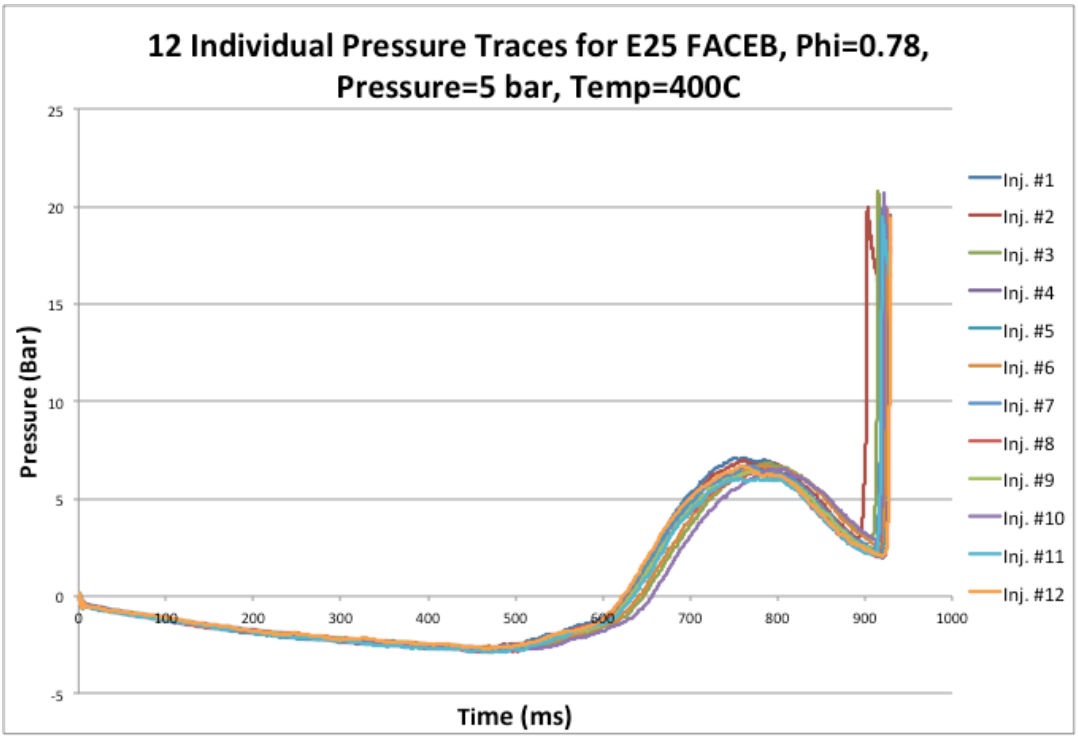

Figure 16: Pressure trace (pressure versus time) for FACE B at 400 °C and 5 bar. The data show the pressure rise and then drop caused by the cycling off, then on, of the chiller.

2.3.6 Advanced Fuel Ignition Delay Analyzer: Gasoline in Piezoelectric Diesel Injector

While the AFIDA was designed to test diesel fuels, NREL intended to study both diesel and gasoline range fuels in the device. The AFIDA uses a commercially available Bosch diesel piezoelectric injector (a common production part used in the Audi/VW/Porsche 3.0L V6 diesel). A schematic of the injector can be seen in Figure 17. The nozzle control is opened and closed by the piezoelectric stack. The stack is housed in the injector, and expands and contracts with an electronic signal. This technology enables a fast response time with multiple injection events per engine cycle. However, the force and displacement from the piezo crystal stack is not great enough to open the needle. To generate the necessary force the piezo stack is coupled with a hydraulic amplification system [38]. The piezo stack exerts a force on a smaller fuel chamber within the injector, and the pressure differential causes the pintle to open.

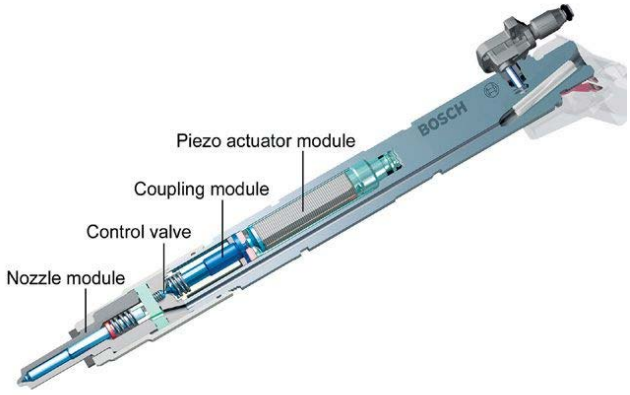

Figure 17: Schematic of Bosch piezoelectric injector. The device consists of a piezo actuator, a coupling module to amplify the force, a control valve, and the nozzle [38].

The function of the injector relies on the fuel that is to be injected. When tests were conducted with iso-octane and n-heptane, leakage back from injector bypass into the AFIDA waste reservoir was observed. While the leak was not significant, even a small amount of internal leakage in the control valve would affect the mass of fuel injected into the chamber. At first the cause of this leak was thought to be a broken backpressure regulator on the AFIDA.

However after this part was replaced leaking continued with lower viscosity fuels. While some injectors functioned better than others, likely due to differences in manufacturing tolerances, which only become apparent with less viscous fuels compared to diesel fuels. Discussions with colleagues at Argonne National Laboratory working on gasoline compression ignition engine research (using common rail injectors) showed that they had to add a diesel fuel lubricity additive to prevent wear on the high pressure pump with low lubricity gasoline range fuels [39]. While the issue with the AFIDA was not the same, discussions with the AFIDA developer, Philipp Seidenspinner and ASG Analytik-Service Gesellschaft mbH, as well as engineers at Bosch, revealed that a related issue could be causing the AFIDA issue, where the control valve within the piezo injector may be sticking. Without the lubricity of diesel fuel, the control valve was essentially sticking; this caused the control valve to not open as desired, to stick open, or to not open at all. As a result 1500 ppm of Infineum R655 lubricant additive is mixed into every low lubricity (gasoline range) sample. While this treat rate may be higher than most related applications, it is not common to run gasoline fuels though diesel injectors. Additionally the additive accounts for less than 0.15% of the fuel composition. This is a conservative treat rate, to avoid complications with the injector. Determining the minimum treat rate that can be used is ongoing at NREL, but outside the scope of this project. The acid-based Infineum R655 lubricity additive is expected to have little effect on ignition delay time; even so it is likely affecting all fuels equally in this study.

2.4 Fuel Set Composition and Preparation

This fuel set had been utilized in previous single cylinder research studies of knock limited engine performance and particulate matter emissions at NREL, and was designed to vary HOV while keeping RON and S close to constant. The basis of the fuel set is renewable

oxygenates blended into gasoline surrogate BOBs, with the exception of FACE B [23]. The gasoline BOB surrogates can be seen in Table 2 and are mixtures of toluene, iso-octane, and n-heptane. The entire fuel set can be seen in Table 3 with the volume percent of each chemical component in the fuel. The majority of these fuels were blended in large batches as part of that study. The fuels were splash blended which refers to the process of blending the fuel and oxygenates by pouring, the sample is not actively mixed. E20 + 6% anisole in TRF88, as well as E25 in TRF88 were blended in small batches by adding the desired oxygenates to premixed TRF88 per the previous study.

Table 2: Surrogate BOB, standardization fuel compositions from detailed hydrocarbon analysis by ASTM D6729, before oxygenate blending [23].

Fuel	toluene (vol. %)	iso-octane (vol. %)	n-heptane (vol. %)
TRF88 (nominally 30 vol. % toluene in PRF70)	28.3	50.4	21.2
TRF71 (nominally 40 vol. % toluene in PRF32)	41.2	18.5	40.3
TSF99.8 (nominally 74 vol. % toluene in PRF38.5)	73.6	10.3	16.1

Table 3: Fuel test set by percent volume of each component in the fuel.

Fuel	toluene (% by vol.)	iso-octane (% by vol.)	n-heptane (% by vol.)	ethanol (% by vol.)	anisole (% by vol.)	p-cresol (% by vol.)	FACE B (% by vol.)
PRF100	0	100	0	0	0	0	0
TSF99.8	74	10	16	0	0	0	0
E25 in TRF88	22.5	36.75	15.75	25	0	0	0
E40 in TRF71	24	11.52	24.48	40	0	0	0
E20 + 2% p-cresol in TRF88	23.4	38.22	16.38	20	0	2	0
E20 + 6% anisole in TRF88	22.2	36.26	15.54	20	6	0	0
TRF88	30	49	21	0	0	0	0
E25 in FACE B	0	0	0	25	0	0	75
FACE B	0	0	0	0	0	0	100

Before the samples were tested in the AFIDA, they were transferred to 40 mL vials, which are compatible with the AFIDA autosampler carousel. During this process 59μL of lubricant Infineum R655 was added to each 40ml of fuel, to achieve 1500 ppm of the additive. The vials were gently rotated to achieve adequate mixing.

2.5 Fuel Set Test Preparation

2.5.1 Fuel Set: Weight Percent Carbon, Hydrogen, And Oxygen Calculations

Before tests could be conducted the ϕ of each fuel needs to be determined per the method outlines in Section 2.3.4. The test conditions are necessary to calculate the ϕ at each set of test parameters. Test parameters were planned for 725 °C – 425 °C in 25 °C increments at 5, 10, 20, and 30 bar. The weight percent carbon (C), hydrogen (H) and oxygen (O) in each fuel as well as the density needed to be calculated from the known volume percent of each component in the fuel. The fuel density is calculated as seen in Equation 2.2, which is the sum of the product of percent volume of each component to the density of each component.

$$\rho_{avg} = \sum_i \rho_i * \%\ \mathrm{vol}_i \tag{2.2}$$

The weight percent C, H, and O are calculated from the percent volume, known densities, molecular mass, and chemical equation of each component. The mass fraction of C, H and O in a given compound is calculated by Equation 2.3, where $n_{C,H,O}$ is the number of moles of C H or O in the compound given by the chemical equation, $ma_{C,H,O}$ is the atomic mass of C, H or O respectively, and $MW_{chemical}$ is the molecular weight of the chemical. This calculation is implemented for each chemical component in the surrogate blend.

$$\text{mass fraction} = \frac{n_{C,H,O} * ma_{C,H,O}}{MW_{chemical}} \tag{2.3}$$

Next, the mass of each chemical in a 100 mL sample is calculated. Equation (2.4) calculates the mass in a 100 mL sample, where $\rho_{chemical}$ is the density of the chemical and % vol is the percent volume of the chemical in the fuel mixture.

$$\text{mass} = \rho_{\text{chemical}} * \%\ \text{vol}_{\text{chemical}} * 100 \tag{2.4}$$

The mass fraction of each chemical in the total fuel mixture is calculated by taking the grams of each chemical in a 100 mL sample, over the sum of the mass of each chemical in a 100 mL sample. Finally the mass fraction of C, H and O in each chemical is calculated, by Equation (2.5) where the mass fraction of each chemical is multiplied by the mass fraction of C, H, and O respectively. To find the total mass fraction of C, H, and O in the fuel blend, the mass fraction of C, H, and O of each chemical component is added. From the total C, H, and O mass fraction and the average density, the ϕ can be calculated for each fuel. The total mass fraction of C, H, and O for each fuel can be seen in Table 4.

$$\text{m fraction}_{\text{C,H,O}} = \text{m fraction}_{\text{Chemical}} * \text{m fraction}_{\text{C,H,O in fuel}} \tag{2.5}$$

Table 4: Calculated mass fraction of C, H, O, and density of each fuel.

Fuel	Weight % C	Weight % H	Weight % O	Density (g/ml)
PRF 100 (iso-octane)	84.09	15.91	0.00	0.692
TSF99.8 (74% toluene)	89.65	10.35	0.00	0.820
E25 in TRF88 (23% toluene)	77.54	13.37	9.09	0.754
E40 in TRF71 (24% toluene)	72.87	12.89	14.24	0.770
E20 + 2% p-cresol in TRF88	79.13	13.22	7.64	0.757
E20 + 6% anisole in TRF88	78.77	12.90	8.32	0.769
TRF88	86.55	13.45	0.00	0.742
E25 FACE B	75.58	14.91	9.52	0.720
FACE B	84.43	15.57	0.00	0.697

Ideally global ϕ would be 1, since it is relevant to stoichiometric SI engine operating conditions. However it was determined with tests in Sections 2.3.4 and 2.3.5 that the upper limit on ϕ is imposed by the maximum amount of fuel that can be injected (2500 μs) and the O_2 concentration required to get relevant ignition delay times (21% O_2). To determine the highest ϕ that could be achieved for the test set, the ϕ of each fuel was calculated at the maximum duration (2500 μs) and 21% O_2. E40 in TRF71 was the fuel with the lowest ϕ, thus each fuel was recalculated with lower durations in order to match the ϕ of TRF71, and attain constant ϕ conditions between fuels. Ideally ϕ would be constant for every test condition, however this was not possible with the AFIDA in its current state. Instead target ϕ is held constant at each pressure among the set of 9 fuels. Target ϕ refers to the ϕ at the highest temperature condition for each pressure. ϕ is not consistent through the tests, as the injection duration is held constant and thus the ϕ is allowed to drift lean as the chamber temperature decreases (and O_2 + N_2 mass, therefore, increases). The change in ϕ as temperature drops can be seen in Table 5. The main reason for allowing the ϕ to drift lean is to be able to run the highest ϕs possible. It is worth noting that while the AFIDA has a high pressure fuel injection system that promotes better mixing than the IQT, it is still expected that Φ gradients exist within the chamber at these timescales and reported Φ is an assumed global average. NREL is working to characterize and model the spray process with Φ and T gradients, but that is ongoing and outside the scope of this thesis project. Past research with the IQT indicates a quasi-homogenous state develops with locally rich gradients where ignition originates, and similar processes likely develop within the AFIDA [33, 35, 40].

Table 5: Calculated ϕ at each temperature and pressure condition.

Chamber Temperature (°C)	ϕ at 5 bar	ϕ at 10 bar	ϕ at 20 bar	ϕ at 30 bar
725	1.04	0.57	0.39	0.20
700	1.02	0.56	0.29	0.20

675	1.00	0.55	0.29	0.19
650	0.98	0.54	0.28	0.19
625	0.96	0.52	0.27	0.19
600	0.94	0.51	0.27	0.18
575	0.92	0.50	0.26	0.18
550	0.90	0.49	0.26	0.17
525	0.88	0.48	0.25	0.17
500	0.86	0.47	0.25	0.17
475	0.84	0.46	0.24	0.16
450	0.82	0.45	0.23	0.16
425	0.80	0.44	0.23	0.15

Additionally a previous study was conducted in the IQT, which experimented with letting the ϕ drift lean at low temperatures, versus changing the amount of fuel injected in steps to hold ϕ near constant (a difficult process requiring manual measurement and adjustment of metal shims to change fuel system pneumatic intensifier stroke) [19]. The results of this study can be seen in Figure 18 .The results of the two tests are very similar even when one test has a constant ϕ (black diamond) and the other has a variance of 0.2 ϕ (open square). From this previous study in the IQT it was determined that allowing the ϕ to drift lean in the AFIDA would have little impact on ID time, compared to temperature or pressure. To hold ϕ constant in the AFIDA, the fuel set would need to be run at 0.20 if the ϕ was allowed to drift lean throughout the test, or 0.15 if it were not. Even if running at an incredibly lean 0.15 ϕ were desirable, it would not be possible to collect data at this point, across every pressure and temperature. For some fuels the ID was already approaching or surpassing the cut off point of 650 ms. If less fuel was injected in order to hold ϕ constant, the ID times would be to long to measure for most of the desired temperature sweep conditions.

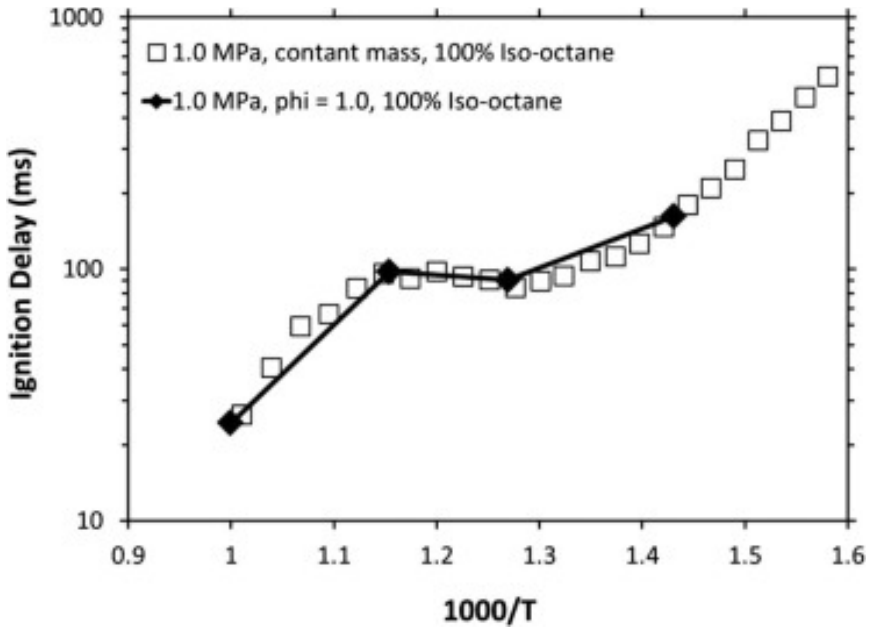

Figure 18: Temperature sweeps at 1.0 MPa. 90 vol.% iso-octane / 10 vol.% ethanol, constant equivalence ratio $\phi = 1.0$ (black diamond), constant mass $0.7 \leq \phi \leq 1.0$ (open square) [19].

2.5.2 Fuel Set: Experimentally And Analytically Determined Properties

For each fuel detailed hydrocarbon analysis (DHA), RON and HOV data were available from a previous study [23]. Neat TRF88 was not originally part of the fuel set, thus data were calculated. For the core fuel set, RON and MON where measured by ASTM D2699 and D2700, respectively [9,10], under subcontract at Southwest Research Institute. HOV was based on chromatographic analysis using ASTM D6729 [41, 42]. For TRF88, the RON was measured according to ASTM D2699 [9]. However, there was no measured value for MON, which is necessary to calculate S. Instead S was estimated based on the method outlined in Morgan et al. [43]. Sensitivity can be predicted from the RON, and percent toluene in the sample. HOV of TRF 88 is calculated based on the DHA data with the help of Earl Christensen at NREL. The properties, experimentally and analytically determined or calculated, of the fuel set can be seen in Table 6.

Table 6: Fuel properties, RON, S, and HOV.

Fuel	RON	S	HOV
PRF 100 (iso-octane)	100.0	0.0	303
TSF99.8 (74% toluene)	99.8	11.1	390
E25 in TRF88 (23% toluene)	101.6	10.7	489
E40 in TRF71 (24% toluene)	99.2	12.2	595
E20 + 2% p-cresol in TRF88	101.1	9.4	472
E20 + 6% anisole in TRF88	99.9	9.6	472
TRF88	87.0	5.2	348
E25- FACE B	105.6	11.8	485
FACE B	95.8	3.4	340

The DHA of each fuel is necessary for later correlation work. Table 7 shows the results of the DHA for TRF88. TRF 88 is blended with toluene, n-heptane, and iso-octane however, the DHA shows impurities; trace amounts of other components. For this study trace amounts of other chemicals were excluded from the correlation work, but a full analysis showing the level of trace compounds (impurities) is shown in Appendix A. Table 8 shows the results of the DHA analysis for each fuel, excluding any trace amounts of other chemicals.

Table 7: DHA analysis results for TRF88. TRF88 by definition is 21% n-heptane, 49% iso-octane, and 30% toluene. Analysis gives components in weight, volume, and mole percent, total C, H and O percent, density and particulate matter index (PMI) [44, 45].

COMPONENT	%WGT	%VOL	%MOL
n-heptane	19.57	21.17	20.16
2-Methylhexane	0.04	0.04	0.04
3-Methylhexane	0.02	0.02	0.02
2,2,4-Trimethylpentane	47.12	50.38	42.57
2,2-Dimethylhexane	0.03	0.03	0.03
Toluene	33.13	28.27	37.11
Methylcyclohexane	0.02	0.02	0.03
Density (g/ml) at 15C	0.7439		
H wt%	13.6		
C wt%	86.4		
PMI	0.51		

Table 8: Table of components in each fuel per the DHA analysis. With the exception of FACE B, which is percent of each component in surrogate.

Fuel	toluene (vol. %)	iso-octane (vol. %)	n-heptane (vol. %)	ethanol (vol. %)	anisole (vol. %)	p-cresol (vol. %)	o-xylene (vol. %)
PRF 100 (iso-octane)	0	99.89	0	0	0	0	0
TSF 99.8	73.59	8.7	16.09	0	0	0	0
E25 in TRF88	21.63	38.55	16.2	23.49	0	0	0
E40 in TRF71	24.95	11.23	24.45	39.44	0	0	0
E20 2pcresol TRF88	24.2	38.8	16.1	20.4	0	2	0
E20 6anisole TRF88	23.3	37.3	15.5	19.7	6.2	0	0
TRF88	28.27	50.38	21.17	0	0	0	0
E25 FACE B	0	65.745	5.085	25	0	0	4.17
FACE B	0	87.66	6.78	0	0	0	5.56

Correlation work will examine the data set based on percent volume of each component. Seven of the fuels are composed mainly of toluene, n-heptane, iso-octane, ethanol, p-cresol, and anisole (six components). Thus the two fuels with FACE B posed a complexity issue. As shown in Appendix A, Figure A-3 the DHA on FACE B identifies 67 different components, making it difficult to compare to the composition of the rest of the fuels. Even if trace amounts of chemicals were excluded, there would still be twice as many components to consider, than are in the rest of the fuel set. To enable correlation work, Dr. Scott Wagnon at Lawrence Livermore National Laboratory (LLNL) was contacted in hopes of suggesting a surrogate blend for FACE B that could be used in the correlation work instead of the DHA data. Dr. Wagnon, proposed a blend of iso-octane, n-heptane, and o-xylene [46]. The FACE B 3-component surrogate can be seen in Table 9 and gives volume, mass and molar percent of each component. Figure 19

compares the FACE B value (target value) to the surrogate value (current value) for RON, S, and the percent paraffin, iso-paraffin and aromatic content.

Table 9: Table of components in FACE B surrogate blend, in volume, molar and mass percent.

FACE B Surrogate	Vol %	Molar %	Mass %
n-heptane	6.78	7.42	6.60
o-xylene	5.56	7.35	6.93
iso-octane	87.66	85.23	86.47

Target Name	Target Value	Current Value
RON	95.8	95.55
SENS	3.4	3.883
HC	2.197	2.178
paraffin_vf	0.079	0.06784
iso-paraffin_vf	0.863	0.8765
aromatic_vf	0.058	0.05561

Figure 19: Comparison of target value properties of FACE B to the current values of the FACE B 3-component surrogate blend [Courtesy of Dr. Wagnon, LLNL].

2.6 Advanced Fuel Ignition Delay Analyzer Temperature Sweep Procedure

Initial functional tests in the AFIDA need to be conducted by the user to ensure the device is working properly. Then a test sequence can be entered for the device to run continuously. The AFIDA software has two main tabs: settings and maintenance. The 'Settings' tab is where the user enters in the test sequence to be conducted, which consists of user inputs for chamber temperature, chamber pressure, injection duration (controls Φ), fuel line pressure, fuel name, Φ value, O_2 concentration and data collection time for each fuel. Each fuel was tested from 725 °C – 425 °C in 25 °C increments at 5, 10, 20, and 30 bar with a 21% O_2 concentration and a fuel pressure of 1190 bar. Each temperature pressure condition consists of 14 injections comprised of 2 pre-injections and 12 main injections the average of which is used to describe the test. The test sequence is set to start at 725 °C, and run all pressure conditions at that temperature before dropping to the next temperature condition in 25 °C increments until 425 °C. The 'Maintenance' tab is where the user can control the AFIDA functions before a test is started. In

order to prepare for the test of each fuel in the set the AFIDA functioning was examined. The chamber was set to around 600 °C and 20 bar. Then the chamber pressure was monitored to ensure no leakage. Additionally 400 ms or more of certification diesel fuel was run through the fuel line after every fuel test, to insure the low viscosity fuels that were being tested would not be sitting in the fuel line while it was unpressurized and thus risk boiling. Additionally a few injections of certification diesel fuel were run under G-CN conditions, of 17.5 bar and 580 °C to ensure that ID time was consistent between fuel samples [36]. After the proper functioning of the AFIDA was confirmed the 40 mL fuel samples with 1500 ppm Infineum R655 were loaded into the autosampling carousel. A flushing vial is designated to flush the test fuel through the line for 340 ms before the test sequence is initiated. The test sequence for 4 pressures as 13 difference temperature conditions each takes around 10 hours and is automated.

CHAPTER 3

Analysis

3.1 AFIDA Data Post Processing

The AFIDA outputs a text file with, pressure transmitter signal data, time, chamber temperature, chamber pressure, injection pressure, injection duration, injection temperature, pressure transmitter temperature, fuel pressure, fuel temperature, and AFIDA software ID time. While the software has its own analysis tool where the user can load a test to be plotted, these plots cannot be exported. The text file must be post processed with an Excel macro created by Jon Luecke at NREL. The macro converts the signals into pressure and time data, as well as smoothens the signal for each of the 12 injections in a test. This code also processed the ID time from the pressure trace data. The ID time definition of the AFIDA (proprietary), is intended for diesel fuels, and like the IQT's ID time definition is typically unable to capture the 2 stage combustion event of gasoline range fuels. The ID time is calculated 4 ways in the macro: maximum dP/dt, 40% of peak pressure, 10% of peak pressure, user defined threshold, and AFDIA definition. Maximum dP/dt finds the time associated with the maximum slope of the pressure trace, defining the greatest rate of pressure rise as the start of combustion, this is calculated for the average pressure trace of the 12 injections. 40% and 10% of peak calculate the ID time based on the time associated with 40 and 10 percent of the maximum pressure in the chamber respectively. This is calculated for each of the 12 injections, and then averaged. User defined, allows the user to choose a threshold pressure much like the NREL designed controls for the IQT defines ID time.

Maximum dP/dt is a commonly accepted definition of ID time. This definition is rooted in the ignition kinetics and relates to the maximum heat release rate. However due to noise this

definition is not always accurate; in these cases 40% of peak is used. 40% of peak is typically very close to the maximum dP/dt values (typically within 2 ms of maximum dP/dt), thus when maximum dP/dt fails to properly identify ignition, 40% is used. Figure 20 illustrates an example of when maximum dP/dt fails to identify ignition; the noise at the beginning of the test causes the ID time to be very low (~4 ms) when in reality it is more like ~180 ms. Another case where 40% of peak is used instead of maximum dP/dt is when the maximum rate of pressure rise is at the very top of the pressure trace which can be seen in Figure 21. In this instance the ID time is more closely identifying the end of the combustion event, not the beginning. Additionally for some fuels ignition did not occur before 650 ms, thus some of the fuels are missing data at low temperatures.

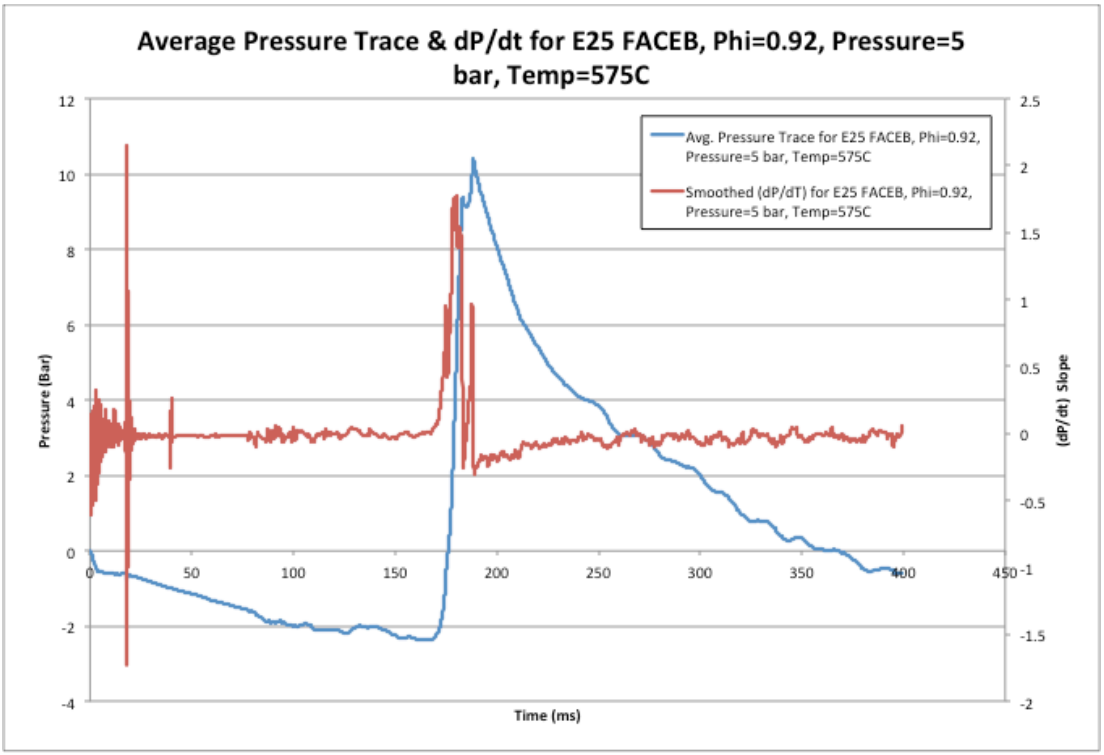

Figure 20: Pressure trace and dP/dt plotted against time for E25 FACE B at a pressure of 5 bar, and temperature of 575 °C.

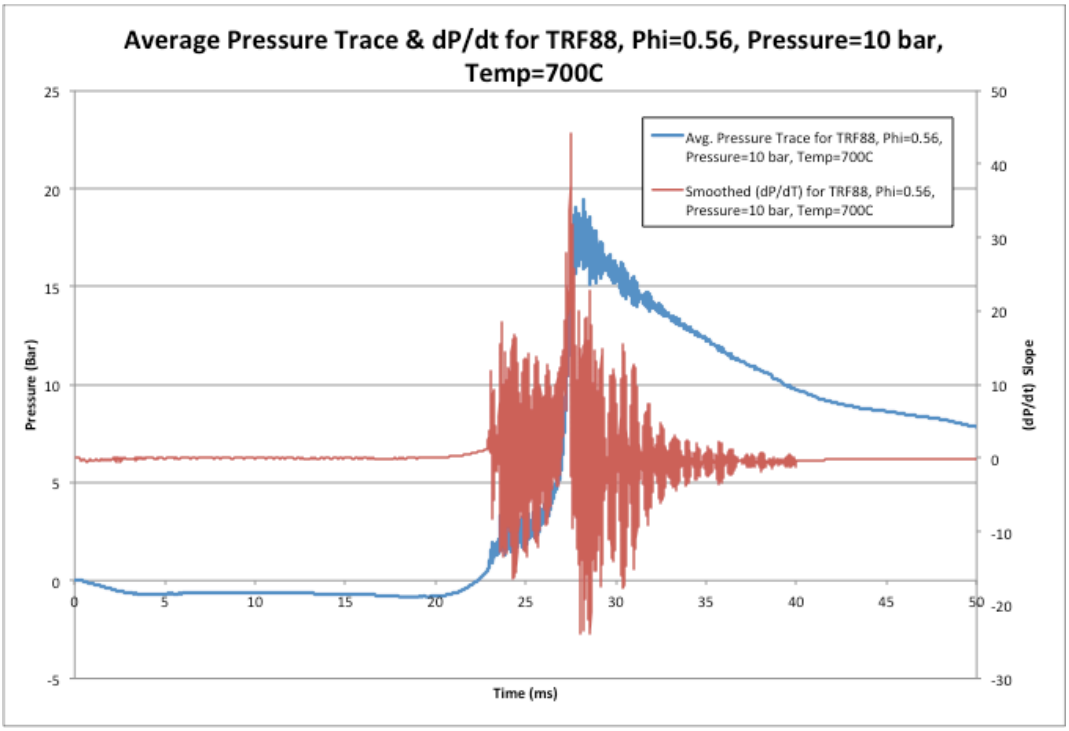

Figure 21: Pressure trace and dP/dt plotted against time for TRF88 at a pressure of 10 bar, and temperature of 700 °C.

3.2 Fuel Set Surface Plots

To evaluate the results the data were plotted two different ways. Figure 22, Figure 23, Figure 24, and Figure 25 show a summary of the temperature sweep for every fuel at 5, 10, 20 and 30 bar respectively. The temperature sweep shows ID time (in ms) on a log scale versus the inverse temperature in typical Arrhenius form (1000/T [Kelvin]. The NTC region can be seen for some of the fuels (TRF88, FACE B) on the 5 and 10 bar plots. The NTC region is defined where increases in temperature result in longer ignition delay, due to competing chemical kinetic chain terminating versus chain propagating and branching pathways at that temperature, which is reflected in a negative slope along the ID time curve.

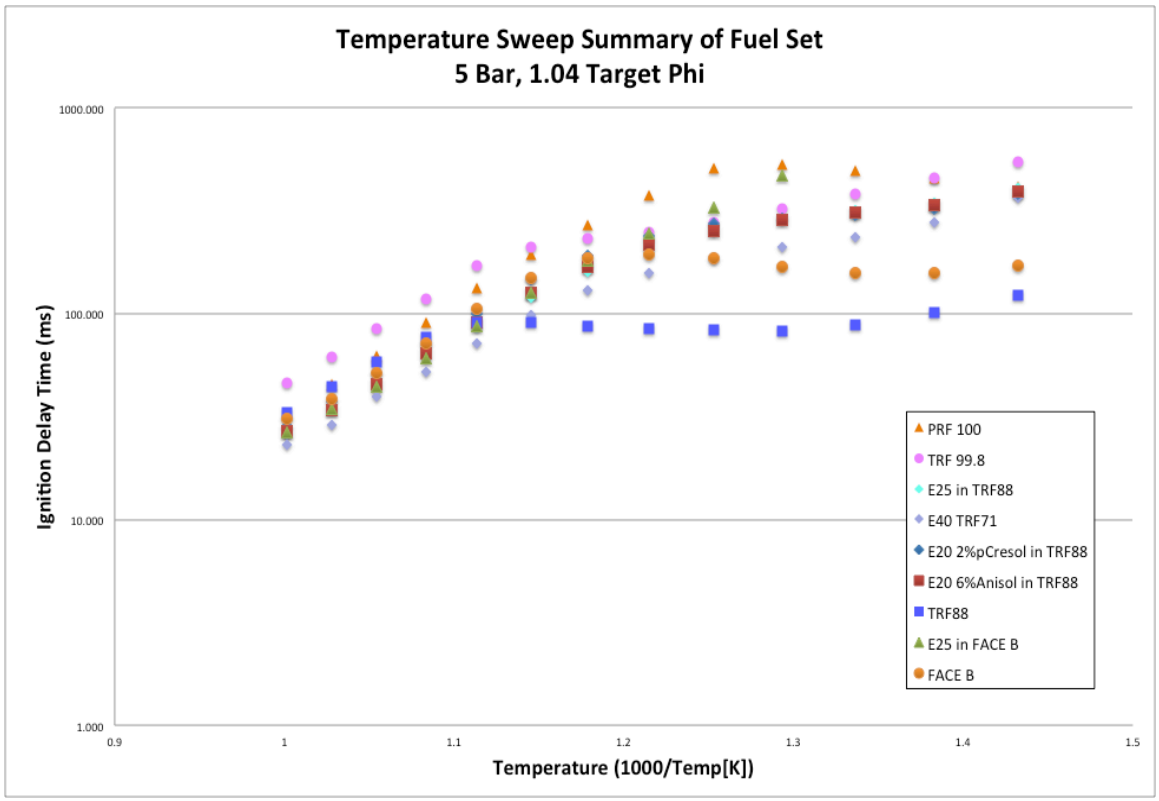

Figure 22: Temperature sweep summary of the fuel set, at 5 bar, with a target Φ of 1.04.

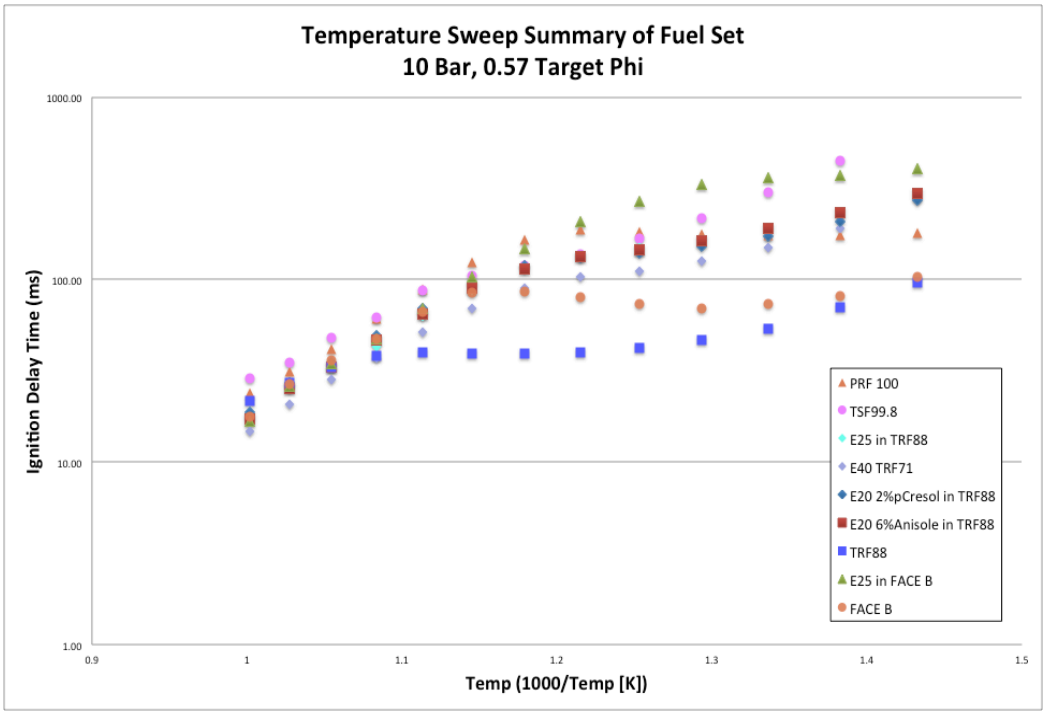

Figure 23: Temperature sweep summary of the fuel set, at 10 bar, with a target Φ of 0.57.

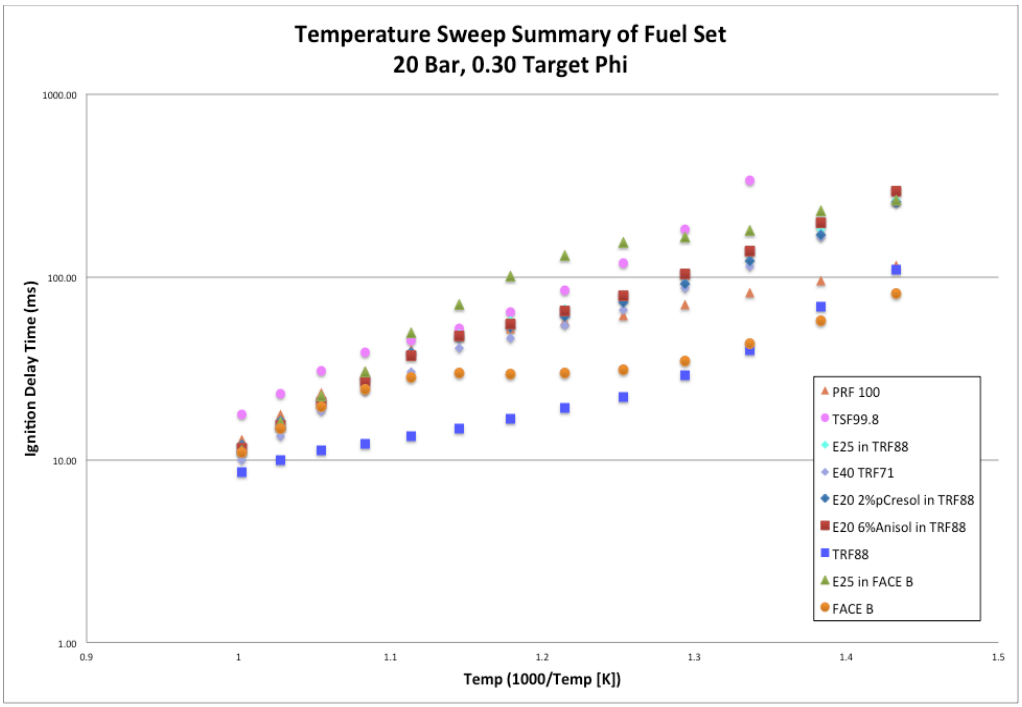

Figure 24: Temperature sweep summary of the fuel set, at 20 bar, with a target Φ of 0.30.

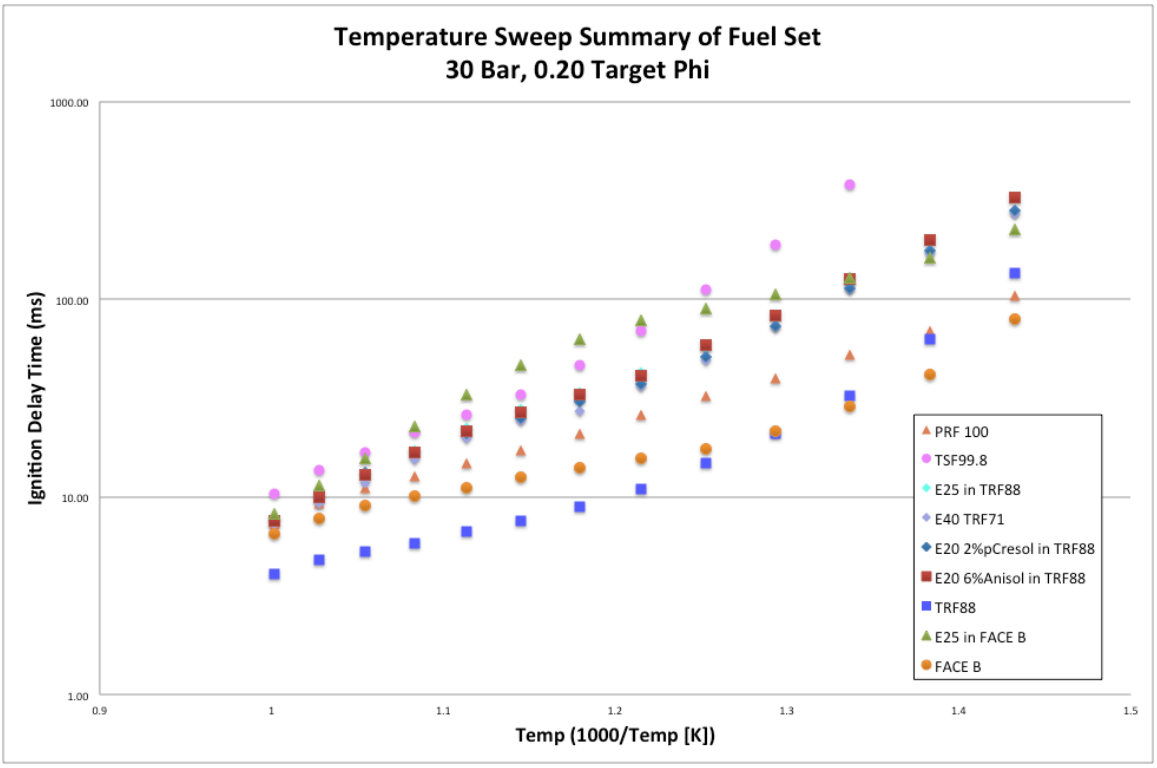

Figure 25: Temperature sweep summary of the fuel set, at 30 bar, with a target Φ of 0.20.

Figure 26, Figure 27, Figure 28 and Figure 29 highlight the differences between TRF88 and E25 in TRF 88; showing the affects of ethanol on the temperature sweep profile at 5, 10, 20

and 30 bar. PRF100 is shown in the background for reference. As the pressure increases the separation between TRF 88 with and without ethanol becomes more pronounced. At 5 bar in Figure 27 the high temperature ID times are closer together and the effects of ethanol are not highly apparent. However, at the lower temperatures the ID time starts to differ and the difference in S of 5.5 between the two fuels become more pronounces as the fuel with the higher S (S=10.7) has higher ID times at low temperatures. As the pressure increases the difference in ID time between the two fuels becomes more noticeable and the E25 blend has higher ID times at every temperature condition.

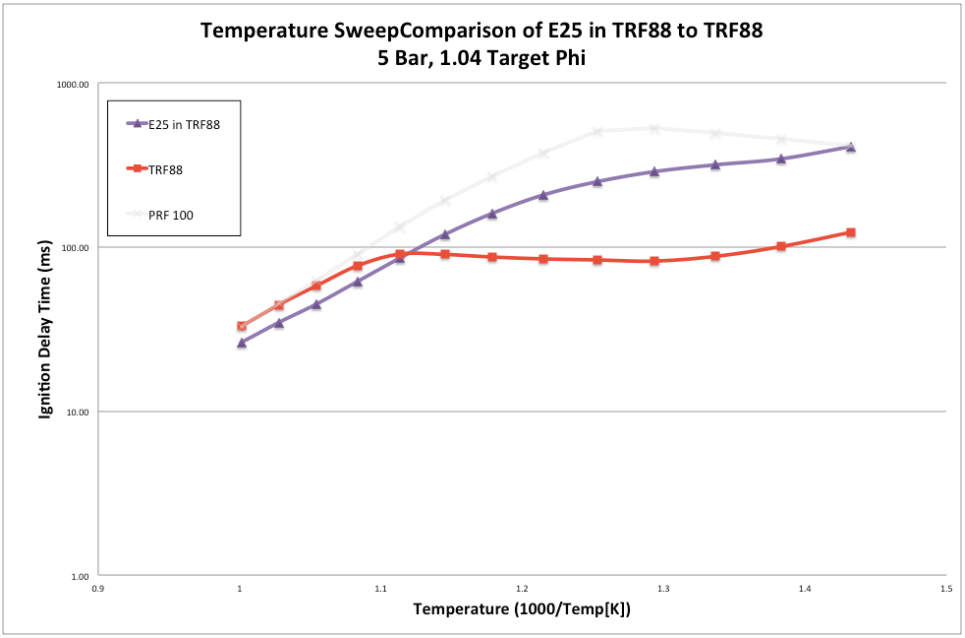

Figure 26: Temperature sweep summary of the TRF88 and E25 TRF88 (with PRF100 in the background for reference) to compare affects of ethanol, at 5 bar, with a target Φ of 1.04.

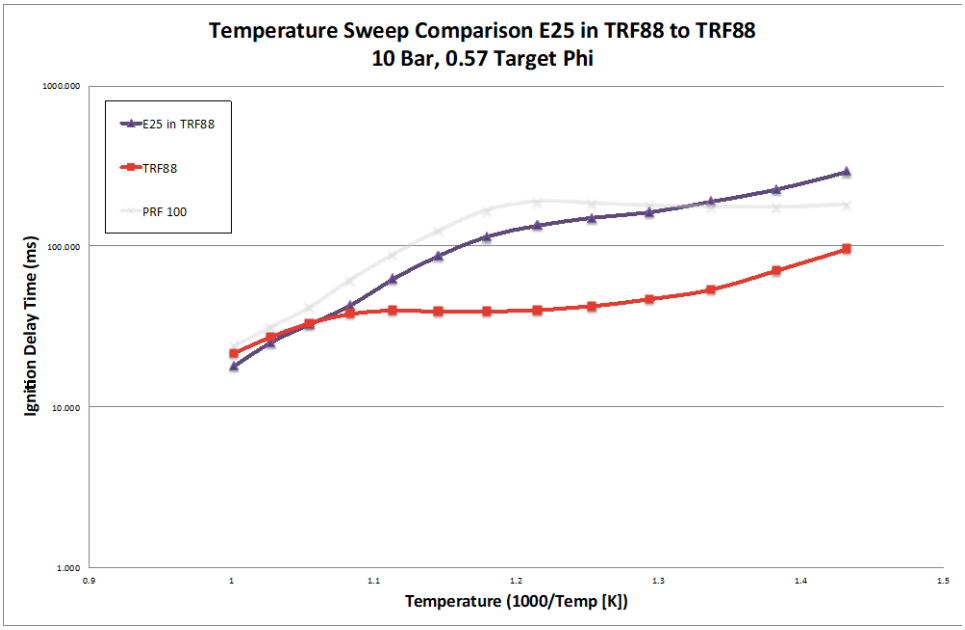

Figure 27: Temperature sweep summary of the TRF88 and E25 TRF88 (with PRF100 in the background for reference) to compare affects of ethanol, at 10 bar, with a target Φ of 0.57.

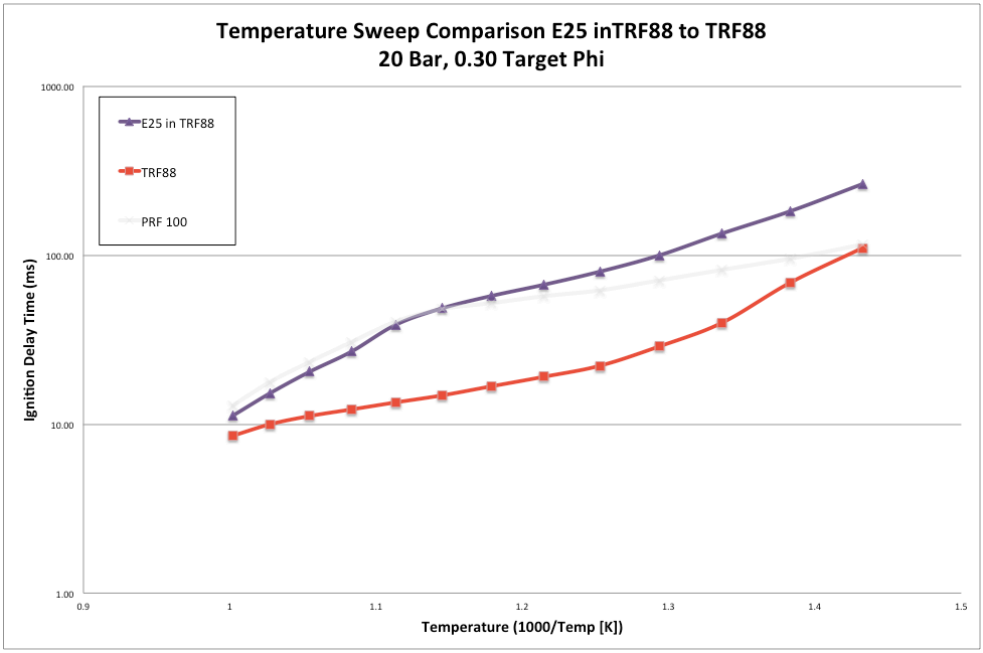

Figure 28: Temperature sweep summary of the TRF88 and E25 TRF88 (with PRF100 in the background for reference) to compare affects of ethanol, at 20 bar, with a target Φ of 0.30.

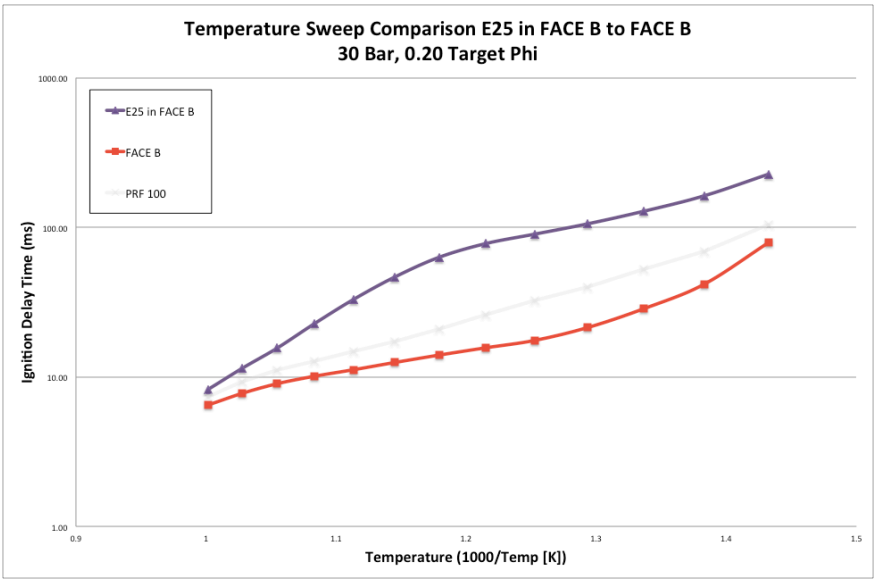

Figure 29: Temperature sweep summary of the TRF88 and E25 TRF88 (with PRF100 in the background for reference) to compare affects of ethanol, at 30 bar, with a target Φ of 0.20.

Figure 30, Figure 31, Figure 32 and Figure 33 highlight the differences between FACE B and E25 in FACE B at 5, 10, 20, and 30 bar respectively. These plots show the effects of ethanol on the temperature sweep profile at various pressures. PRF100 is shown in the background for reference. Figure 30 is missing some data for E25 FACE B at low pressures, because the ID times became to long to record. This shows there is a large difference between FACE B with, and without, ethanol. As the pressure increases, the two fuels start to exhibit different behavior at high temperatures and spread apart as they have a difference of 8.4 in S. However the Φ is changing between each pressure as well. Thus the differences in temperature sweeps for all the fuels will be partially from change in pressure and partially from changing Φ.

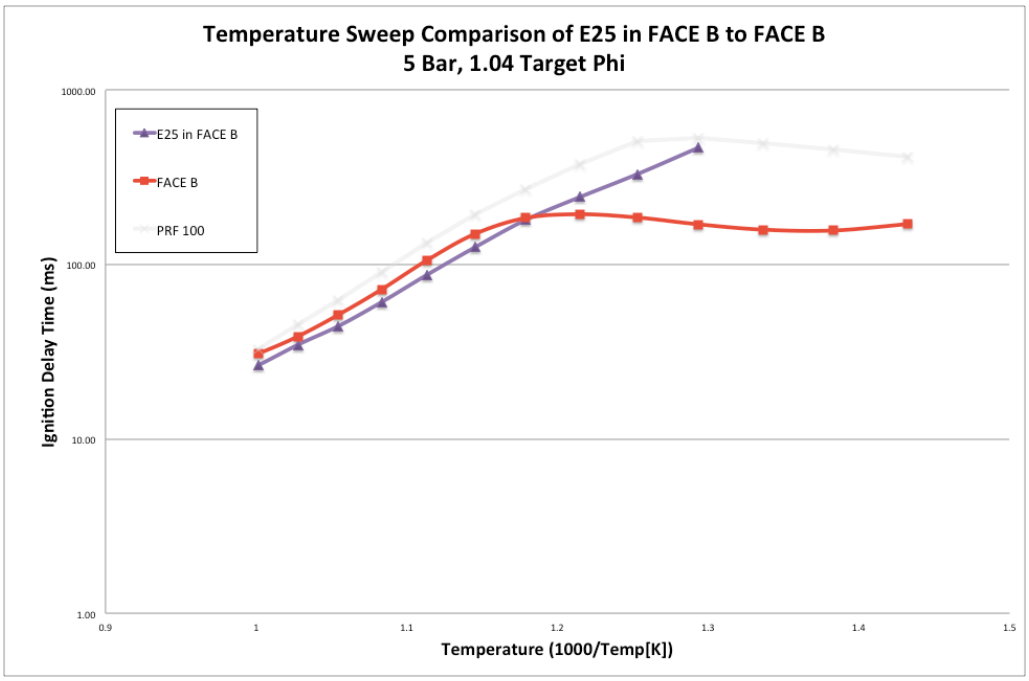

Figure 30: Temperature sweep summary of the FACE B and E25 FACE B (with PRF100 in the background for reference) to compare affects of ethanol, at 5 bar, with a target Φ of 1.04.

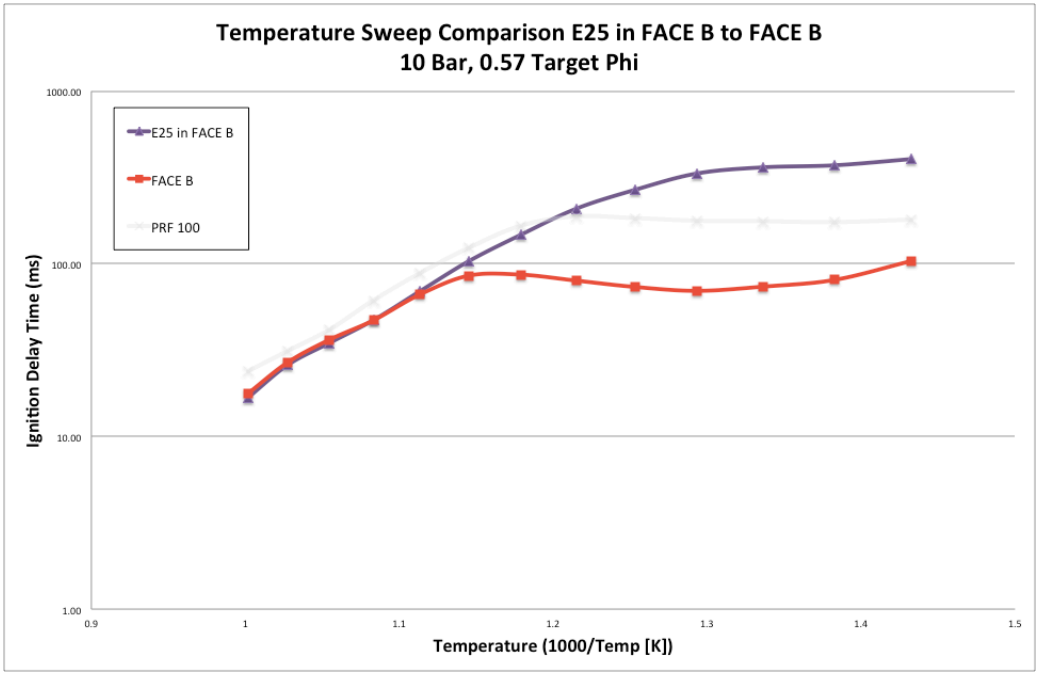

Figure 31: Temperature sweep summary of the FACE B and E25 FACE B (with PRF100 in the background for reference) to compare affects of ethanol, at 10 bar, with a target Φ of 0.57.

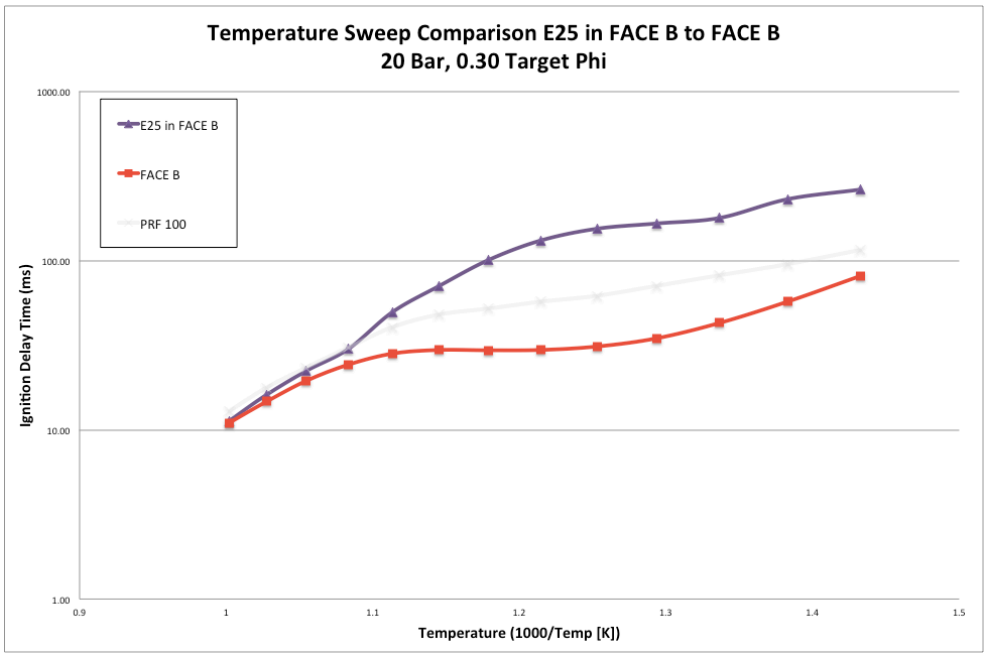

Figure 32: Temperature sweep summary of the FACE B and E25 FACE B (with PRF100 in the background for reference) to compare affects of ethanol, at 20 bar, with a target Φ of 0.30.

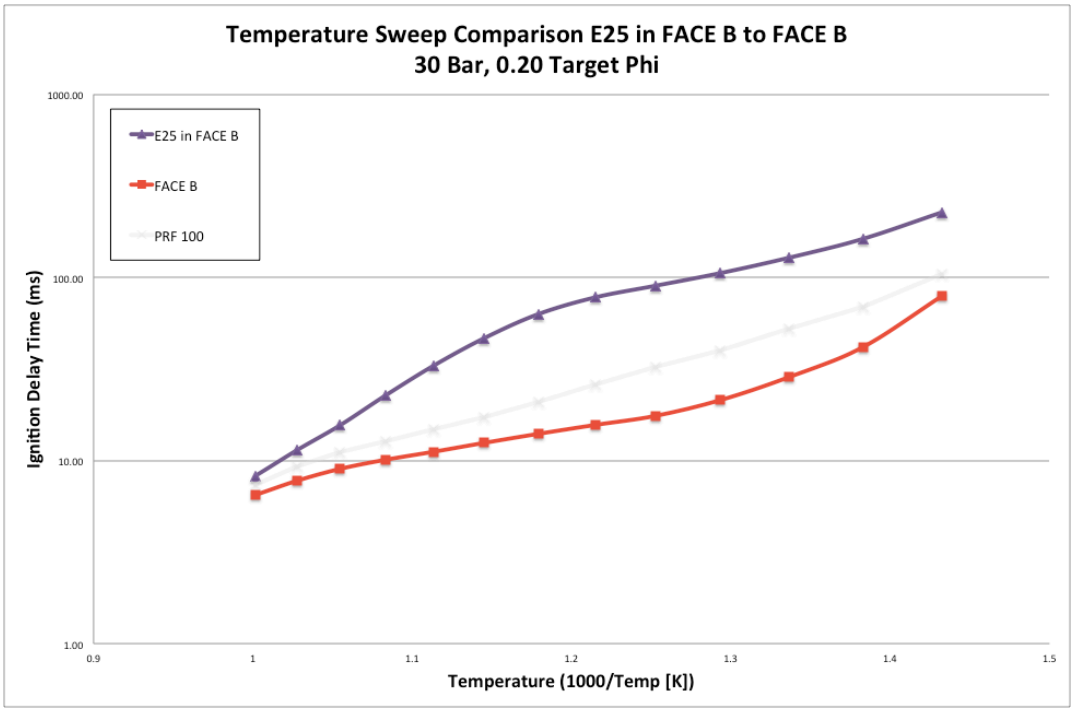

Figure 33: Temperature sweep summary of the FACE B and E25 FACE B (with PRF100 in the background for reference) to compare affects of ethanol, at 30 bar, with a target Φ of 0.20.

The results have also been plotted as generated 3D surfaces for each fuel. The surface fit equation is a 3rd order polynomial in pressure and a 4th order polynomial in temperature. 3D

surface plots can be seen in Figure 34-Figure 42 for PRF100, TRF99.8, E20 in TRF 88, E40 in TRF71, E20 + 2% p-cresol in TRF 88, E20 + 6% anisole in TRF88, TRF88, E25 in FACE B, and FACE B respectively. Figure 41 shows the surface of ID time as pressure and temperature change for E25 FACE B, this surface is what a typical ID time surface should look like as a function of temperature and pressure. ID time is expected to decrease with pressure thus the ID time at 5 bar should be higher than 10 bar, and so on. However, in some of the surfaces the opposite is happing, and at low temperatures the ID time is increasing as the pressure increases. This effect can be seen in Figure 39, which is the surface for E20 plus 6% anisole in TRF88. This abnormal behavior can be explained by the decreasing fuel-air equivalence ratio, Φ. The tests are leaner both as the pressure increases, and as the temperature decreases. At high temperatures the fuel injected creates a rich zone and combusts before the fuel has time to disperse, which gives the expected result despite Φ changing between pressures and temperatures. However, at the very low temperatures and low Φ / high pressures, the rich pocket of fuel has time to disperse before combustion, thus the fuel becomes a less rich pocket or even a lean pocket and takes even longer to combust. At high temperatures, Φ has less of an effect on the ID than compared to low temperatures. While this behavior is not typical of a temperature sweep across pressures, the Φ is typically help constant, and close to 1. These results can be well explained by the changing Φ through the temperature and pressure tests.

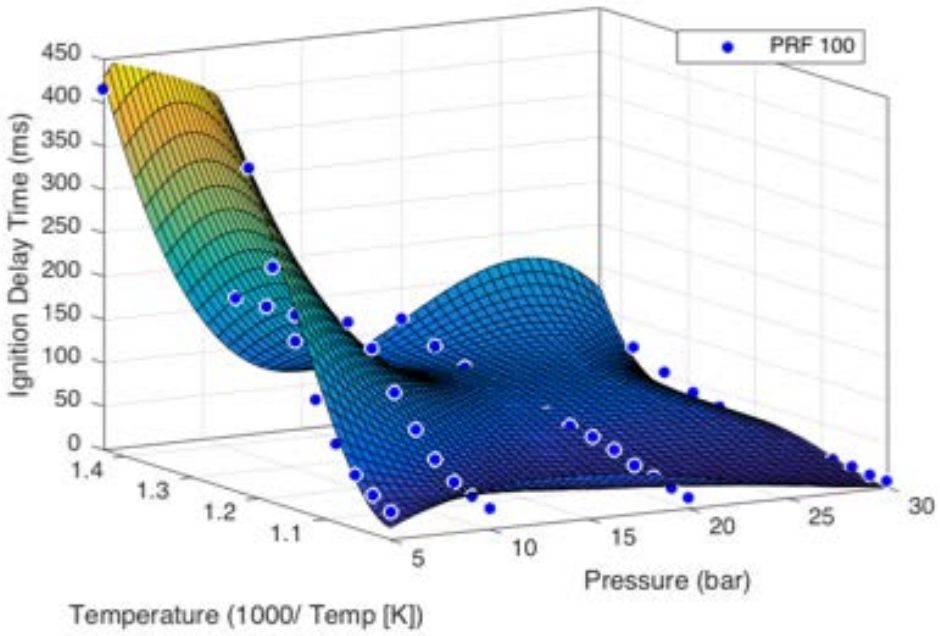

Figure 34: 3D surface of ID time as temperature and pressure change for REF 100 The surface is a 4th order polynomial in temperature and a 3rd order polynomial in pressure.

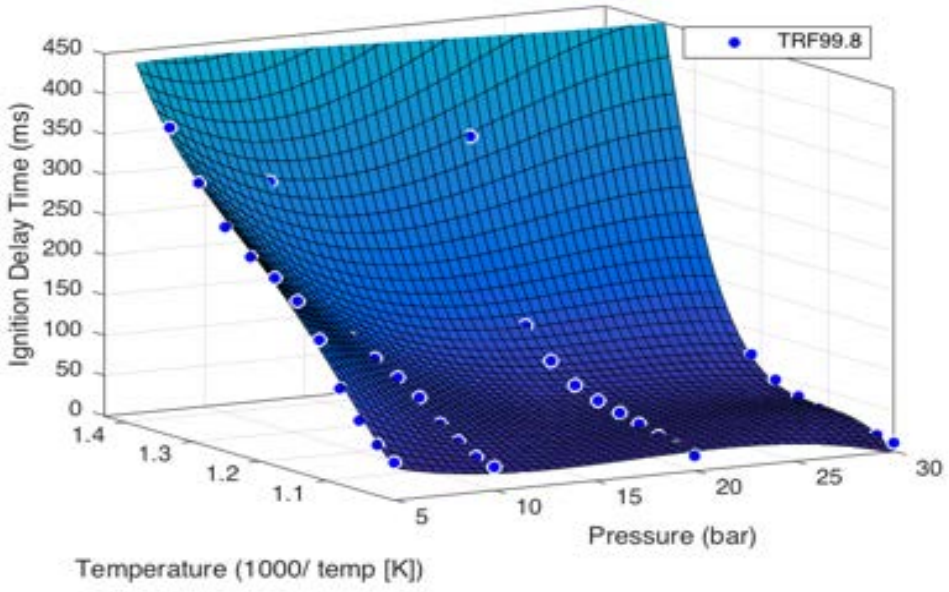

Figure 35: 3D surface of ID time as temperature and pressure change for TRF99.8. The surface is a 4th order polynomial in temperature and a 3rd order polynomial in pressure.

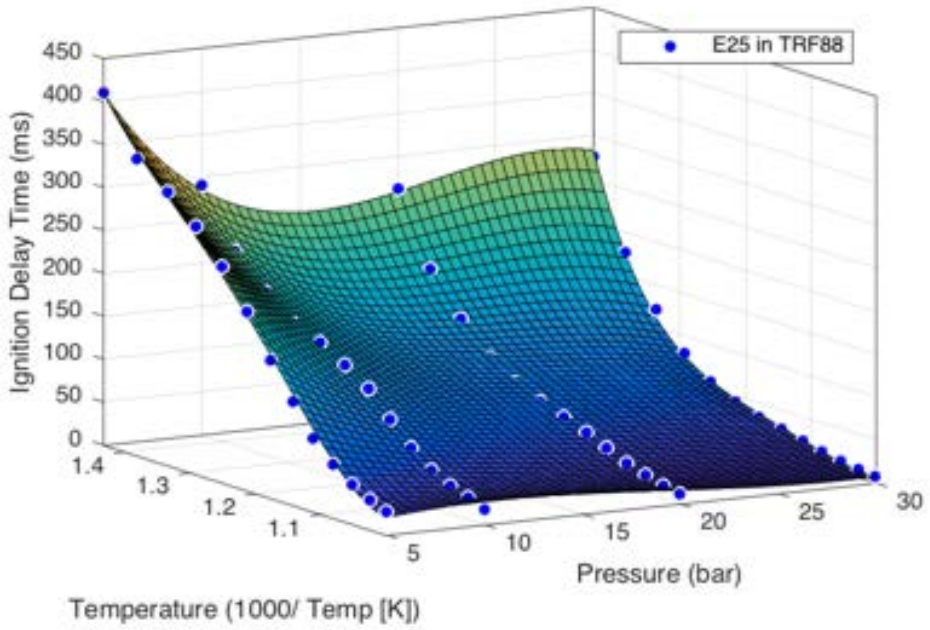

Figure 36: 3D surface of ID time as temperature and pressure change for E25 in TRF88. The surface is a 4th order polynomial in temperature and a 3rd order polynomial in pressure.

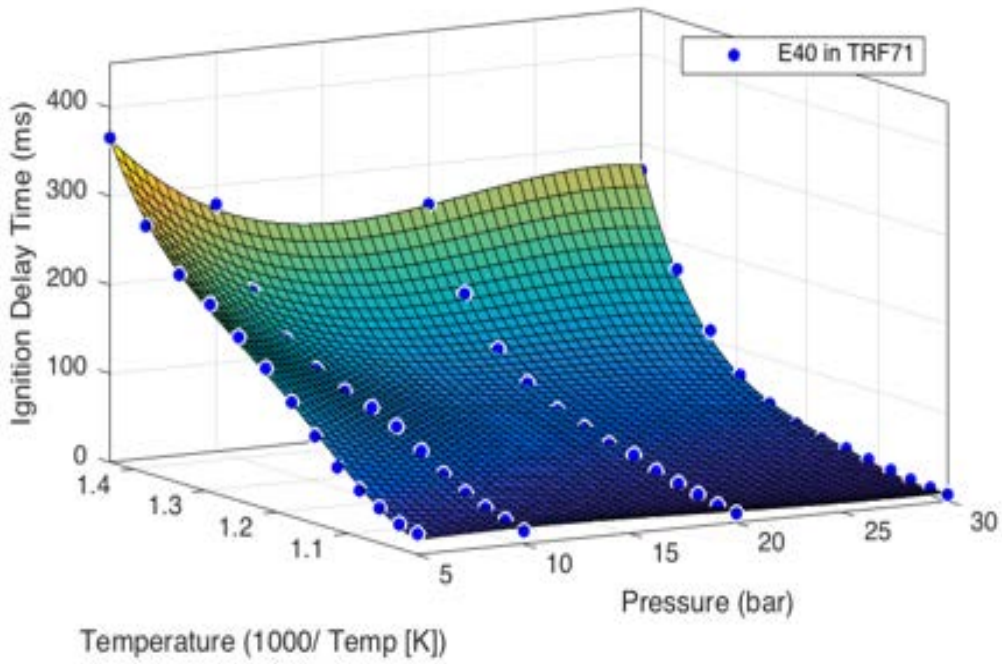

Figure 37: 3D surface of ID time as temperature and pressure change for E40 in TRF71. The surface is a 4th order polynomial in temperature and a 3rd order polynomial in pressure.

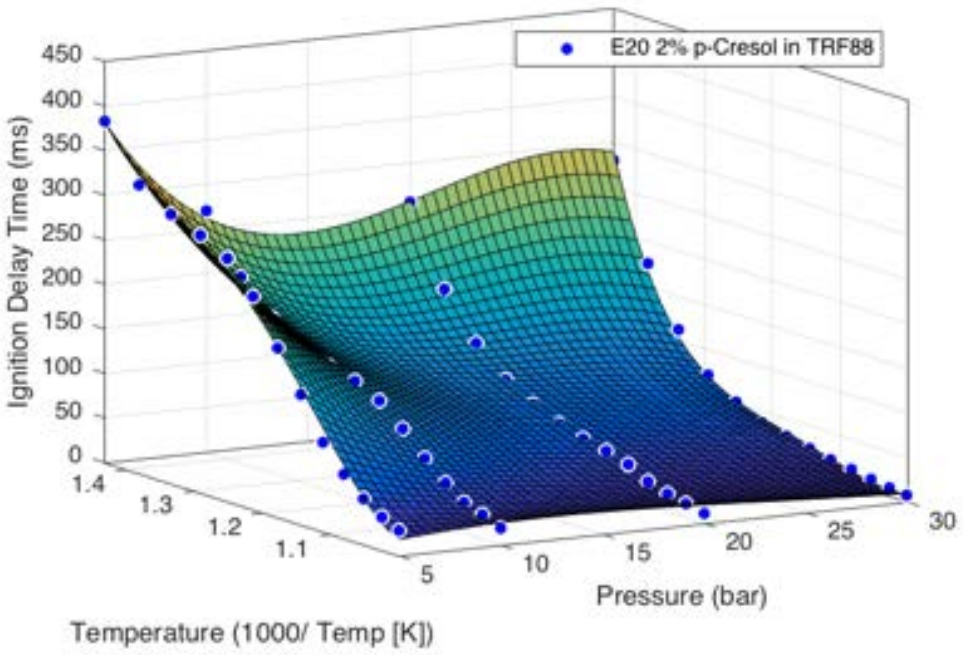

Figure 38: 3D surface of ID time as temperature and pressure change for E20 +2% p-cresol in TRF88. The surface is a 4th order polynomial in temperature and a 3rd order polynomial in pressure.

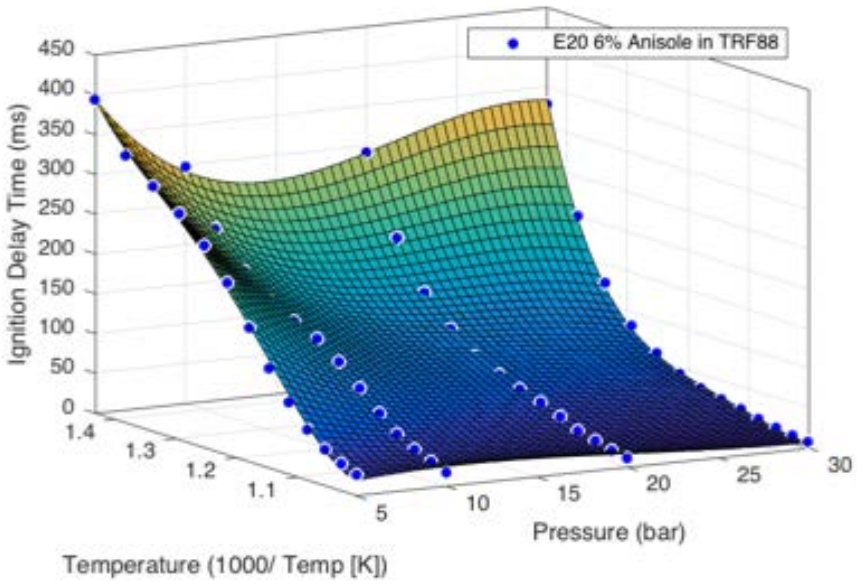

Figure 39: 3D surface of ID time as temperature and pressure change for E20 +6% anisole in TRF88. The surface is a 4th order polynomial in temperature and a 3rd order polynomial in pressure.

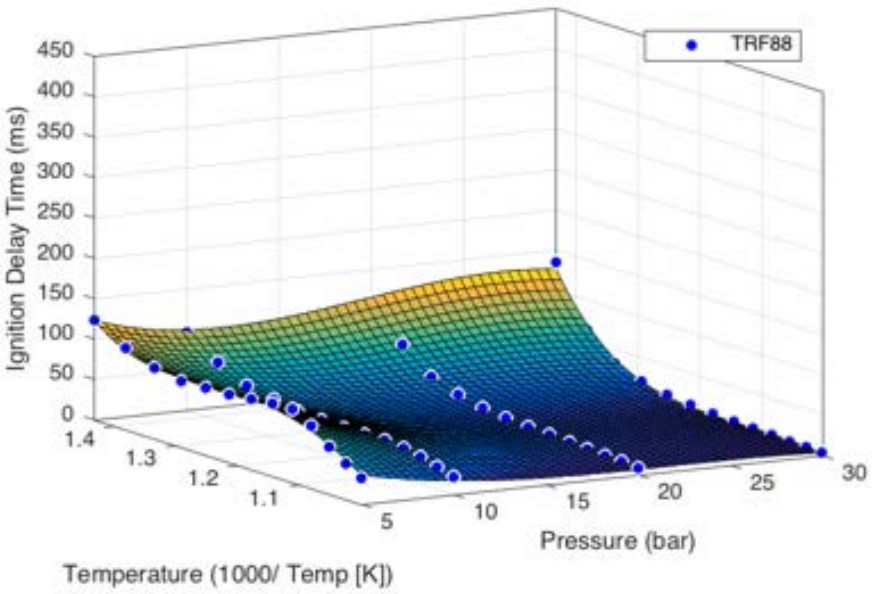

Figure 40: 3D surface of ID time as temperature and pressure change for TRF88. The surface is a 4th order polynomial in temperature and a 3rd order polynomial in pressure.

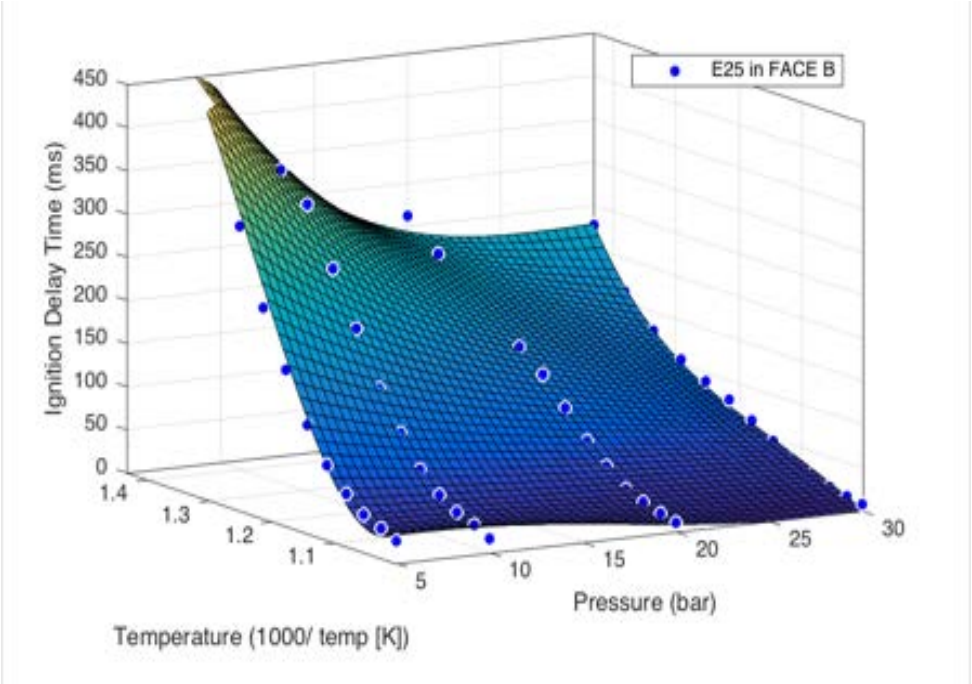

Figure 41: 3D surface of ID time as temperature and pressure change for E25 in FACE B. The surface is a 4th order polynomial in temperature and a 3rd order polynomial in pressure.

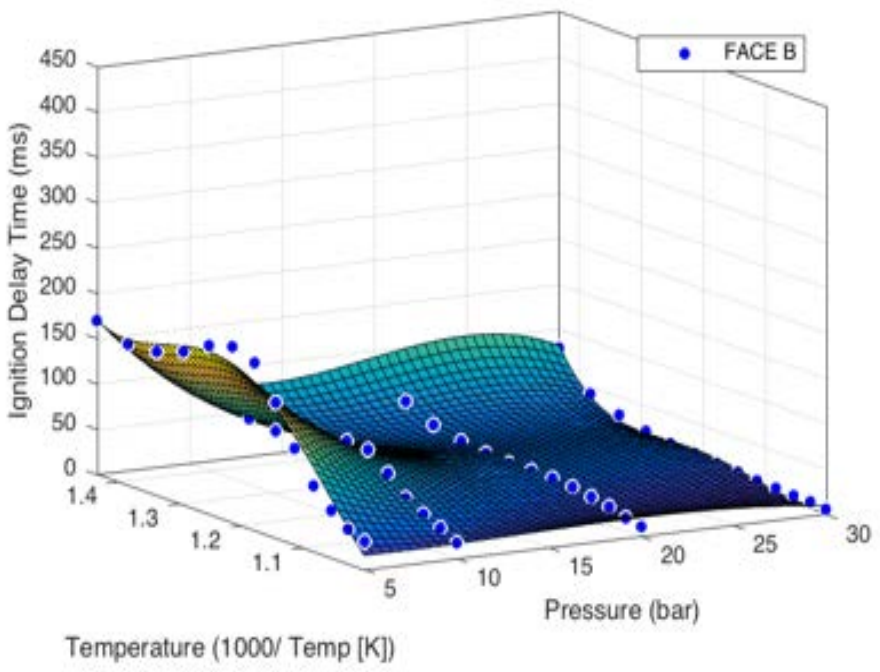

Figure 42: 3D surface of ID time as temperature and pressure change for FACE B. The surface is a 4th order polynomial in temperature and a 3rd order polynomial in pressure.

3.3 Correlation

The original plan for correlation with the AVFL-20 fuel set was to correlate the 3D surface plot of ID time as a function of pressure and temperature of each fuel to the major chemical compounds identified in the DHA. This plan was modified with the new fuel set, since the fuels were simple blends of up to 4 components (from a palette of 7 components, as shown in Table 8), thus making this a more tractable problem. Linear regression was preformed in MATLAB on the fuel set in numerous ways with the assistance from Dr. Daily. Initially a linear regression was performed between RON and weight percent of C, H, and O of each of the 9 fuels. This showed poor correlations R^2 of 0.31, but this result is not unexpected. Next a linear regression was performed between RON and the composition of each of the 9 fuels (7 components in total). While this regression was perfect with an R^2 value of 1, it wasn't meaningful. A point was deleted from the set, the regression performed again, and then the

deleted point was used with the regression equation to predict RON. The value was incorrect which shows this correlation is not useful for fuels outside those used in the regression. Unfortunately with such a small set of 9 fuels by 7 components, it is easy to find a perfect but meaningless correlation. Next a regression was performed on the entire set of data: temperature, pressure, Φ, composition, HOV, RON, and S. Figure 43 shows the results of this regression. While the correlation between ID time and 'fit' ID time is not valuable, there is a pattern within the data. Since pressure and thus Φ changes significantly throughout the fuel set, the data was parsed by pressure, and regressed against temperature and Φ. The results for 5, 10, 20, and 30 bar can be seen in Figure 44, Figure 45, Figure 46 and Figure 47 respectively. The R^2 values are 0.63, 0.59, 0.59, and 0.54 for 5, 10, 20, and 30 bar respectively. While the correlation still isn't significant the ID time is clearly dependent on phi and temperature for the fuels. One would not expect a meaningful correlation for this regression, as it does not account for chemical differences between the fuels at all. Finally a regression was performed at each pressure against 1000/temperature [K], phi, composition, HOV, RON and S. The regressions for 5, 10, 20, and 30 bar are shown in Figure 48, Figure 49, Figure 50 and Figure 51 respectively with R^2 values of 0.81, 0.77, 0.76, and 0.66. While these correlations still are not significant, and ID time cannot be predicted from the regression, the regression ID times are correlating better to the actual ID times. This is useful as there should be some correlation between composition of fuel and their parametric ID times.

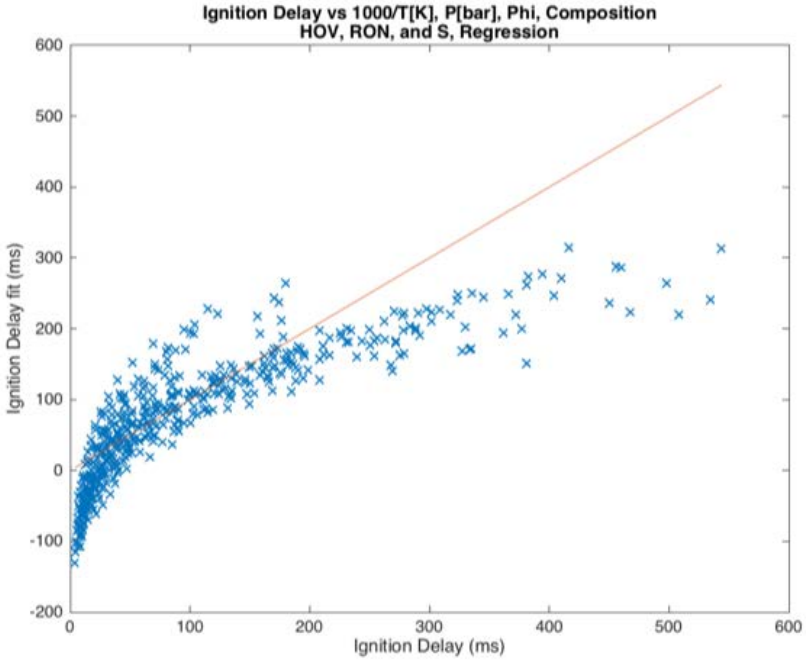

Figure 43: Linear regression of ID time versus: 1000/T [K], Pressure(bar), Φ, composition (vol.% toluene, iso-octane, n-heptane, ethanol, anisole, p-cresol, and o-xylene), HOV, RON, and S.

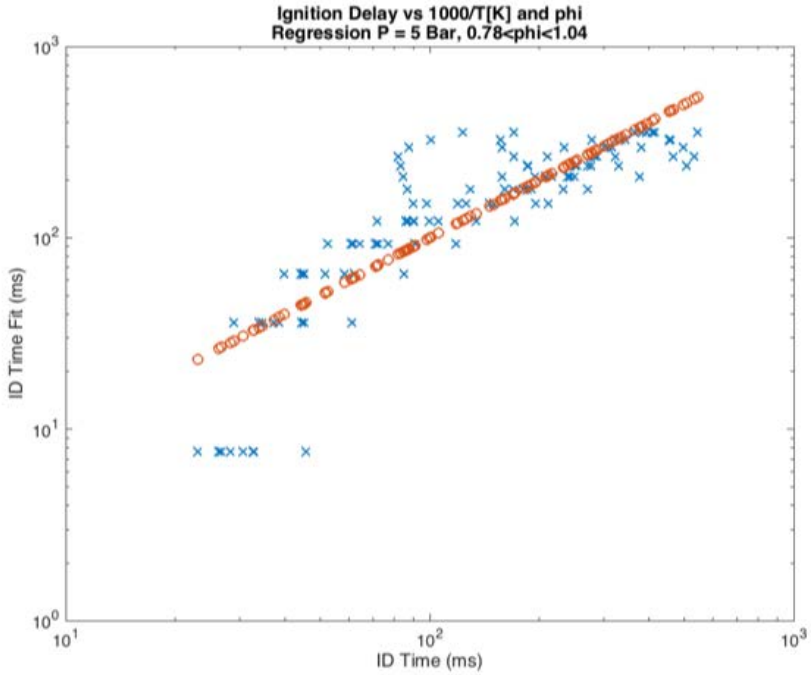

Figure 44: Linear regression of ID time versus: 1000/T [K] and Φ for fuels at 5 bar.

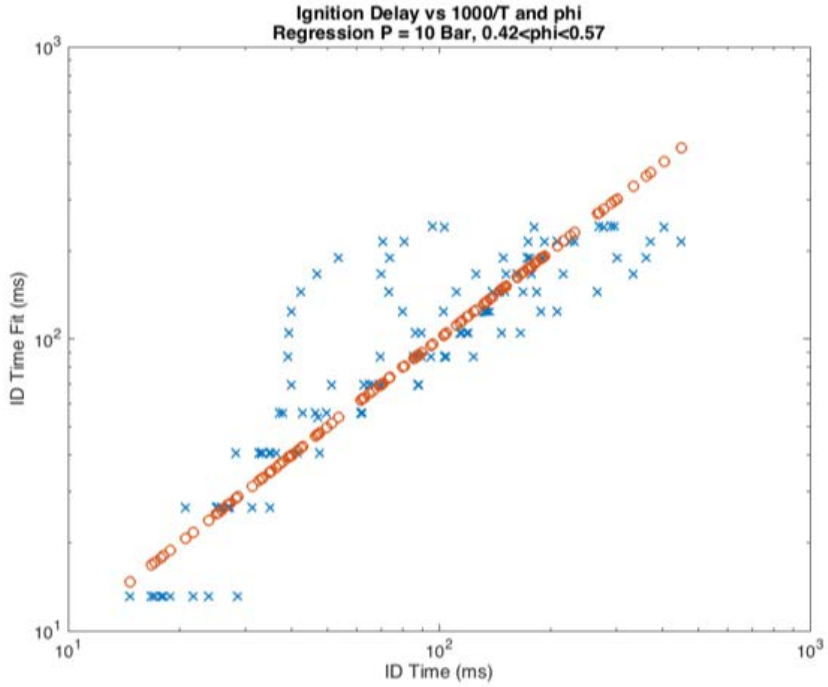

Figure 45: Linear regression of ID time versus: 1000/T [K] and Φ for fuels at 10 bar.

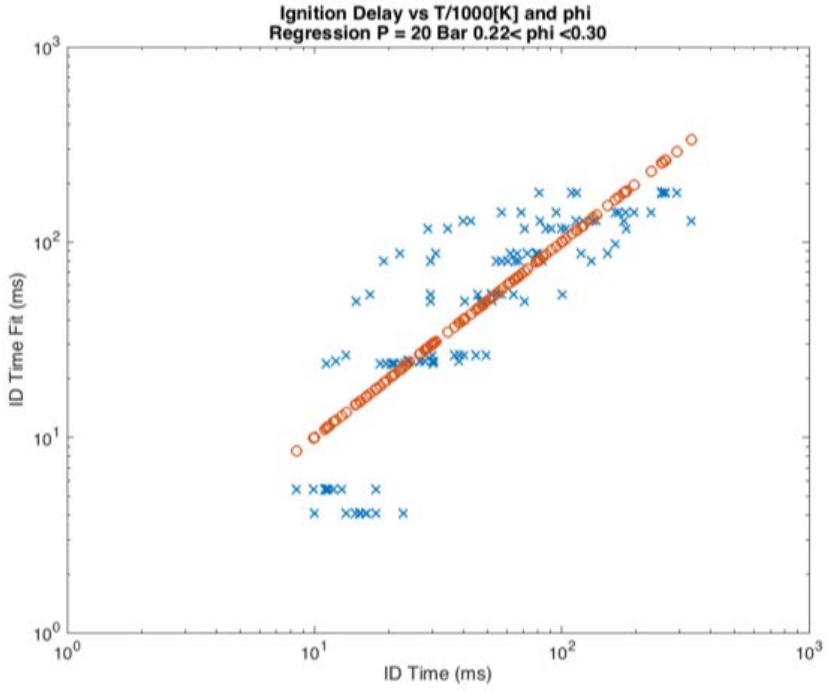

Figure 46: Linear regression of ID time versus: 1000/T [K] and Φ for fuels at 20 bar.

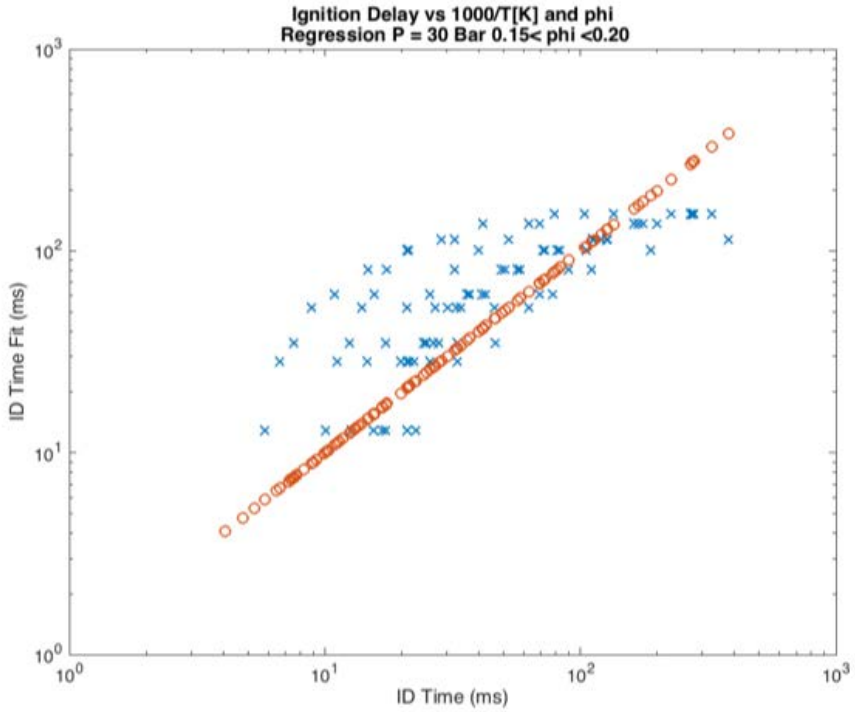

Figure 47: Linear regression of ID time versus: 1000/T [K] and Φ for fuels at 30 bar.

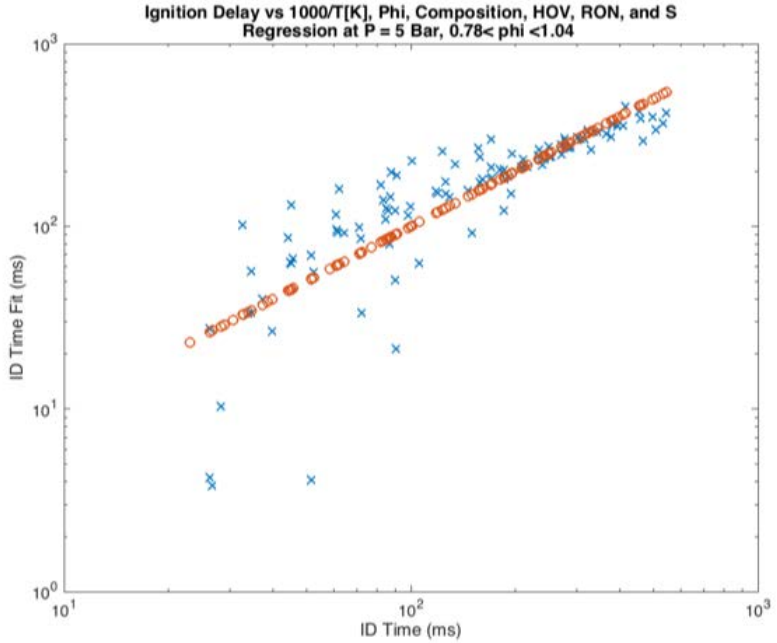

Figure 48: Linear regression of ID time versus: 1000/T [K], Φ, composition (vol.% toluene, iso-octane, n-heptane, ethanol, anisole, p-cresol, and o-xylene), HOV, RON, and S at 5 bar.

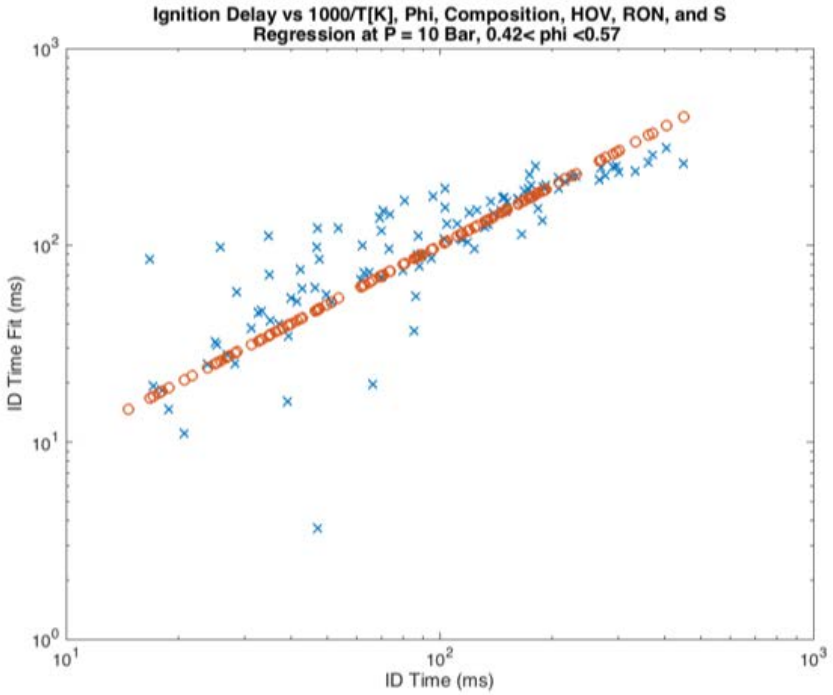

Figure 49: Linear regression of ID time versus: 1000/T [K], Φ, composition (vol.% toluene, iso-octane, n-heptane, ethanol, anisole, p-cresol, and o-xylene), HOV, RON, and S at 10 bar.

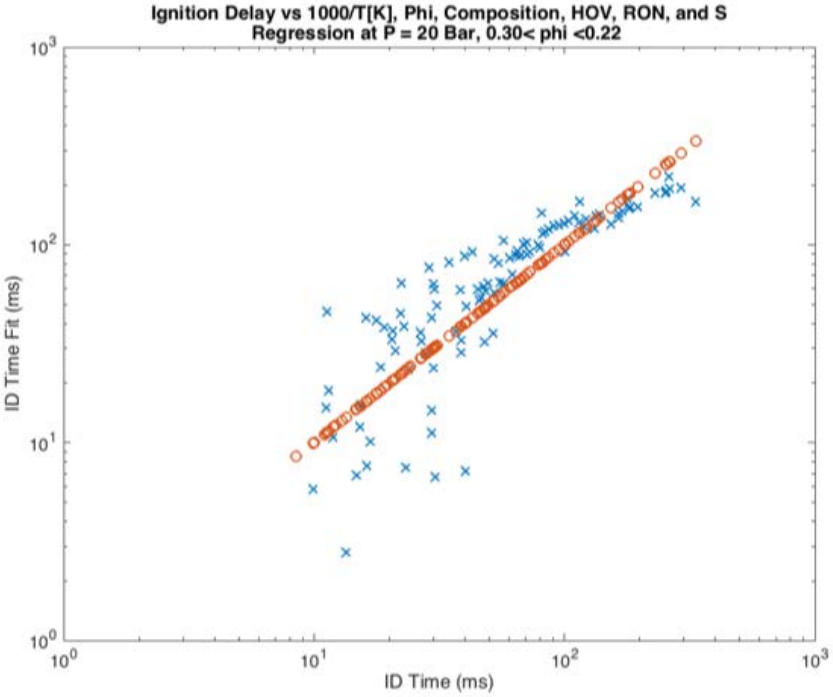

Figure 50: Linear regression of ID time versus: 1000/T [K], Φ, composition (vol.% toluene, iso-octane, n-heptane, ethanol, anisole, p-cresol, and o-xylene), HOV, RON, and S at 20 bar.

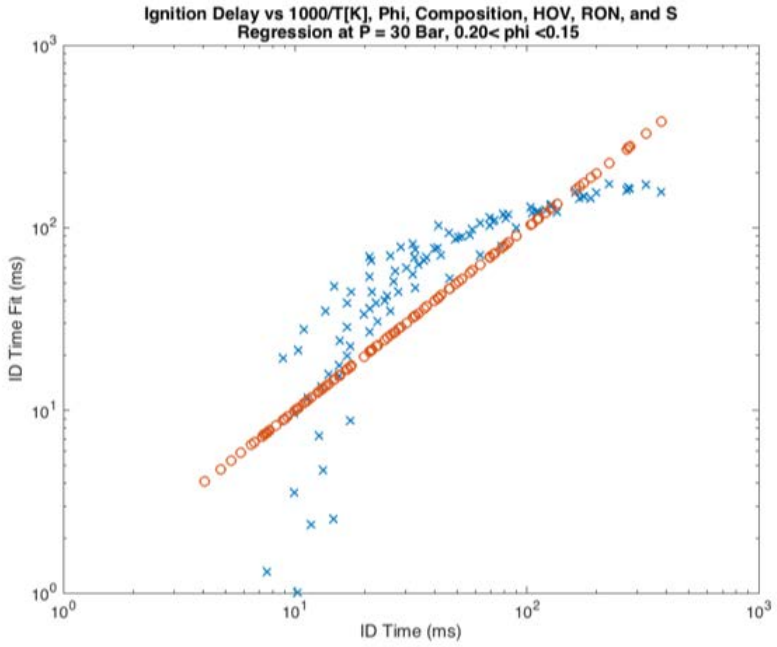

Figure 51: Linear regression of ID time versus: 1000/T [K], Φ, composition (vol.% toluene, iso-octane, n-heptane, ethanol, anisole, p-cresol, and o-xylene), HOV, RON, and S at 30 bar.

CHAPTER 4

Conclusion

4.1 Conclusions

Significant correlation between parametric ID and composition was not found with the regression methodologies used in this research. While the linear regression analysis on all fuel properties and composition at each pressure was an improved correlation to the previous attempts, it is clear that the data do not fit a linear model. More advanced regression work would need to be conducted to determine a consistent correlation between fuel autoignition and its composition, without resorting to building kinetic mechanisms. The ID time should relate back to the chemical composition as well as the temperature and pressure conditions of the test. Though a clear correlation was not determined, the research provided valuable information about the fuel set and 3D surfaces of fuel ID are more indicative of knock resistance that the two engine conditions run with RON and MON tests. Most importantly, crucial information was learned about the AFIDA and progress was made in the ability to test gasoline range fuels in this new highly flexible CVCC. While the IQT has been extremely useful for the study of PRFs and other simple component blends, research was approaching the limits of its capabilities. In order to examine fuels with lower boiling fractions more reflective of gasolines, it is necessary to migrate research to the AFIDA. This study is valuable as it is the first study of its kind in the AFIDA with gasoline range fuels. It is possible a more meaningful correlation could be made with more advanced regression analysis.

4.2 Future Work

Going forward the surrogate blend for FACE B will be tested in the AFIDA, under the same conditions as the fuel set in this study, to determine its success in replicating FACE B. This

study was more focused on testing the fuel set, while performing simple correlation work. Future work will be conducted with these results to implement a more complex regression analysis between the ID time and the fuel composition. Currently the significant change in Φ from 1.04 to 0.20 is not desirable and adds another changing variable, which most similar studies keep relatively constant. For more studies like this to progress with gasoline range fuels in the AFIDA it will be important to modify the fuel injection system with a larger rail volume in order to reach a Φ of 1 at all desirable test conditions (up to 30 bar and down to 400 °C). Future work will also look to study more complex gasoline surrogates and blends, which are not able to be studied in tho other CVCCs, RCMs, or shock tubes that are currently used in this area of research.

Citations

[1] Energy Information Administration, Monthly Energy Review, August 2017, Tables 2.1 and 2.5. https://www.eia.gov/totalenergy/data/monthly/archive/00351708.pdf

[2] U.S. Department of Energy, Vehicle Technologies Office, "Transportation Analysis Fact of the Week #996", September 27, 2017. https://energy.gov/eere/vehicles/articles/fact-996-september-25-2017-transportation-accounts-nearly-three-quarters

[3] Oak Ridge National Laboratory, Transportation Energy Data Book: Edition 35, October 2016, ORNL-6992, Table 1.16. http://cta.ornl.gov/data/tedb35/Edition35_Full_Doc.pdf

[4] Mittal, V., Heywood, J.B., 2009. The Shift in Relevance of Fuel RON and MON to Knock Onset in Modern SI Engines Over the Last 70 Years. SAE International Journal of Engines 2, 1–10. https://doi.org/10.4271/2009-01-2622

[5] Mittal, V., Heywood, J.B., 2008. The Relevance of Fuel RON and MON to Knock Onset in Modern SI Engines. https://doi.org/10.4271/2008-01-2414

[6] Dr, Y.A.C., Boles, M.A., 2014. Thermodynamics: An Engineering Approach, 8 edition. ed. McGraw-Hill Education, New York, NY.

[7] Tatarevic, B., n.d. The Truth About Gas! Does Premium Fuel Perform Better? – Hoonable.

[8] Szybist, J.P., Splitter, D.A., 2017. Pressure and temperature effects on fuels with varying octane sensitivity at high load in SI engines. Combustion and Flame 177, 49–66. https://doi.org/10.1016/j.combustflame.2016.12.002

[9] ASTM D2699 - 13b, Standard Test Method for Research Octane Number of Spark-Ignition Engine Fuel. Annual Book of ASTM Standards, Vol. 5.05, 2013. https://doi.org/10.1520/D2699

[10] ASTM D2700 - 13b, Standard Test Method for Motor Octane Number of Spark-Ignition Engine Fuel. Annual Book of ASTM Standards, Vol. 5.05, 2013. https://doi.org/10.1520/D2700-17

[11] Sluder, C.S., Szybist, J.P., McCormick, R.L., Ratcliff, M.A., Zigler, B.T., 2016. Exploring the Relationship Between Octane Sensitivity and Heat-of-Vaporization. SAE International Journal of Fuels and Lubricants 9, 80–90. https://doi.org/10.4271/2016-01-0836

[12] Stein, R.A., Polovina, D., Roth, K., Foster, M., Lynskey, M., Whiting, T., Anderson, J.E., Shelby, M.H., Leone, T.G., VanderGriend, S., 2012. Effect of Heat of Vaporization, Chemical Octane, and Sensitivity on Knock Limit for Ethanol - Gasoline Blends. SAE International Journal of Fuels and Lubricants 5, 823–843. https://doi.org/10.4271/2012-01-1277

[13] Anderson, J.E., Leone, T.G., Shelby, M.H., Wallington, T.J., Bizub, J.J., Foster, M., Lynskey, M.G., Polovina, D., 2012. Octane Numbers of Ethanol-Gasoline Blends: Measurements and Novel Estimation Method from Molar Composition. https://doi.org/10.4271/2012-01-1274

[14] Davidson, D.F., Haylett, D.R., Hanson, R.K., 2008. Development of an aerosol shock tube for kinetic studies of low-vapor-pressure fuels. Combustion and Flame 155, 108–117. https://doi.org/10.1016/j.combustflame.2008.01.006

[15] Shen, H.-P.S., Oehlschlaeger, M.A., 2009. The autoignition of C8H10 aromatics at moderate temperatures and elevated pressures. Combustion and Flame 156, 1053–1062. https://doi.org/10.1016/j.combustflame.2008.11.015

[16] Allen, C., Mittal, G., Sung, C.-J., Toulson, E., Lee, T., 2011. An aerosol rapid compression machine for studying energetic-nanoparticle-enhanced combustion of liquid fuels. Proceedings of the Combustion Institute 33, 3367–3374. https://doi.org/10.1016/j.proci.2010.06.007

[17] Karwat, D.M.A., Wagnon, S.W., Teini, P.D., Wooldridge, M.S., 2011. On the Chemical Kinetics of n-Butanol: Ignition and Speciation Studies. J. Phys. Chem. A 115, 4909–4921. https://doi.org/10.1021/jp200905n

[18] Fisher, B.T., Allen, J.C., Hancock, R.L., Bittle, J.A., 2017. Evaluating the Potential of a Direct-Injection Constant-Volume Combustion Chamber as a Tool to Validate Chemical-Kinetic Models for Liquid Fuels. Combustion Science and Technology 189, 1–23. https://doi.org/10.1080/00102202.2016.1193015

[19] Bogin, G., Dean, A.M., Ratcliff, M.A., Luecke, J., Zigler, B.T., 2010. Expanding the Experimental Capabilities of the Ignition Quality Tester for Autoigniting Fuels. SAE Int. J. Fuels Lubr. 3, 353–367. https://doi.org/10.4271/2010-01-0741

[20] Tekawade, A., Oehlschlaeger, M.A., 2016. An experimental study of the spray ignition of alkanes. Fuel 185, 381–393. https://doi.org/10.1016/j.fuel.2016.07.108

[21] Coordinating Research Council,. About CRC. https://crcao.org/about/index.html.

[22] Coordinating Research Council, INC, 2017. CRC ANNUAL REPORT 2017.

[23] M. A. Ratcliff, J. Burton, P. Sindler, R. L. McCormick, L. Fouts, and E. Christensen,. Effects of Heat of Vaporization and Octane Sensitivity on Knock-Limited Spark Ignition Engine Performance. under review by SAE International.

[24] Foong, T.M., Morganti, K.J., Brear, M.J., da Silva, G., Yang, Y., Dryer, F.L., 2014. The octane numbers of ethanol blended with gasoline and its surrogates. Fuel 115, 727–739. https://doi.org/10.1016/j.fuel.2013.07.105

[25] Morgan, N., Smallbone, A., Bhave, A., Kraft, M., Cracknell, R., Kalghatgi, G., 2010. Mapping surrogate gasoline compositions into RON/MON space. Combustion and Flame 157, 1122–1131. https://doi.org/10.1016/j.combustflame.2010.02.003

[26] Cannella, W., Foster, M., Gunter, G., Leppard, W., 2014. FACE GASOLINES AND BLENDS WITH ETHANOL: DETAILED CHARACTERIZATION OF PHYSICAL AND CHEMICAL PROPERTIES (No. AVFL-24). Coordinating Research Council, Inc.

[27] Allard, L.N., Webster, G.D., Hole, N.J., Ryan, T.W., Ott, D., Fairbridge, C.W., 1996. Diesel Fuel Ignition Quality as Determined in the Ignition Quality Tester (IQT). https://doi.org/10.4271/961182

[28] Allard, L.N., Hole, N.J., Webster, G.D., Ryan, T.W., Ott, D., Beregszazy, A., Fairbridge, C.W., Cooley, J., Mitchell, K., Richardson, E.K., Elliot, N.G., Rickeard, D.J., 1997. Diesel Fuel Ignition Quality as Determined in the Ignition Quality Tester (IQT) - Part II. https://doi.org/10.4271/971636

[29] Allard, L.N., Webster, G.D., Ryan, T.W., Baker, G., Beregszaszy, A., Fairbridge, C.W., Ecker, A., Rath, J., 1999. Analysis of the Ignition Behaviour of the ASTM D-613 Primary Reference Fuels and Full Boiling Range Diesel Fuels in the Ignition Quality Tester (IQT™) - Part III. https://doi.org/10.4271/1999-01-3591

[30] Allard, L.N., Webster, G.D., Ryan, T.W., Matheaus, A.C., Baker, G., Beregszaszy, A., Read, H., Mortimer, K., Jones, G., 2001. Diesel Fuel Ignition Quality as Determined in the Ignition Quality Tester (IQT™) - Part IV. https://doi.org/10.4271/2001-01-3527

[31] ASTM D6890-16e1, Standard Test Method for Determination of Ignition Delay and Derived Cetane Number (DCN) of Diesel Fuel Oils by Combustion in a Constant Volume Chamber. ASTM International. West Conshohocken, PA, 2016. https://doi.org/10.1520/D6890-16E01

[32] ASTM D613-17b, Standard Test Method for Cetane Number of Diesel Fuel Oil. ASTM International. West Conshohocken, PA, 2017. https://doi.org/10.1520/D0613-17B

[33] Bogin, G.E., Jr., Luecke, J., Ratcliff, M.A., Osecky, E., Zigler, B.T., 2016. Effects of iso-octane/ethanol blend ratios on the observance of negative temperature coefficient behavior within the Ignition Quality Tester. Fuel 186, 82–90. https://doi.org/10.1016/j.fuel.2016.08.021

[34] Webster, G., n.d. Ignition Quality Tester (IQT(tm)) [WWW Document]. URL http://aet.ca/files/resourcesmodule/@random428b4e06ecd32/1254780127_IQT_Brochure___June_18__2009_with_EN590__stainless_steel_mod.pdf

[35] Bogin, G.E., Osecky, E., Ratcliff, M.A., Luecke, J., He, X., Zigler, B.T., Dean, A.M., 2013. Ignition Quality Tester (IQT) Investigation of the Negative Temperature Coefficient Region of Alkane Autoignition. Energy Fuels 27, 1632–1642. https://doi.org/10.1021/ef301738b

[36] Seidenspinner, P., Härtl, M., Wilharm, T., and Wachtmeister, G., 2015. Cetane Number Determination by Advanced Fuel Ignition Delay Analysis in a New Constant Volume Combustion Chamber. http://doi.org/10.4271/2015-01-0798.

[37] AFIDA manual, ASG Analytik-Service Gesellschaft mbH, Germany

[38] Audi Technology Portal - Piezo-Injektoren [WWW Document], n.d. . Audi Technology Portal. URL https://www.audi-technology-portal.de/de/antrieb/tdi-motoren/piezo-injektoren?c=image:506 (accessed 11.1.17).

[39] Kolodziej, C., Kodavasal, J., Ciatti, S., Som, S. et al., 2015. Achieving Stable Engine Operation of Gasoline Compression Ignition Using 87 AKI Gasoline Down to Idle. SAE Technical Paper 2015-01-0832. http://doi.org/10.4271/2015-01-0832.

[40] Osecky, E.M., Bogin, G.E., Jr., Villano, S.M., Ratcliff, M.A., Luecke, J., Zigler, B.T., Dean, A.M., 2016. Investigation of Iso-octane Ignition and Validation of a Multizone Modeling Method in an Ignition Quality Tester. Energy and Fuels 30, 9761–9771. https://doi.org/10.1021/acs.energyfuels.6b01406

[41] Chupka, G.M., Christensen, E., Fouts, L., Alleman, T.L., Ratcliff, M.A., McCormick, R.L., 2015. Heat of Vaporization Measurements for Ethanol Blends Up To 50 Volume Percent in Several Hydrocarbon Blendstocks and Implications for Knock in SI Engines. SAE International Journal of Fuels and Lubricants 8. https://doi.org/10.4271/2015-01-0763

[42] ASTM D6729-14, Standard Test Method for Determination of Individual Components in Spark Ignition Engine Fuels by 100 Metre Capillary High Resolution Gas Chromatography, ASTM International. West Conshohocken, PA, 2014. https://doi.org/10.1520/D6729-14

[43] Morgan, N., Smallbone, A., Bhave, A., Kraft, M., Cracknell, R., Kalghatgi, G., 2010. Mapping surrogate gasoline compositions into RON/MON space. Combustion and Flame 157, 1122–1131. https://doi.org/10.1016/j.combustflame.2010.02.003

[44] Ratcliff, M.A., Burton, J., Sindler, P., Christensen, E., Fouts, L., Chupka, G.M., McCormick, R.L., 2016. Knock Resistance and Fine Particle Emissions for Several Biomass-Derived Oxygenates in a Direct-Injection Spark-Ignition Engine. SAE International Journal of Fuels and Lubricants 9, 59–70. https://doi.org/10.4271/2016-01-0705

[45] Aikawa, K., Sakurai, T., Jetter, J.J., 2010. Development of a Predictive Model for Gasoline Vehicle Particulate Matter Emissions. SAE International Journal of Fuels and Lubricants 3, 610–622. https://doi.org/10.4271/2010-01-2115

[46] October 31, 2017, Personal communication with Dr. Scott Wagnon, Lawrence Livermore National Laboratory.

Appendix A:

Detailed Hydrocarbon Analysis

Table A- 1: Detailed hydrocarbon analysis of FACE B summary by group, courtesy of Earl Christensen of NREL.

GROUP	%WGT	%VOL	%MOL	AREA	AVERAGE_ MW	AVERAGE_ SG
Paraffin	6.530	7.476	10.143	1722.538	6.614	0.045
I-Paraffins	85.635	86.251	82.486	22854.648	86.742	0.592
Aromatics	7.440	5.936	7.098	2140.812	7.537	0.051
Mono-Aromatics	7.440	5.936	7.098	2140.812	7.537	0.051
Naphthalenes	0.000	0.000	0.000	0.000	0.000	0.000
Indanes	0.000	0.000	0.000	0.000	0.000	0.000
Indenes	0.000	0.000	0.000	0.000	0.000	0.000
Naphthenes	0.004	0.004	0.006	1.146	0.004	0.000
Mono-Naphthenes	0.004	0.004	0.006	1.146	0.004	0.000
Di/Bicyclo-Naphthenes	0.000	0.000	0.000	0.000	0.000	0.000
Olefins	0.025	0.024	0.019	6.737	0.025	0.000
n-Olefins	0.016	0.015	0.013	4.401	0.016	0.000
Iso-Olefins	0.009	0.008	0.006	2.337	0.009	0.000
Naphtheno-Olefins	0.000	0.000	0.000	0.000	0.000	0.000
Di-Olefins	0.000	0.000	0.000	0.000	0.000	0.000
Oxygenates	0.000	0.000	0.000	0.000	0.000	0.000
Unidentified	0.366	0.309	0.247	108.902	0.371	0.003
Plus	0.000	0.000	0.000	0.000	0.000	0.000

Table A- 2: Detailed hydrocarbon analysis of FACE B summary by carbon weight percent, courtesy of Earl Christensen of NREL.

Carbon#	Paraffin	I-Paraffins	Aromatics	Naphthenes	Olefins	Oxygenates	Plus	Total
1	--	--	--	--	--	--	--	0.000
2	--	--	--	--	--	--	--	0.000
3	--	--	--	--	--	--	--	0.000
4	3.146	0.070	--	--	--	--	--	3.215
5	3.237	9.088	--	0.004	--	--	--	12.329
6	0.017	1.240	--	--	--	--	--	1.257
7	0.005	13.501	--	--	--	--	--	13.506
8	--	59.626	7.434	--	--	--	--	67.060
9	0.100	1.672	0.006	--	0.016	--	--	1.794
10	--	0.388	--	--	0.009	--	--	0.397
11	--	0.050	--	--	--	--	--	0.050
12	--	--	--	--	--	--	--	0.000
13	--	--	--	--	--	--	--	0.000

14	0.025	--	--	--	--	--	--	0.025
15	--	--	--	--	--	--	--	0.000
TOTAL	6.530	85.635	7.440	0.004	0.025	0.000	0.000	99.634
						UNKNOWNS		0.366
						GRAND_TOTAL		100.000

Table A- 3: DHA components listed by group in weight volume and mole percent, courtesy of Earl Christensen of NREL.

Group	Time	Ri	Component	%Wgt	%Vol	%Mol	Area	Average_ MW	Average_ SG
Paraffin	10.142	400.00	n-Butane	3.146	3.759	5.482	826.590	3.186	0.022
Paraffin	18.046	500.00	n-Pentane	3.237	3.575	4.545	856.556	3.279	0.022
Paraffin	34.923	600.00	n-Hexane	0.017	0.018	0.020	4.580	0.017	0.000
Paraffin	55.643	700.00	n-heptane	0.005	0.005	0.005	1.311	0.005	0.000
Paraffin	87.368	900.00	n-Nonane	0.100	0.096	0.079	26.686	0.101	0.001
Paraffin	122.200	1400.00	n-Tetradecane	0.025	0.023	0.013	6.815	0.026	0.000
I-Paraffins	8.959	354.37	i-Butane	0.070	0.086	0.121	18.304	0.071	0.000
I-Paraffins	10.753	410.19	2,2-Dimethylpropane	0.012	0.014	0.016	3.096	0.012	0.000
I-Paraffins	15.085	468.92	i-Pentane	9.076	10.131	12.742	2401.562	9.193	0.063
I-Paraffins	27.840	565.68	2,3-Dimethylbutane	0.851	0.889	1.000	225.967	0.862	0.006
I-Paraffins	28.873	571.19	2-Methylpentane	0.259	0.275	0.305	68.930	0.263	0.002
I-Paraffins	31.387	583.84	3-Methylpentane	0.130	0.136	0.153	34.592	0.132	0.001
I-Paraffins	40.913	633.97	2,4-Dimethylpentane	4.226	4.345	4.271	1127.057	4.280	0.029
I-Paraffins	41.435	636.69	2,2,3-Trimethylbutane	0.017	0.017	0.017	4.587	0.017	0.000
I-Paraffins	48.803	671.80	2-Methylhexane	9.083	9.257	9.181	2422.565	9.200	0.063
I-Paraffins	50.462	678.98	3-Methylhexane	0.176	0.177	0.178	46.986	0.178	0.001
I-Paraffins	53.104	689.93	2,2,4-Trimethylpentane	39.137	39.123	34.704	10459.763	39.643	0.271
I-Paraffins	61.933	736.59	2,2,3-	0.673	0.650	0.596	179.776	0.681	0.005

			Trimethylpentane						
I-Paraffins	62.192	738.02	2,5-Dimethylhexane	1.308	1.304	1.159	349.470	1.325	0.009
I-Paraffins	62.503	739.73	2,4-Dimethylhexane	1.865	1.842	1.654	498.519	1.889	0.013
I-Paraffins	65.393	755.21	2,3,4-Trimethylpentane	8.645	8.316	7.666	2310.388	8.756	0.060
I-Paraffins	66.013	758.44	2,3,3-Trimethylpentane	5.852	5.574	5.189	1564.075	5.928	0.040
I-Paraffins	67.666	766.91	2,3-Dimethylhexane	1.735	1.686	1.539	463.822	1.758	0.012
I-Paraffins	67.778	767.47	2-Methyl-3-ethylpentane	0.051	0.049	0.045	13.552	0.051	0.000
I-Paraffins	68.919	773.19	2-Methylheptane	0.032	0.032	0.029	8.620	0.033	0.000
I-Paraffins	69.143	774.31	4-Methylheptane	0.147	0.145	0.131	39.358	0.149	0.001
I-Paraffins	69.268	774.92	3,4-Dimethylhexane	0.148	0.142	0.131	39.445	0.149	0.001
I-Paraffins	70.186	779.43	3-Methylheptane	0.033	0.033	0.030	8.892	0.034	0.000
I-Paraffins	71.987	788.11	2,2,5-Trimethylhexane	1.203	1.176	0.950	322.096	1.218	0.008
I-Paraffins	72.896	792.40	2,2,4-Trimethylhexane	0.020	0.019	0.016	5.355	0.020	0.000
I-Paraffins	76.818	819.00	2,3,5-Trimethylhexane	0.210	0.201	0.166	56.124	0.212	0.001
I-Paraffins	77.944	828.15	2,4-Dimethylheptane	0.037	0.036	0.030	10.006	0.038	0.000
I-Paraffins	78.849	835.41	2,6-Dimethylheptane	0.013	0.013	0.011	3.613	0.014	0.000
I-Paraffins	79.702	842.17	2,5-Dimethylheptane	0.061	0.059	0.048	16.392	0.062	0.000
I-Paraffins	79.846	843.31	2-Methyl-4-ethylhexane	0.006	0.006	0.005	1.703	0.006	0.000

I-Paraffins	81.250	854.27	3,3-Diethylpentane	0.016	0.015	0.013	4.330	0.016	0.000
I-Paraffins	82.328	862.56	2,3-Dimethylheptane	0.067	0.064	0.053	17.913	0.068	0.000
I-Paraffins	82.558	864.30	3,5-Dimethylheptane	0.007	0.007	0.006	1.985	0.008	0.000
I-Paraffins	82.658	865.07	4-Ethylheptane	0.010	0.010	0.008	2.795	0.011	0.000
I-Paraffins	83.321	870.09	Heptane, 3-ethyl-	0.005	0.005	0.004	1.379	0.005	0.000
I-Paraffins	83.448	871.04	2-Methyloctane	0.007	0.006	0.005	1.746	0.007	0.000
I-Paraffins	84.240	876.99	3-Methyloctane	0.008	0.008	0.007	2.241	0.008	0.000
I-Paraffins	85.206	884.15	C10 - Isoparaffin - 2	0.104	0.099	0.074	27.993	0.106	0.001
I-Paraffins	85.966	889.74	2,2,4-trimethylheptane	0.185	0.175	0.131	49.508	0.187	0.001
I-Paraffins	89.351	920.43	2,3,6-trimethylheptane	0.049	0.034	0.035	13.208	0.050	0.000
I-Paraffins	89.553	922.50	2,2-Dimethyloctane	0.019	0.018	0.014	5.111	0.019	0.000
I-Paraffins	90.321	930.33	C10 - IsoParaffin - 2(1)	0.004	0.004	0.003	1.084	0.004	0.000
I-Paraffins	90.849	935.68	2,4-Dimethyloctane	0.011	0.011	0.008	3.019	0.011	0.000
I-Paraffins	93.326	960.33	2,3-Dimethyloctane(1)	0.006	0.006	0.004	1.679	0.006	0.000
I-Paraffins	94.166	968.54	C11-Isoparaffin-1	0.050	0.047	0.033	13.512	0.051	0.000
I-Paraffins	95.398	980.45	C10 - IsoParaffin - 5	0.009	0.009	0.007	2.535	0.010	0.000
Mono-Aromatics	80.863	851.26	Ethylbenzene	1.125	0.898	1.074	323.755	1.140	0.008
Mono-Aromatics	82.011	860.13	m-Xylene	3.421	2.738	3.264	984.294	3.465	0.024
Mono-Aromatics	82.142	861.13	p-Xylene	1.471	1.182	1.404	423.287	1.490	0.010
Mono-Aromatics	84.737	880.68	o-Xylene	1.417	1.113	1.352	407.643	1.435	0.010

Mono-Aromatics	88.603	912.73	i-Propylbenzene	0.006	0.005	0.005	1.833	0.006	0.000
Mono-Naphthenes	27.168	561.98	Cyclopentane	0.004	0.004	0.006	1.146	0.004	0.000
n-Olefins	84.638	879.95	C9-isoolefin	0.009	0.009	0.007	2.437	0.009	0.000
n-Olefins	88.917	915.97	c-Nonene-2	0.007	0.006	0.006	1.964	0.007	0.000
Iso-Olefins	87.443	900.66	C10 - IsoOlefin - 1	0.009	0.008	0.006	2.337	0.009	0.000
Unidentified	75.343	806.81	Unidentified	0.050	0.042	0.034	14.966	0.051	0.000
Unidentified	81.039	852.63	Unidentified	0.016	0.014	0.011	4.799	0.016	0.000
Unidentified	88.816	914.93	Unidentified	0.007	0.006	0.005	2.120	0.007	0.000
Unidentified	95.771	984.03	Unidentified	0.005	0.004	0.003	1.416	0.005	0.000
Unidentified	133.832	2153.76	Unidentified	0.013	0.011	0.009	3.887	0.013	0.000
Unidentified	141.383	2599.19	Unidentified	0.275	0.232	0.186	81.713	0.278	0.002

Table A- 4: DHA for PRF100 in weight, volume and molar percent of the components; the percent carbon, hydrogen and oxygen; and particulate matter index, average density.

COMPONENT	%WGT	%VOL	%MOL
2-Methylhexane	0.04	0.04	0.05
2,2,4-Trimethylpentane	99.89	99.89	99.88
2,2-Dimethylhexane	0.07	0.07	0.07
%H	15.9		
PMI	0.19		

Table A- 5: DHA for TRF99.8 in weight, volume and molar percent of the components; the percent carbon, hydrogen and oxygen; and particulate matter index, average density.

COMPONENT	%WGT	%VOL	%MOL
n-heptane	13.42	16.09	12.69
2,2,4-Trimethylpentane	8.70	10.30	7.21
Toluene	77.86	73.59	80.08
Ethylbenzene	0.02	0.02	0.02
Density (g/mL)at 15C	0.8235		
%H	10.4		
PMI	0.96		

Table A- 6: DHA for TRF88 in weight, volume and molar percent of the components; the percent carbon, hydrogen and oxygen; and particulate matter index, average density.

COMPONENT	%WGT	%VOL	%MOL
n-heptane	19.57	21.17	20.16
2-Methylhexane	0.04	0.04	0.04
3-Methylhexane	0.02	0.02	0.02
2,2,4-Trimethylpentane	47.12	50.38	42.57
2,2-Dimethylhexane	0.03	0.03	0.03
Toluene	33.13	28.27	37.11
Methylcyclohexane	0.02	0.02	0.03
Density (g/mL) at 15C	0.7439		
H wt%	13.6		
C wt%	86.4		
PMI	0.51		

Table A- 7: DHA for E25 TRF88 in weight, volume and molar percent of the components; the percent carbon, hydrogen and oxygen; and particulate matter index, average density, average molecular weight, HOV, LHV.

COMPONENT	%WGT	%VOL
n-heptane	14.76	16.20
2-Methylhexane	0.03	0.03
3-Methylhexane	0.02	0.02
2,2,4-Trimethylpentane	35.54	38.55
2,2-Dimethylhexane	0.02	0.03
Toluene	24.99	21.63
Methylcyclohexane	0.02	0.02
Ethanol	24.58	23.49
Density at 15C	0.7583	
C wt%	78.0	
H wt%	13.4	
O wt%	8.5	
PMI	0.40	

Table A- 8: DHA for E40 + 2% TRF81 in weight, volume and molar percent of the components; the percent carbon, hydrogen and oxygen; and particulate matter index, average density, average molecular weight, HOV, LHV.

COMPONENT	WT%	VOL%	MOL%
n-heptane	21.6	24.45	14.6
2,2,4-Trimethylpentane	10.1	11.23	5.9
Toluene	28.0	24.95	20.5
Ethanol	40.3	39.44	59.0
Sum	100.0	100.1	100.0

C wt%	73.2		
H wt%	12.8		
O wt%	14.0		
Ave MW	67.5		
PMI	0.41		
HOV kJ/kg	594.6		
Density (g/mL) at 15C	0.7725		
LHV J/g	36213		

Table A- 9: DHA for E20 + 2% p-cresol in TRF88 in weight, volume and molar percent of the components; the percent carbon, hydrogen and oxygen; and particulate matter index, average density, average molecular weight, HOV, LHV.

COMPONENT	WT%	VOL%	MOL%
n-heptane	14.5	16.1	11.9
2,2,4-Trimethylpentane	35.4	38.8	25.5
Toluene	27.6	24.2	24.6
Ethanol	20.4	19.7	36.5
Cresol	2.0	1.5	1.5
C wt%	79.3		
H wt%	13.3		
O wt%	7.4		
Ave MW	82.2		
PMI	0.70		
HOV kJ/kg, 25C	472.0		
Density (g/mL)at 15C	0.7592		

Table A- 10: DHA for E20 + 6% Anisole in TRF88 in weight, volume and molar percent of the components; the percent carbon, hydrogen and oxygen; and particulate matter index, average density, average molecular weight, HOV, LHV.

COMPONENT	WT%	VOL%	MOL%
n-heptane	13.8	15.5	11.3
2,2,4-Trimethylpentane	33.6	37.3	24.2
Toluene	26.2	23.3	23.5
ethanol	20.3	19.7	36.3
anisole	6.2	4.8	4.7
C wt%	79.0		
H wt%	13.0		
O wt%	8.0		
Ave MW	82.5		
PMI	0.61		
HOV kJ/kg, 25C	471.7		
Density at 15C	0.7691		

Appendix B:

ID Data

Table B- 1: Ignition delay time at specified pressure, temperature, and Φ for PRF 100 from the tests in the AFIDA.

Fuel ID	PRF 100			
Temp °C	1000/Temp [K]	ID time (ms)	Pressure (bar)	Φ
725	1.001853429	32.761	5	1.04
700	1.027590813	45.203	5	1.02
675	1.05468544	62.353	5	1.00
650	1.083247576	91.276	5	0.98
625	1.113399766	134.203	5	0.96
600	1.145278589	195.253	5	0.94
575	1.179036727	271.709	5	0.92
550	1.214845411	377.08	5	0.90
525	1.252897325	508.349	5	0.88
500	1.293410076	534.553	5	0.86
475	1.336630355	497.769	5	0.84
450	1.382838968	455.886	5	0.82
425	1.432356943	416.139	5	0.80
725	1.001853429	23.90	10	0.57
700	1.027590813	31.323	10	0.56
675	1.05468544	41.56	10	0.55
650	1.083247576	61.494	10	0.54
625	1.113399766	88.303	10	0.52
600	1.145278589	123.849	10	0.51
575	1.179036727	166.336	10	0.50
550	1.214845411	188.396	10	0.49
525	1.252897325	183.996	10	0.48
500	1.293410076	177.653	10	0.47
475	1.336630355	176.363	10	0.46
450	1.382838968	174.289	10	0.45
425	1.432356943	180.24	10	0.43
725	1.001853429	12.88	20	0.30
700	1.027590813	17.76	20	0.29
675	1.05468544	23.34	20	0.29
650	1.083247576	30.607	20	0.28
625	1.113399766	40.426	20	0.27
600	1.145278589	47.96	20	0.27

575	1.179036727	52.04	20	0.26
550	1.214845411	57.16	20	0.26
525	1.252897325	61.88	20	0.25
500	1.293410076	70.76	20	0.25
475	1.336630355	81.88	20	0.24
450	1.382838968	95.20	20	0.23
425	1.432356943	115.373	20	0.23
725	1.001853429	7.37	30	0.20
700	1.027590813	9.242	30	0.20
675	1.05468544	11.16	30	0.19
650	1.083247576	12.76	30	0.19
625	1.113399766	14.72	30	0.19
600	1.145278589	17.32	30	0.18
575	1.179036727	20.95	30	0.18
550	1.214845411	25.87	30	0.17
525	1.252897325	32.32	30	0.17
500	1.293410076	39.85	30	0.17
475	1.336630355	52.40	30	0.16
450	1.382838968	69.473	30	0.16
425	1.432356943	104.039	30	0.15

Table B- 2: Ignition delay time at specified pressure, temperature, and Φ for TSF 99.8 from the tests in the AFIDA.

Fuel ID	TSF 99.8			
Temp °C	1000/Temp [K]	ID time (ms)	Pressure (bar)	Φ
725	1.001853429	45.80	5	1.04
700	1.027590813	61.323	5	1.02
675	1.05468544	85.006	5	1.00
650	1.083247576	117.963	5	0.98
625	1.113399766	171.403	5	0.96
600	1.145278589	212.176	5	0.94
575	1.179036727	232.88	5	0.92
550	1.214845411	250.059	5	0.90
525	1.252897325	277.799	5	0.88
500	1.293410076	323.336	5	0.86
475	1.336630355	381.256	5	0.84
450	1.382838968	460.106	5	0.82
425	1.432356943	543.76	5	0.80
725	1.001853429	28.74	10	0.57
700	1.027590813	35.13	10	0.56
675	1.05468544	47.80	10	0.55

650	1.083247576	62.36	10	0.54
625	1.113399766	87.72	10	0.52
600	1.145278589	104.536	10	0.51
575	1.179036727	120.00	10	0.50
550	1.214845411	136.796	10	0.49
525	1.252897325	168.88	10	0.48
500	1.293410076	216.52	10	0.47
475	1.336630355	301.52	10	0.46
450	1.382838968	450.16	10	0.45
725	1.001853429	17.70	20	0.30
700	1.027590813	22.89	20	0.29
675	1.05468544	30.38	20	0.29
650	1.083247576	38.51	20	0.28
625	1.113399766	45.04	20	0.27
600	1.145278589	52.28	20	0.27
575	1.179036727	63.80	20	0.26
550	1.214845411	84.08	20	0.26
525	1.252897325	119.52	20	0.25
500	1.293410076	182.24	20	0.25
475	1.336630355	334.853	20	0.24
725	1.001853429	10.324	30	0.20
700	1.027590813	13.56	30	0.20
675	1.05468544	16.84	30	0.19
650	1.083247576	21.03	30	0.19
625	1.113399766	25.86	30	0.19
600	1.145278589	33.05	30	0.18
575	1.179036727	46.16	30	0.18
550	1.214845411	69.04	30	0.17
525	1.252897325	111.12	30	0.17
500	1.293410076	188.24	30	0.17
475	1.336630355	381.236	30	0.16

Table B- 3: Ignition delay time at specified pressure, temperature, and Φ for E25 in TSF 88 from the tests in the AFIDA.

Fuel ID	E25 in TRF88			
Temp °C	1000/Temp [K]	ID time (ms)	Pressure (bar)	Φ
725	1.001853429	26.32	5	1.04
700	1.027590813	34.655	5	1.02
675	1.05468544	45.08	5	1.00
650	1.083247576	61.643	5	0.98
625	1.113399766	85.766	5	0.96

600	1.145278589	119.626	5	0.94
575	1.179036727	160.989	5	0.92
550	1.214845411	208.079	5	0.90
525	1.252897325	250.613	5	0.88
500	1.293410076	288.52	5	0.86
475	1.336630355	317.526	5	0.84
450	1.382838968	345.163	5	0.82
425	1.432356943	410.08	5	0.80
725	1.001853429	18.070	10	0.57
700	1.027590813	25.345	10	0.56
675	1.05468544	32.704	10	0.55
650	1.083247576	42.92	10	0.54
625	1.113399766	62.776	10	0.52
600	1.145278589	87.399	10	0.51
575	1.179036727	115.013	10	0.50
550	1.214845411	134.739	10	0.49
525	1.252897325	150.68	10	0.48
500	1.293410076	162.88	10	0.47
475	1.336630355	189.52	10	0.46
450	1.382838968	225.946	10	0.45
425	1.432356943	290.719	10	0.44
725	1.001853429	11.16	20	0.30
700	1.027590813	15.24	20	0.29
675	1.05468544	20.42	20	0.29
650	1.083247576	26.88	20	0.28
625	1.113399766	38.66	20	0.27
600	1.145278589	48.52	20	0.27
575	1.179036727	57.40	20	0.26
550	1.214845411	66.84	20	0.26
525	1.252897325	79.84	20	0.25
500	1.293410076	99.609	20	0.25
475	1.336630355	134.40	20	0.24
450	1.382838968	181.52	20	0.23
425	1.432356943	263.12	20	0.23
725	1.001853429	7.39	30	0.20
700	1.027590813	9.95	30	0.20
675	1.05468544	12.713	30	0.19
650	1.083247576	17.28	30	0.19
625	1.113399766	22.41	30	0.19
600	1.145278589	27.92	30	0.18
575	1.179036727	34.00	30	0.18

550	1.214845411	42.68	30	0.17
525	1.252897325	56.76	30	0.17
500	1.293410076	81.04	30	0.17
475	1.336630355	120.88	30	0.16
450	1.382838968	176.40	30	0.16
425	1.432356943	275.44	30	0.15

Table B- 4: Ignition delay time at specified pressure, temperature, and Φ for E40 in TRF71 from the tests in the AFIDA.

Fuel ID	E40 TRF71			
Temp °C	1000/Temp [K]	ID time (ms)	Pressure (bar)	Φ
725	1.001853429	23.09	5	1.04
700	1.027590813	28.90	5	1.02
675	1.05468544	39.85	5	1.00
650	1.083247576	52.513	5	0.98
625	1.113399766	71.859	5	0.96
600	1.145278589	98.283	5	0.94
575	1.179036727	129.499	5	0.92
550	1.214845411	158.473	5	0.90
525	1.252897325	185.24	5	0.88
500	1.293410076	211.08	5	0.86
475	1.336630355	234.64	5	0.84
450	1.382838968	278.84	5	0.82
425	1.432356943	365.736	5	0.80
725	1.001853429	14.72	10	0.57
700	1.027590813	20.72	10	0.56
675	1.05468544	28.364	10	0.55
650	1.083247576	37.12	10	0.54
625	1.113399766	51.306	10	0.52
600	1.145278589	69.509	10	0.51
575	1.179036727	89.625	10	0.50
550	1.214845411	102.843	10	0.49
525	1.252897325	111.44	10	0.48
500	1.293410076	125.64	10	0.47
475	1.336630355	149.44	10	0.46
450	1.382838968	192.20	10	0.45
425	1.432356943	278.093	10	0.43
725	1.001853429	9.90	20	0.30
700	1.027590813	13.48	20	0.29
675	1.05468544	18.43	20	0.29
650	1.083247576	23.92	20	0.28

625	1.113399766	30.08	20	0.27
600	1.145278589	40.76	20	0.27
575	1.179036727	45.959	20	0.26
550	1.214845411	54.536	20	0.26
525	1.252897325	66.133	20	0.25
500	1.293410076	86.52	20	0.25
475	1.336630355	114.60	20	0.24
450	1.382838968	165.16	20	0.23
425	1.432356943	254.28	20	0.23
725	1.001853429	7.20	30	0.20
700	1.027590813	9.28	30	0.20
675	1.05468544	11.744	30	0.19
650	1.083247576	15.52	30	0.19
625	1.113399766	19.78	30	0.19
600	1.145278589	24.42	30	0.18
575	1.179036727	27.02	30	0.18
550	1.214845411	36.02	30	0.17
525	1.252897325	49.04	30	0.17
500	1.293410076	71.60	30	0.17
475	1.336630355	111.36	30	0.16
450	1.382838968	168.88	30	0.16
425	1.432356943	269.32	30	0.15

Table B- 5: Ignition delay time at specified pressure, temperature, and Φ for E20 + 2% p-cresol in TRF88 from the tests in the AFIDA.

Fuel ID	E20 2%pCresol in TRF88			
Temp °C	1000/Temp [K]	ID time (ms)	Pressure (bar)	Φ
725	1.001853429	28.319	5	1.04
700	1.027590813	37.290	5	1.02
675	1.05468544	51.64	5	1.00
650	1.083247576	71.183	5	0.98
625	1.113399766	99.583	5	0.96
600	1.145278589	146.413	5	0.94
575	1.179036727	190.516	5	0.92
550	1.214845411	239.769	5	0.90
525	1.252897325	272.326	5	0.88
500	1.293410076	288.383	5	0.86
475	1.336630355	301.913	5	0.84
450	1.382838968	323.709	5	0.82
425	1.432356943	382.929	5	0.80
725	1.001853429	18.858	10	0.57

700	1.027590813	27.100	10	0.56
675	1.05468544	35.23	10	0.55
650	1.083247576	49.72	10	0.54
625	1.113399766	69.803	10	0.52
600	1.145278589	94.979	10	0.51
575	1.179036727	119.029	10	0.50
550	1.214845411	132.04	10	0.49
525	1.252897325	139.383	10	0.48
500	1.293410076	151.76	10	0.47
475	1.336630355	173.24	10	0.46
450	1.382838968	208.719	10	0.45
425	1.432356943	270.80	10	0.44
725	1.001853429	11.96	20	0.30
700	1.027590813	16.32	20	0.29
675	1.05468544	21.10	20	0.29
650	1.083247576	27.94	20	0.28
625	1.113399766	38.64	20	0.27
600	1.145278589	46.56	20	0.27
575	1.179036727	52.60	20	0.26
550	1.214845411	60.64	20	0.26
525	1.252897325	72.88	20	0.25
500	1.293410076	90.989	20	0.25
475	1.336630355	121.48	20	0.24
450	1.382838968	169.84	20	0.23
425	1.432356943	256.12	20	0.23
725	1.001853429	7.70	30	0.20
700	1.027590813	10.27	30	0.20
675	1.05468544	13.27	30	0.19
650	1.083247576	16.80	30	0.19
625	1.113399766	20.96	30	0.19
600	1.145278589	25.09	30	0.18
575	1.179036727	30.18	30	0.18
550	1.214845411	37.021	30	0.17
525	1.252897325	50.88	30	0.17
500	1.293410076	72.48	30	0.17
475	1.336630355	112.64	30	0.16
450	1.382838968	175.32	30	0.16
425	1.432356943	279.223	30	0.15

Table B- 6: Ignition delay time at specified pressure, temperature, and Φ for E20 + 6% anisole in TRF88 from the tests in the AFIDA.

Fuel ID	E20 6% anisole in TRF88			
Temp °C	1000/Temp [K]	ID time (ms)	Pressure (bar)	Φ
725	1.001853429	26.78	5	1.04
700	1.027590813	33.95	5	1.02
675	1.05468544	45.20	5	1.00
650	1.083247576	64.109	5	0.98
625	1.113399766	90.156	5	0.96
600	1.145278589	125.929	5	0.94
575	1.179036727	169.219	5	0.92
550	1.214845411	216.763	5	0.90
525	1.252897325	253.829	5	0.88
500	1.293410076	283.979	5	0.86
475	1.336630355	308.566	5	0.84
450	1.382838968	335.76	5	0.82
425	1.432356943	394.28	5	0.80
725	1.001853429	17.15	10	0.57
700	1.027590813	25.158	10	0.56
675	1.05468544	33.39	10	0.55
650	1.083247576	46.376	10	0.54
625	1.113399766	64.923	10	0.52
600	1.145278589	89.503	10	0.51
575	1.179036727	113.92	10	0.50
550	1.214845411	133.52	10	0.49
525	1.252897325	146.303	10	0.48
500	1.293410076	162.24	10	0.47
475	1.336630355	190.56	10	0.46
450	1.382838968	231.48	10	0.45
425	1.432356943	297.36	10	0.44
725	1.001853429	11.47	20	0.30
700	1.027590813	15.36	20	0.29
675	1.05468544	20.630	20	0.29
650	1.083247576	26.595	20	0.28
625	1.113399766	36.840	20	0.27
600	1.145278589	47.52	20	0.27
575	1.179036727	55.40	20	0.26
550	1.214845411	64.80	20	0.26
525	1.252897325	78.836	20	0.25
500	1.293410076	103.60	20	0.25
475	1.336630355	138.44	20	0.24

450	1.382838968	196.28	20	0.23
425	1.432356943	292.04	20	0.23
725	1.001853429	7.50	30	0.20
700	1.027590813	9.90	30	0.20
675	1.05468544	12.99	30	0.19
650	1.083247576	16.86	30	0.19
625	1.113399766	21.55	30	0.19
600	1.145278589	26.74	30	0.18
575	1.179036727	32.84	30	0.18
550	1.214845411	41.156	30	0.17
525	1.252897325	58.24	30	0.17
500	1.293410076	83.056	30	0.17
475	1.336630355	126.993	30	0.16
450	1.382838968	199.036	30	0.16
425	1.432356943	327.423	30	0.15

Table B- 7: Ignition delay time at specified pressure, temperature, and Φ for TRF88 from the tests in the AFIDA.

Fuel ID	TRF88			
Temp	1000/Temp	ID time (ms)	Pressure	Phi
725	1.001853429	32.90	5	1.04
700	1.027590813	44.44	5	1.02
675	1.05468544	58.24	5	1.00
650	1.083247576	76.88	5	0.98
625	1.113399766	90.709	5	0.96
600	1.145278589	90.193	5	0.94
575	1.179036727	86.92	5	0.92
550	1.214845411	84.68	5	0.90
525	1.252897325	83.48	5	0.88
500	1.293410076	82.16	5	0.86
475	1.336630355	87.80	5	0.84
450	1.382838968	100.733	5	0.82
425	1.432356943	123.179	5	0.80
725	1.001853429	21.72	10	0.57
700	1.027590813	27.36	10	0.56
675	1.05468544	33.299	10	0.55
650	1.083247576	38.008	10	0.54
625	1.113399766	39.938	10	0.52
600	1.145278589	39.197	10	0.51
575	1.179036727	39.421	10	0.50
550	1.214845411	40.042	10	0.49

525	1.252897325	42.429	10	0.48
500	1.293410076	46.949	10	0.47
475	1.336630355	53.720	10	0.46
450	1.382838968	70.727	10	0.45
425	1.432356943	96.16	10	0.44
725	1.001853429	8.50	20	0.30
700	1.027590813	9.98	20	0.29
675	1.05468544	11.16	20	0.29
650	1.083247576	12.22	20	0.28
625	1.113399766	13.44	20	0.27
600	1.145278589	14.80	20	0.27
575	1.179036727	16.75	20	0.26
550	1.214845411	19.06	20	0.26
525	1.252897325	22.14	20	0.25
500	1.293410076	28.78	20	0.25
475	1.336630355	39.85	20	0.24
450	1.382838968	68.52	20	0.23
425	1.432356943	110.08	20	0.23
725	1.001853429	4.08	30	0.20
700	1.027590813	4.77	30	0.20
675	1.05468544	5.29	30	0.19
650	1.083247576	5.85	30	0.19
625	1.113399766	6.67	30	0.19
600	1.145278589	7.57	30	0.18
575	1.179036727	8.86	30	0.18
550	1.214845411	10.95	30	0.17
525	1.252897325	14.77	30	0.17
500	1.293410076	20.92	30	0.17
475	1.336630355	32.228	30	0.16
450	1.382838968	62.793	30	0.16
425	1.432356943	135.036	30	0.15

Table B- 8: Ignition delay time at specified pressure, temperature, and Φ for E25 FACE B from the tests in the AFIDA.

Fuel ID	E25 in FACE B			
Temp °C	1000/Temp [K]	ID time (ms)	Pressure (bar)	Phi
725	1.001853429	26.37	5	1.04
700	1.027590813	34.62	5	1.02
675	1.05468544	44.40	5	1.00
650	1.083247576	60.886	5	0.98
625	1.113399766	87.319	5	0.96

600	1.145278589	125.676	5	0.94
575	1.179036727	180.633	5	0.92
550	1.214845411	243.833	5	0.90
525	1.252897325	329.96	5	0.88
500	1.293410076	467.56	5	0.86
725	1.001853429	16.80	10	0.57
700	1.027590813	25.943	10	0.56
675	1.05468544	34.80	10	0.55
650	1.083247576	47.20	10	0.53
625	1.113399766	69.32	10	0.52
600	1.145278589	103.68	10	0.51
575	1.179036727	147.360	10	0.50
550	1.214845411	208.28	10	0.49
525	1.252897325	267.76	10	0.48
500	1.293410076	333.463	10	0.47
475	1.336630355	362.04	10	0.46
450	1.382838968	371.96	10	0.45
425	1.432356943	403.76	10	0.43
725	1.001853429	11.28	20	0.30
700	1.027590813	16.11	20	0.29
675	1.05468544	22.29	20	0.29
650	1.083247576	29.98	20	0.28
625	1.113399766	49.56	20	0.27
600	1.145278589	70.76	20	0.27
575	1.179036727	100.84	20	0.26
550	1.214845411	131.56	20	0.26
525	1.252897325	154.08	20	0.25
500	1.293410076	165.48	20	0.24
475	1.336630355	178.56	20	0.24
450	1.382838968	230.20	20	0.23
425	1.432356943	262.40	20	0.23
725	1.001853429	8.25	30	0.20
700	1.027590813	11.38	30	0.20
675	1.05468544	15.57	30	0.19
650	1.083247576	22.66	30	0.19
625	1.113399766	32.94	30	0.19
600	1.145278589	46.60	30	0.18
575	1.179036727	62.96	30	0.18
550	1.214845411	77.76	30	0.17
525	1.252897325	90.08	30	0.17
500	1.293410076	105.52	30	0.17

475	1.336630355	128.12	30	0.16
450	1.382838968	162.32	30	0.16
425	1.432356943	226.52	30	0.15

Table B- 9: Ignition delay time at specified pressure, temperature, and Φ for FACE B from the tests in the AFIDA.

Fuel ID	FACE B			
Temp °C	1000/Temp [K]	ID time (ms)	Pressure (bar)	Phi
725	1.001853429	30.75	5	1.04
700	1.027590813	38.66	5	1.02
675	1.05468544	51.56	5	1.00
650	1.083247576	72.00	5	0.98
625	1.113399766	105.819	5	0.96
600	1.145278589	149.919	5	0.94
575	1.179036727	185.086	5	0.92
550	1.214845411	194.28	5	0.90
525	1.252897325	186.153	5	0.88
500	1.293410076	170.12	5	0.86
475	1.336630355	158.48	5	0.84
450	1.382838968	156.676	5	0.82
425	1.432356943	170.579	5	0.80
725	1.001853429	17.777	10	0.57
700	1.027590813	26.88	10	0.56
675	1.05468544	36.35	10	0.55
650	1.083247576	47.08	10	0.53
625	1.113399766	66.40	10	0.52
600	1.145278589	85.40	10	0.51
575	1.179036727	86.52	10	0.50
550	1.214845411	79.92	10	0.49
525	1.252897325	73.456	10	0.48
500	1.293410076	69.72	10	0.47
475	1.336630355	73.76	10	0.46
450	1.382838968	80.72	10	0.45
425	1.432356943	103.60	10	0.43
725	1.001853429	10.99	20	0.30
700	1.027590813	14.69	20	0.29
675	1.05468544	19.48	20	0.29
650	1.083247576	24.25	20	0.28
625	1.113399766	28.187	20	0.27
600	1.145278589	29.62	20	0.27
575	1.179036727	29.50	20	0.26

550	1.214845411	29.64	20	0.26
525	1.252897325	31.04	20	0.25
500	1.293410076	34.68	20	0.25
475	1.336630355	42.80	20	0.24
450	1.382838968	57.12	20	0.23
425	1.432356943	80.88	20	0.23
725	1.001853429	6.48	30	0.20
700	1.027590813	7.746	30	0.20
675	1.05468544	9.00	30	0.19
650	1.083247576	10.09	30	0.19
625	1.113399766	11.16	30	0.19
600	1.145278589	12.48	30	0.18
575	1.179036727	13.97	30	0.18
550	1.214845411	15.63	30	0.17
525	1.252897325	17.54	30	0.17
500	1.293410076	21.36	30	0.17
475	1.336630355	28.56	30	0.16
450	1.382838968	41.599	30	0.16
425	1.432356943	79.00	30	0.15

Appendix C:

MATLAB Code

C-1: MATLAB Code To Create Surface Plot And Polynomial Curve Fit To Data.

```
%%% importing data
%clear workspace
clear

%import data from excel sheets
Fuel = xlsread('Summary_E40_TRF6x.xlsx');

%assign data to specific arrays for each pressure
pressure = Fuel(1:52,4);
pressure = pressure(:);
ignition_delay = Fuel(1:52,3);
ignition_delay = ignition_delay(:);
temperature = Fuel(1:52,2);
temperature = temperature(:);

%% find polynomial surface fit

[xData, yData, zData] = prepareSurfaceData( pressure, temperature,
ignition_delay );

% Set up fittype and options.
ft = fittype( 'poly34' );

% Fit model to data.
[fitresult, gof] = fit( [xData, yData], zData, ft );

% Create a figure for the plots.
figure( 'Name', 'untitled fit 1' );

% Plot fit with data.
subplot( 2, 1, 1 );
h = plot( fitresult, [xData, yData], zData );
legend( 'E40 in TRF71', 'Location', 'NorthEast' );
% Label axes
xlabel 'Pressure (bar)'
ylabel 'Temperature (1000/ Temp [K])'
zlabel 'Ignition Delay Time (ms)'
grid on
zlim([0 450])
view( -30, 15 );;

% Plot residuals.
subplot( 2, 1, 2 );
h = plot( fitresult, [xData, yData], zData, 'Style', 'Residual' );
legend( h, 'untitled fit 1 - residuals', 'Location', 'NorthEast' );
```

```
% Label axes
xlabel 'Temperature (1000/ temp [K])'
ylabel 'Pressure (bar)'
zlabel 'Ignition Delay Time (ms)'
grid on
view( -83.5, 13.2 );

%% outputt fitt coefficents

p00 = fitresult.p00
p10 = fitresult.p10
p01 = fitresult.p01
p20 = fitresult.p20
p02 = fitresult.p02
p30 = fitresult.p30
p03 = fitresult.p03
p04 = fitresult.p04
p11 = fitresult.p11
p12 = fitresult.p12
p21 = fitresult.p21
p31 = fitresult.p31
p13 = fitresult.p13
p22 = fitresult.p22

E40_TRF6x_coef = [p00, p01, p10, p20, p02, p03, p30, p04, p11, p12, p22, p21,
p13]
```

C-2: MATLAB Code To Apply Linear Regression of ID time to Temperature 1000/T [K] and Φ.

```
Linear regression with the help of Dr. Daily
% Examine Drew's data

close all;clear all;clc;

filedata = 'data/FuelDatathesisall';

load(filedata)


Tinvp5 = Tinv(P==5,:);
phip5 = phi(P==5,:);
IDp5 = ID(P==5,:);


%set up regression wrt 1000/T and phi

x = [ones(size(Tinvp5)) Tinvp5 phip5 ];
y = IDp5;

[b bint,r,rint,stats] = regress(y, x)
stats5=stats

%yfit = b(1)+b(2)*Tinvp5;
```

```
yfit = b(1)+b(2)*Tinvp5+ b(3)*phip5;

figure
loglog(y,yfit,'x',y,y,'o')
xlabel('ID Time (ms)','fontsize',12)
ylabel('ID Time Fit (ms)', 'fontsize',12)
title({'Ignition Delay vs 1000/T[K] and phi',' Regression P = 5 Bar,
0.78<phi<1.04 '}, 'fontsize',14)

% plot and regress P = 10 atm and narrow phi range

Tinvp10 = Tinv(P==10,:);
phip10 = phi(P==10,:);
IDp10 = ID(P==10,:);

% set up regression wrt 1000/T

x = [ones(size(Tinvp10)) Tinvp10 phip10 ];
y = IDp10;

[b bint,r,rint,stats] = regress(y, x)
stats10=stats

%yfit = b(1)+b(2)*Tinvp10;
yfit = b(1)+b(2)*Tinvp10+ b(3)*phip10;

figure
loglog(y,yfit,'x',y,y,'o')
xlabel('ID Time (ms)','fontsize',12)
ylabel('ID Time Fit (ms)', 'fontsize',12)
title({'Ignition Delay vs 1000/T and phi',' Regression P = 10 Bar,
0.42<phi<0.57 '},'fontsize',14)

% plot and regress P = 20 atm and narrow phi range

Tinvp20 = Tinv(P==20,:);
phip20 = phi(P==20,:);
IDp20 = ID(P==20,:);

% set up regression wrt 1000/T

x = [ones(size(Tinvp20)) Tinvp20 phip20 ];
y = IDp20;

[b bint,r,rint,stats] = regress(y, x)
stats20=stats

%yfit = b(1)+b(2)*Tinvp20;
yfit = b(1)+b(2)*Tinvp20+ b(3)*phip20;

figure
loglog(y,yfit,'x',y,y,'o')
xlabel('ID Time (ms)','fontsize',12)
ylabel('ID Time Fit (ms)', 'fontsize',12)
title({'Ignition Delay vs T/1000[K] and phi ','Regression P = 20 Bar 0.22<
```

```
phi <0.30'},'fontsize',14)

% plot and regress P = 30 atm and narrow phi range

Tinvp30 = Tinv(P==30,:);
phip30 = phi(P==30,:);
IDp30 = ID(P==30,:);

% set up regression wrt 1000/T

x = [ones(size(Tinvp30)) Tinvp30 phip30];
y = IDp30;

[b bint,r,rint,stats] = regress(y, x)
stats30=stats

yfit = b(1)+b(2)*Tinvp30+ b(3)*phip30;

figure
loglog(y,yfit,'x',y,y,'o')
xlabel('ID Time (ms)','fontsize',12)
ylabel('ID Time Fit (ms)', 'fontsize',12)
title({'Ignition Delay vs 1000/T[K] and phi',' Regression P = 30 Bar 0.15<
phi <0.20'}, 'fontsize',14)
```

C-3: MATLAB Code To Apply Linear Regression of ID time to temperature (1000/T[K]), Φ, composition, HOV, RON, and S.

```
close all;clear all;clc;

filedata = 'data/FuelDatathesisall';

load(filedata)

Tinvp5 = Tinv(P==5,:);
phip5 = phi(P==5,:);
IDp5 = ID(P==5,:);
C1p5 = C1(P==5,:);
C2p5 = C2(P==5,:);
C3p5 = C3(P==5,:);
C4p5 = C4(P==5,:);
C5p5 = C5(P==5,:);
C6p5 = C6(P==5,:);;
C7p5 = C7(P==5,:);
HOVp5 = HOV(P==5,:);
RONp5 = RON(P==5,:);
Sp5 = S(P==5,:);

% set up regression wrt 1000/T and phi

x = [ones(size(Tinvp5)) Tinvp5 phip5 C1p5 C2p5 C3p5 C4p5 C5p5 C6p5 C7p5 HOVp5
RONp5 Sp5 ];
y = IDp5;
```

```
[b bint,r,rint,stats] = regress(y, x)
stats5=stats

    % Removes NaN data

yfit =
b(1)+b(2)*Tinvp5+b(3)*phip5+b(4)*C1p5+b(5)*C2p5+b(6)*C3p5+b(7)*C4p5+b(8)*C5p5
+b(9)*C6p5+b(10)*C7p5+b(11)*HOVp5+b(12)*RONp5+b(13)*Sp5;

figure
loglog(y,yfit,'x',y,y,'o')
xlabel('ID Time (ms)','fontsize',12)
ylabel('ID Time Fit (ms)', 'fontsize',12)
title( {'Ignition Delay vs 1000/T[K], Phi, Composition, HOV, RON, and S',
'Regression at P = 5 Bar, 0.78< phi <1.04 '},'fontsize',14)

% plot and regress P = 10 atm and narrow phi range

Tinvp10 = Tinv(P==10,:);
phip10 = phi(P==10,:);
IDp10 = ID(P==10,:);
C1p10 = C1(P==10,:);
C2p10 = C2(P==10,:);
C3p10 = C3(P==10,:);
C4p10 = C4(P==10,:);
C5p10 = C5(P==10,:);
C6p10 = C6(P==10,:);
C7p10 = C7(P==10,:);
HOVp10 = HOV(P==10,:);
RONp10 = RON(P==10,:);
Sp10 = S(P==10,:);

% set up regression wrt 1000/T

x = [ones(size(Tinvp10)) Tinvp10 phip10 C1p10 C2p10 C3p10 C4p10 C5p10 C6p10
C7p10 HOVp10 RONp10 Sp10 ];
y = IDp10;

[b,bint,r,rint,stats]= regress(y,x)     % Removes NaN data
stats10=stats

yfit =
b(1)+b(2)*Tinvp10+b(3)*phip10+b(4)*C1p10+b(5)*C2p10+b(6)*C3p10+b(7)*C4p10+b(8
)*C5p10+b(9)*C6p10+b(10)*C7p10+b(11)*HOVp10+b(12)*RONp10+b(13)*Sp10;

figure
loglog(y,yfit,'x',y,y,'o')
xlabel('ID Time (ms)','fontsize',12)
ylabel('ID Time Fit (ms)', 'fontsize',12)
title({'Ignition Delay vs 1000/T[K], Phi, Composition, HOV, RON, and S',
'Regression at P = 10 Bar, 0.42< phi <0.57 '}, 'fontsize', 14)

% plot and regress P = 20 atm and narrow phi range
Tinvp20 = Tinv(P==20,:);
phip20 = phi(P==20,:);
IDp20 = ID(P==20,:);
```

```
C1p20 = C1(P==20,:);
C2p20 = C2(P==20,:);
C3p20 = C3(P==20,:);
C4p20 = C4(P==20,:);
C5p20 = C5(P==20,:);
C6p20 = C6(P==20,:);
C7p20 = C7(P==20,:);
HOVp20 = HOV(P==20,:);
RONp20 = RON(P==20,:);
Sp20 = S(P==20,:);

% set up regression wrt 1000/T

x = [ones(size(Tinvp20)) Tinvp20 phip20 C1p20 C2p20 C3p20 C4p20 C5p20 C6p20
C7p20 HOVp20 RONp20 Sp20 ];

y = IDp20;

[b,bint,r,rint,stats] = regress(y,x)     % Removes NaN data
stats20=stats

yfit =
b(1)+b(2)*Tinvp20+b(3)*phip20+b(4)*C1p20+b(5)*C2p20+b(6)*C3p20+b(7)*C4p20+b(8
)*C5p20+b(9)*C6p20+b(10)*C7p20+b(11)*HOVp20+b(12)*RONp20+b(13)*Sp20;

figure
loglog(y,yfit,'x',y,y,'o')
xlabel('ID Time (ms)','fontsize',12)
ylabel('ID Time Fit (ms)', 'fontsize',12)
title({'Ignition Delay vs 1000/T[K], Phi, Composition, HOV, RON, and S',
'Regression at P = 20 Bar, 0.30< phi <0.22 '}, 'fontsize', 14)

% plot and regress P = 30 atm and narrow phi range

Tinvp30 = Tinv(P==30,:);
phip30 = phi(P==30,:);
IDp30 = ID(P==30,:);
C1p30 = C1(P==30,:);
C2p30 = C2(P==30,:);
C3p30 = C3(P==30,:);
C4p30 = C4(P==30,:);
C5p30 = C5(P==30,:);
C6p30 = C6(P==30,:);
C7p30 = C7(P==30,:);
HOVp30 = HOV(P==30,:);
RONp30 = RON(P==30,:);
Sp30 = S(P==30,:);

% set up regression wrt 1000/T

x = [ones(size(Tinvp30)) Tinvp30 phip30 C1p30 C2p30 C3p30 C4p30 C5p30 C6p30
C7p30 HOVp30 RONp30 Sp30];

y = IDp30;

[b,bint,r,rint,stats] = regress(y,x)     % Removes NaN data
```

```
stats30=stats

yfit =
b(1)+b(2)*Tinvp30+b(3)*phip30+b(4)*C1p30+b(5)*C2p30+b(6)*C3p30+b(7)*C4p30+b(8
)*C5p30+b(9)*C6p30+b(10)*C7p30+b(11)*HOVp30+b(12)*RONp30+b(13)*Sp30;

figure
loglog(y,yfit,'x',y,y,'o')
xlabel('ID Time (ms)','fontsize',12)
ylabel('ID Time Fit (ms)', 'fontsize',12)
title({'Ignition Delay vs 1000/T[K], Phi, Composition, HOV, RON, and S',
'Regression at P = 30 Bar, 0.20< phi <0.15 '}, 'fontsize', 14)
```